STAR FORMATION RATES AND STELLAR CONTRIBUTIONS IN ELLIPTICAL GALAXIES AT 12- AND 22- μm

NUR HIDAYAH BINTI MOHD ALI

FACULTY OF SCIENCE
UNIVERSITY OF MALAYA
KUALA LUMPUR

2018

STAR FORMATION RATES AND STELLAR CONTRIBUTIONS IN ELLIPTICAL GALAXIES AT 12- AND 22- μm

NUR HIDAYAH BINTI MOHD ALI

DISSERTATION SUBMITTED IN FULFILMENT OF THE REQUIREMENTS FOR THE DEGREE OF MASTER OF SCIENCE

DEPARTMENT OF PHYSICS
FACULTY OF SCIENCE
UNIVERSITY OF MALAYA
KUALA LUMPUR

2018

UNIVERSITY OF MALAYA

ORIGINAL LITERARY WORK DECLARATION

Name of Candidate: **NUR HIDAYAH BINTI MOHD ALI**

Matric No: **SGR150003**

Name of Degree: **MASTER OF SCIENCE**

Title of Project Paper/Research Report/Dissertation/Thesis ("this Work"):

STAR FORMATION RATES AND STELLAR CONTRIBUTIONS IN ELLIPTICAL GALAXIES AT 12- AND 22- μm

Field of Study: **EXPERIMENTAL PHYSICS**

I do solemnly and sincerely declare that:

(1) I am the sole author/writer of this Work;
(2) This Work is original;
(3) Any use of any work in which copyright exists was done by way of fair dealing and for permitted purposes and any excerpt or extract from, or reference to or reproduction of any copyright work has been disclosed expressly and sufficiently and the title of the Work and its authorship have been acknowledged in this Work;
(4) I do not have any actual knowledge nor do I ought reasonably to know that the making of this work constitutes an infringement of any copyright work;
(5) I hereby assign all and every rights in the copyright to this Work to the University of Malaya ("UM"), who henceforth shall be owner of the copyright in this Work and that any reproduction or use in any form or by any means whatsoever is prohibited without the written consent of UM having been first had and obtained;
(6) I am fully aware that if in the course of making this Work I have infringed any copyright whether intentionally or otherwise, I may be subject to legal action or any other action as may be determined by UM.

Candidate"s Signature Date:

Subscribed and solemnly declared before,

Witness"s Signature Date:

Name:

Designation:

STAR FORMATION RATES AND STELLAR CONTRIBUTIONS IN ELLIPTICAL GALAXIES AT 12- AND 22- μm

ABSTRACT

The star formation rates (SFRs) is one of the most important characteristics in determining galaxy evolution. Investigations on star formation were done using the mid-infrared indicators. In this study, the SFRs were investigated from a sample of selected galaxies from the Sloan Digital Sky Survey (SDSS) MPA-JHU catalogue with morphologically-classified elliptical galaxies by Galaxy Zoo. The sample galaxies were astrometric-matched for the mid-infrared emission data from the Wide-field Infrared Survey Explorer (*WISE*), which was equipped with the four mid-infrared bandpass filters centered at 3.4, 4.6, 12, and 22 μm. The highly sensitive W3 (12 μm) and W4 (22 μm) bands that cover the emission for hot dust and polycyclic hydrocarbon were used to estimate the SFRs of the sources. Due to the stellar emission, this could overestimate the W3- and W4-based derived SFRs in the low star forming galaxy. The fractions of stellar contributions at W3 and W4 bands respective to W1 band were found to be about 0.125 $\pm$ 0.001 and 0.0107 $\pm$ 0.0003, respectively. Better SFRs were proposed by subtracting the stellar contributions of the sources. The study of intrinsic properties of galaxies that are highly affected by stellar contributions suggests that the star forming elliptical galaxies (SFEGs) show different star formation properties with stellar populations of different ages and masses at their central regions. By implementing the model of star formation history (SFH), the SFEGs have also showed continuous star formation activities that are comparable to spiral galaxies at the central regions. The results highlighted the possibility of unknown mechanism exists in triggering the star formation activities in the elliptical galaxies.

Keywords : galaxies, elliptical and spiral, star formation, mid-infrared.

KADAR PEMBENTUKKAN BINTANG DAN SUMBANGAN BINTANG DALAM GALAKSI ELIPS PADA 12- AND 22- μm

ABSTRAK

Kadar pembentukan bintang (SFR) adalah salah satu ciri-ciri yang paling penting dalam menentukan evolusi pembentukan sesebuah galaksi. Penyelidikan ke atas pembentukan bintang telah dilakukan dengan menggunakan penunjuk dalam frekuensi inframerah pertengahan. Kajian ini menggunakan sampel galaksi yang telah dipilih daripada katalog *Sloan Digital Sky Survey* (SDSS) MPA-JHU yang telah diklasifikasikan secara morfologi sebagai galaksi elips oleh Zoo Galaxy. Sampel telah dipadankan secara astrometrik untuk mendapatkan data inframerah pertengahan dari katalog *Wide-field Infrared Survey Explorer* (*WISE*), yang dilengkapi dengan empat penapis turas jalur yang berpusat pada 3.4, 4.6, 12, dan 22 22 μm. Turas jalur W3(12 μm) dan W4(22 μm) sangat sensitif terhadap debu panas dan hidrokarbon polisiklik yang digunakan sebagai penunjuk kepada kadar pembentukkan bintang untuk sesuatu sumber. Disebabkan oleh pancaran bintang, ini boleh memberi anggaran yang berlebihan terhadap kadar pembentukan bintang yang diterbitkan daripada turas jalur W3 dan W4 lebih-lebih lagi daripada galaksi yang mempunyai kadar pembentukkan bintang yang rendah. Pecahan sumbangan bintang dalam turas jalur W3 dan W4 relatif kepada W1 masing-masing mencatatkan kira-kira 0.125 ± 0.001 and 0.0107 ± 0.0003. Untuk kajian yang lebih baik, sumbangan bintang haruslah ditolakkan daripada kadar pembentukkan bintang oleh sesuatu sumber. Kajian terhadap sifat intrinsik sesebuah galaksi yang terjejas akibat sumbangan bintang telah mengsyorkan bahawa galaksi elips yang mempunyai pembentukkan bintang (SFEGs) menunjukkan sifat pembentukkan bintang yang berbeza-beza. Dengan melaksanakan Model Sejarah Pembentukkan bintang (SFH), SFEGs juga telah menunjukkan aktiviti pembentukan bintang yang

berterusan di dalam galaksi ini setanding dengan galaksi pilin, di kawasan tengah galaksi. Keputusan yang diperoleh menekankan tentang kemungkinan wujudnya mekanisma yang tidak diketahui yang mencetuskan aktiviti pembentukan bintang dalam galaksi elips.

Kata kunci: galaksi, elips dan pilin, pembentukkan bintang, pertengahan inframerah.

ACKNOWLEDGEMENTS

Foremost, Alhamdullilah. I am very grateful to The Almighty God for all the blessing and strength that have given been to me throughout these years. This thesis becomes possible with the kind support of many individuals, who I would like to extend my sincere thanks to.

Firstly, I would like to express my deepest appreciation and thanks to my supervisor, Assc. Prof. Dr. Zamri Zainal Abidin for all his valuable comments, supervision and words of encouragement throughout my master study. I also highly indebted to Professor Dr. Hwang Chorng-Yuan (from National Central University,Taiwan), who always and constantly provide me with guidance and endless supervision on my study. Also thousand of thanks for giving me a priceless experience during my study visit in NCU, Taiwan and also in Lulin Observatory. I also take this opportunity to thanks all my wonderful friends from Radio Cosmology Lab, UM and also from Extragalactic Group, NCU.

The completion of this study could not have been possible without the affection, encouragement and prays from my family. Especially from my beloved husband, Anis Norsyafiq who always inspired me to achieve my goals. Thank you again.

TABLE OF CONTENTS

LIST OF FIGURES

LIST OF TABLES

LIST OF SYMBOLS AND ABBREVIATIONS

η_{w3}	:	Coefficient of stellar contribution at 12 μm
η_{w4}	:	Coefficient of stellar contribution at 22 μm
H_0	:	Hubble constant
Ω_m	:	Matter density
z	:	Spectroscopic redshift
Ω_Λ	:	Vacuum energy density or cosmological constant
AGB	:	Asymptotic Giant Branch
AGN	:	Active Galactic Nuclei
IR	:	Infrared
MIR	:	Mid-Infrared
PAH	:	Polycyclic Aromatic Hydrocarbons
PSF	:	Point Spread Function
RMSE	:	Root-mean-square error
RSR	:	Relative System Response
SFEG	:	Star forming Elliptical Galaxies
SFR	:	Star Formation Rate

LIST OF APPENDICES

CHAPTER 1: INTRODUCTION

1.1 Star Formation Activities in the Galaxies

Over the last 13 billion years, the Universe has evolved from an almost uniform state to the rich diversity of galaxies that locally can be seen today. Matter began to coalesce into gas clouds, galaxies, stars and planets as the Universe expanded. There are about $\sim 10^{11}$ galaxies within the observable universe. They formed in varies types and characteristics. Some experienced merging, some are quiescent, while some experienced a burst of star formation activity in the nucleus. All these differences have directly influenced the properties of the gas and the process of star formation which takes place within the galaxy. In the quest to understand when galaxies formed their stars and assembled their mass, direct observation technique can be employed to measure the star formation rates in the galaxy at different epoch. One of the best ways to understand this crucial phenomenon is by measuring the accurate star formation rate (SFR) of the galaxies (Kennicutt, 1998). This SFR parameter estimates the recent rate of star forming in a galaxy, which will describe the numbers of new born stars in a limited period of time. In 1936, a schema for classifying the galaxies has been proposed by Edwin Hubble, known as "tuning fork" diagram (shown in Figure 1.1). For the past 80 years up untill now, Hubble classification method of galaxies remains relevant and only subsequent refinements have been proposed by others. Anyhow, it does not change the fundamental ideas. In the diagram, the elliptical galaxies are generally smooth, usually round and almost featureless. There are no observable spiral arms or any dust lanes, lacking in cool gas, hence consisting only few young blue stars. On the other hand, spiral galaxies have dust lanes or bright spiral arms, which are prominent in bright OB stars. The classification of spirals is based on the importance of their central bulge, disk, and the linear bar. Between elliptical and spiral classes, there is a transition class called

as lenticular, which has a rotating disk in addition to central elliptical bulge without any disk spiral arms or dust lanes. By looking at the properties of subsystems within the galaxies (e.g., the disks, spheroids, halos), these could be related in deducing their origins and evolution. Hubble interpreted the classification diagram as an evolutionary sequence, where the ellipticals are called as "early-type" and spirals as "late-type" galaxies. However, his idea is not supported by many modern researches.

Morphology of the galaxies along the Hubble sequence is strongly correlated with the SFR of galaxies, where the late-type galaxies actively performed the star formation compared to the early-type galaxies that are typically considered as quiescent, non-star forming galaxies. The study done by Kennicutt & Kent (1983) showed that the *Hα* equivalent width increases from the early-type to late-type galaxies, suggesting the early-type galaxies are lacking in young, bright stars and *HII* star forming regions compared to the late-type galaxies. In the spiral galaxies, the distribution of young and bright stars generally dominates in the dense spiral features, while the central bulge consists of older stars. The spiral arm features showed that the spiral galaxies are able to maintain the spiral structure dynamically and hence the star forming activities in the galaxy. With the help from the density waves mechanism, the molecular clouds in high density regions of spiral arms compressed by density waves could enhance the star formation activities and hence been conserved within a longer timescale. In general, SFRs of the disk of spiral galaxies have the range between 0 to 20 $M_{\odot}\mathrm{yr}^{-1}$. On the other hand, the star formation activities in the elliptical galaxies still remain a hot debate in this field. Majority of elliptical galaxies constitute of the red galaxies as classified in the bimodal color distribution. The most massive ($>10^{10}\,M_{\odot}$) elliptical galaxies are red and with little star formation (Temi et al., 2009). Their stellar population has been transitioned from blue to red as their star formation ceased (Faber et al., 2007; Hughes & Cortese, 2009). From traditional view, elliptical galaxies are the old systems that

formed at higher redshift and passively evolved to present without further star formation activity (Eggen et al., 1962; Tinsley & Gunn, 1976). Hence, the stellar component was formed at an early epoch and passively evolved at the present (Trager et al., 2000; Cimatti et al., 2004; Temi et al., 2005).

In recent decades, beside the monolithic model, the formation of elliptical galaxies has also been proposed by hierarchical models; formed by merger of galaxies either rich ("wet" merger) or poor ("dry" merger) in gas. Recently, advanced observational data have revealed the unique and unusual elliptical with bluer optical color than the typical elliptical (Schade et al., 1999; Im et al., 2001; Schawinski et al., 2009) with lower stellar mass (Im et al., 2001; Kannappan et al., 2009; Salim et al., 2010). The higher SFR and the presence of strong, centrally-concentrated burst of star formation in these galaxies have built the modern merger hypothesis. This hypothesis is the most recently accepted that able to well-described the prediction of blue-to-red migration theory. Some of the researchers have proposed that blue elliptical galaxies have younger stellar population and on-going star formation activities in the central region (Phillips et al., 1986).

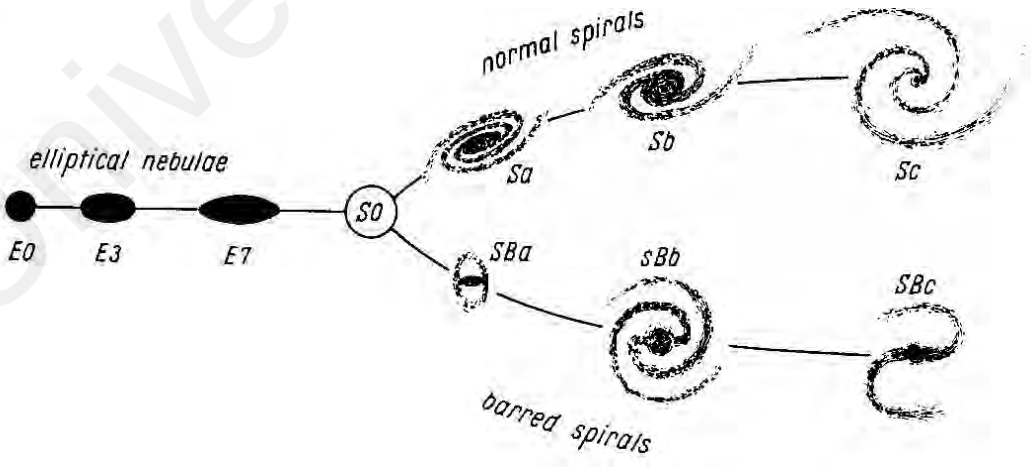

Figure 1.1: Tuning-fork diagram from Hubble (1936), where galaxies are broadly classified into elliptical (E), lenticular (S0) and spiral (S and B).

1.2 The Study of Mid-Infrared SFR Indicators

Recently, various observational diagnostics have been employed to estimate the SFR of a galaxy. These studies have been carried out almost at all frequencies, covering from the lowest to the highest frequencies of electromagnetic wave radiation. In radio studies, the radio continuum emission at 1.4 GHz (21 cm) is claimed as a good SFR tracer (e.g., Condon, 1992; Kennicutt Jr, 1998; Wu et al., 2005; Alonso-Herrero et al., 2006; Rieke et al., 2009; Murphy et al., 2011). The emission mainly originates from the non-thermal synchoroton radiation of generated relativistic electrons that are accelerated by Type II supernovae (SNe) from stars with mass ≥ 7 - 8 $M_{\odot}$ (Condon, 1992; Cram et al., 1998). Going down to the IR spectrum, the SFR traced by far-infrared (FIR) luminosities arising from thermal emission produced via dust-absorbed ultraviolet (UV) radiation of massive stars (Rowan-Robinson et al., 1997; Blain et al., 1999). The UV and optical line diagnostics have measured the SFRs using hydrogen recombination emission and forbidden lines (e.g., *Hα*, *Hβ*, *[OIII]*) and UV continuum. Meanwhile, SFRs derived from X-ray binary emission (e.g., Calzetti et al., 2005; Schmitt et al., 2006) were commonly used in X-ray studies. The extensive growth of SFR studies in infrared observation is attributed by the impact of dust extinction in shorter wavelength observations (e.g., UV, hydrogen and nebular emission). It is well understood that gas is the fundamental element to form stars. The gas components are important to estimate the SFRs of the galaxies, which can be measured from their UV and optical emission. In estimating the SFR, the young, massive stars used to represent as new born stars, which could only span a short lifetime (e.g., Lilly et al., 1996; Treyer et al., 1998; Cowie et al., 1999; Steidel et al., 1999; Sullivan et al., 2000). The young, massive stars that dominate in UV continuum, thus give direct information to trace the star forming activities in the galaxy. Meanwhile, line emissions are due to the transition of gas stimulated by stellar radiation. The emission lines from hydrogen series (i.e., Balmer or Lyman) or other

nebular emission lines, are generated by the ionizing photons from massive ($\geq 10\ M_{\odot}$), short-lived ($\simeq 20$ Myr) and early-type (e.g., Gallego et al., 1995; Tresse & Maddox, 1998; Glazebrook et al., 1999; Moorwood et al., 2000) stars (OB) in the star forming regions in the galaxies. However, a major source of uncertainty is the likelihood that these diagnostics are affected by the dust extinction. These SFR tracers could be severely biased as most of the star formation takes place in the regions with the presence of obscuring dust (Helou et al., 2004; Wu et al., 2005). Thus, infrared observations were proposed to trace the star forming activities of the galaxy, especially in dusty galaxies. The star forming activities determined by infrared emission, produced via the re-emitted emission in FIR or mid-infrared (MIR) by the dust that are heated by the young and hot stars (normally enshrouded by dust). In addition, the prominence of strong polycyclic aromatic hydrocarbons (PAHs) features present in the spectrum of most star forming galaxies. The infrared spectral features which have been attributed to emission from highly vibrationally excited PAHs are mainly shown in MIR wavelengths ($3 \sim 30$ μm). Therefore, MIR emission could be a reliable tracer that experienced negligible dust extinction and give more accurate SFR estimation of the galaxies. Rieke et al. (2009), Elbaz et al. (2011) and Goto et al. (2010) have shown that the MIR luminosities tightly correlated to the total infrared luminosities in the normal star forming galaxies. There have been a number of studies that calibrate the SFR based on the MIR indicator from the available IR survey telescope, such as using Spitzer 8 and 24 μm luminosities (e.g., Wu et al., 2005; Calzetti et al., 2007; Zhu et al., 2008), AKARI 9 and 18 μm luminosities (e.g., Yuan et al., 2011; Goto et al., 2010), IRAS 12 and 25 μm luminosities (e.g., Helou, 1986) and also derived from the latest infrared survey of *WISE* 12- and 22-μm (e.g., Donoso et al., 2012; Shi et al., 2012; Jarrett et al., 2012).

1.3 AGN in Mid-Infrared Study

Active Galactic Nucleis (AGNs) are the very bright nuclei of an active galaxy and are the most powerful sources of luminosity in the Universe. The emission is coming from the cold matter (gas and dust) that formed the accretion disks surround the super massive black hole (SMBH) at the center of the galaxy. For some of the AGN (∼10 %), the interaction between the accretion disks and the SMBH produces a powerful radio jet that is ejected at nearly the speed of light outward in opposite directions away from the disk. The emitted energy from the whole AGN system is widely spread across the electromagnetic spectrum, with more significant luminosity in infrared and X-ray bands, but often found peaking in the Ultraviolet (UV) band. The AGN is typically divided into two classes according to the existence of any jet-related emission categorized as radio-quiet and radio-loud nuclei. Seyfert galaxy is radio-quiet AGN that have been subdivided into two groups (Type 1 and Type 2) based on the obscuration of their emission lines by dust and gas. Besides, there are similar galaxies to Seyfert 2 with strong low ionization lines (such as *[OI]* and *[NII]*) classified as Low Ionization Nuclear Emission-line Region galaxies (LINERs). The radio-loud galaxy is commonly classified into Broad-line radio galaxies (BLRGs) and Narrow-line radio galaxies (NLRGs), which are analogous to Seyfert 1 and Seyfert 2, respectively. They are the elliptical galaxies with strong radio emission accompanied by single or twin radio lobes. Quasars and Quasi-stellar objects (QSOs) are another AGN subdivisions that possess different radio loudness and particularly numerous at a higher redshift. Both sources located distant enough to appear as star-like object. The classification of AGN depends on the obscuration of dusty torus and the apparent differences due to the orientation of the system relative to the observer‟s line of sight (e.g., Pier & Krolik, 1992; Efstathiou & Rowan-Robinson, 1995; Stalevski et al., 2012; Siebenmorgen et al., 2015). Many orientation-based AGN unification models (shown in Figure 1.2) have been proposed to

account for the variety of observational differences in viewing geometry for many years (e.g., Antonucci & Miller, 1985; Antonucci, 1993; Urry & Padovani, 1995; Urry, 2003; Tadhunter, 2008). The AGN unification model requires modification from time to time to enhance the efficiency of AGN classification (e.g., Heckman & Best, 2014; Netzer, 2015) and modern revisions have been done by several studies (e.g., Kewley et al., 2006; Stasińska et al., 2006; Kewley et al., 2013). In infrared observations, AGN activities in the host galaxy play an important role as the sources of infrared emission. The circum-nuclear dust or usually referred as dusty torus, absorbs a fraction of the optical and UV light and re-emits the energy in the infrared regime, peaking in the mid-infrared (MIR; ∼5 - 30 μm). Prominent features in the MIR spectrum of AGN are the 9.7 μm silicate feature and the Polycyclic Aromatic Hydrocarbon (PAH) emission bands.

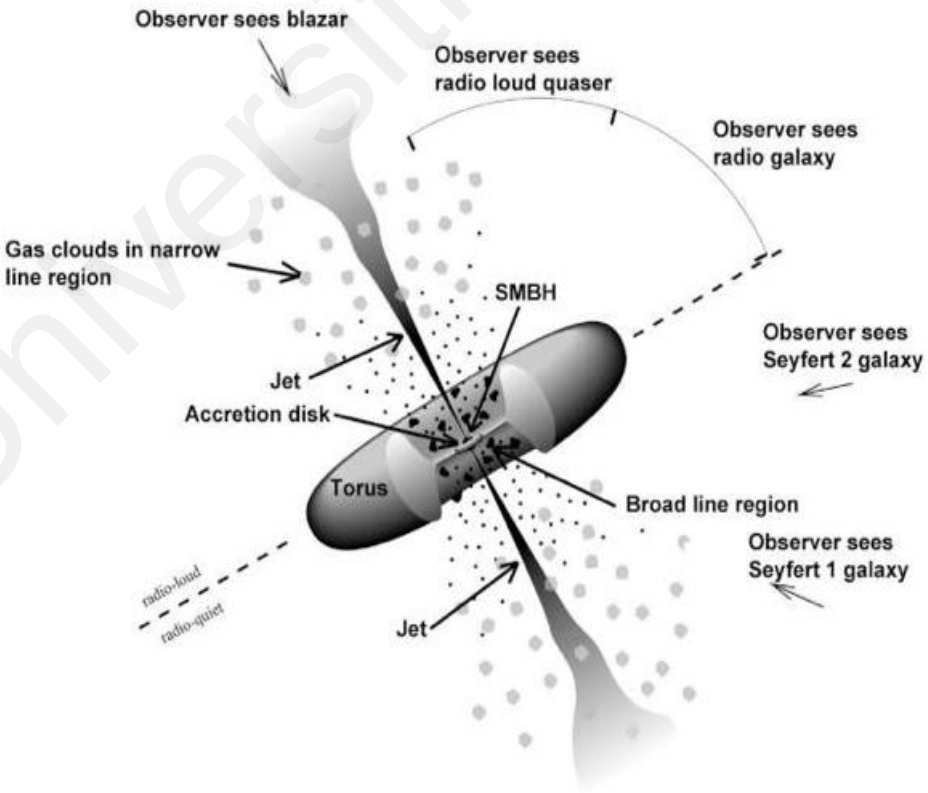

Figure 2.2: Unified model of Active Galactic Nuclei (AGN).

1.4 Literature Review

Over more than 30 years, since IRAS times, infrared indicators have been calibrated to measure the SFR of the galaxies conveniently at local Universe as well at intermediate and high redshift (e.g., Lonsdale et al., 1987; Rowan-Robinson & Crawford, 1989; Daddi et al., 2005; Wu et al., 2005). The interest in IR-based SFR arises because of the transparency of infrared emission against the dust reddening, and hence reducing effect of dust is much challenging in UV-optical indicators. Kennicutt Jr (1998) has shown the bolometric infrared luminosities, LIR (between ~3 – 1100 μm) is directly proportional to the SFR. Previous findings claimed that PAHs are an essential component in MIR that traces the star forming activities in the galaxies (Sauvage et al., 1996; Dale et al., 2000; Roussel et al., 2001). However, Boselli et al., (2003) showed that the MIR emissions of optically selected normal, early-type galaxies are dominated by the Rayleigh-Jeans (R-J) tail of old stellar populations. Whereas, the IR emission of late-type galaxies are dominated by the thermal emission from the dust heated by young stellar populations. Also, Lonsdale Persson & Helou (1987), Sauvage & Thuan (1994) and Mazzei & De Zotti (1994) have proposed the significant contribution of the IR emission in early-type galaxies is originated from dust heating by the general stellar radiation. Hence, a clear excess over stellar emission can be observed in MIR wavelengths (9.62 - 15.0 μm) for elliptical galaxies (e.g., Athey et al., 2002; Xilouris et al., 2004), where the spectrum energy distribution (SED) of the galaxy can be well-fitted to the blackbody profile of T ~3500 K from 6 - 7.75 μm. This situation makes it unclear whether these MIR-based SFR indicators are applicable to the galaxies with low star forming activities, since the early-type galaxies are mostly composed of old K- and M-type stars. Additionally, the small amount of dust opacities in the early-type galaxies have brought up the usage of MIR-based SFR for these galaxies into question. Generally, lower metallicity and more dust-poor galaxies might be significantly affected

by this stellar contribution (Calzetti et al., 2007), but showed only small contribution in high metallicity, dusty galaxies (e.g., Calzetti et al., 2005).

The reliability of strong correlation between star formation rates and the mid-infrared luminosities, as well as the advance in infrared telescope, have broaden the study of star formation activities in the galaxy. There are several studies that empirically modeled the SFR functions by using MIR indicators by using the latest infrared telescope, Wield-field Infrared Survey Explorer (*WISE*), such as Shi et al., (2012); Donoso et al. (2012); Jarrett et al. (2012); Lee et al. (2013); Chang et al. (2015). The derived SFR conversion factors from these studies have been widely used to estimate the SFR of the galaxies, thus brings up the concern in the estimation of SFR for early-type or elliptical galaxies. Even though all these studies use similar *WISE* selected SDSS galaxies, the largest discrepancies occur for these studies that are limited to galaxies with relatively high luminosities (i.e., $L_{H\alpha} > 10^{40}$ ergs^{-1}). Jarrett et al. (2012) and Lee et al. (2013) claimed that the average estimation for the contribution of stellar continuum at 12 μm are ∼0.15 and ∼0.1, respectively. Hence, these stellar fractions have been ignored in the SFR calibration of the literature, as the corresponding contribution of stellar continuum to the flux density shows only a few percent and give negligible affects on the scatter of the data (Jarrett et al., 2012; Lee et al., 2013; Cluver et al., 2014). As a consequence, the contamination from the stellar continuum can severely bias the derivations of MIR-based SFRs for early-type galaxies that essentially have low star forming activities.

Although the stellar contribution is pivotal in many early-type galaxies, there is some population of elliptical galaxies that provide convincing evidence of substantial recent star formation from their strong *Hα* emission (e.g., Fukugita et al., 2004). Evidence has also been reported that a small fraction of early-type galaxies retain a

signature of star formation that occurred in the recent past (Zabludoff et al., 1995; Quintero et al., 2004; Goto et al., 2003). The traditional ideas of elliptical or early-type galaxy are this population used to be a quiescent galaxy (passive with no on-going star formation) and tended to be redder than spirals (e.g., Hubble, 1926; Holmberg, 1958) is not longer completely true. The advert of large imaging and spectroscopic surveys from Sloan Digital Sky Survey (SDSS) and visual inspection from Galaxy Zoo, has increased the discoveries of unusually young luminosity-weighted stellar ages of elliptical population, which also classified as “blue elliptical” (e.g., McIntosh et al., 2014; Schawinski et al., 2009; Tojeiro et al., 2013). This population show remarkable of star formation compare to normal elliptical galaxies, hence the estimation of SFR is vital to ensure no excessive emission from non-star forming sources. Since the literatures have convinced that there is no compelling reason to apply the exclusion of stellar continuum for the MIR-based SFR calibration, this will result in an overestimation of SFR especially for elliptical galaxies.

1.5 Problem Statements and Objectives of the Study

The contamination of old stellar continuum will give a significant contribution in the mid-infrared SFR calibration. This matter might reveal the problem in the SFR calibration of MIR indicators. Besides that, the stellar continuum emissions contribute differently at different wavelength, hence resulting the estimated SFRs from two SFR indicators might yield inconsistency in the results obtained. In addition, the derived SFR conversions of MIR indicators from previous studies might not be applicable to estimate the SFR of low star forming or the early-type galaxies. Since most of the derived SFR conversion depending on the samples with high SFRs, the employment could overestimate the "expected" SFR of the galaxies. Therefore, the discrepancies in SFR calibration are hence questionable.

The specific objectives to be achieved in this study are:

- To examine the correlation between the galaxy SFR in MIR emission using *WISE* W3 and W4 bands
- To estimate the contribution of stellar continuum at 12- and 22- μm emission of the galaxy
- To estimate the MIR SFR of the galaxy exclusively from star forming activities in the galaxy
- To identify the intrinsic properties of the elliptical galaxies that affected by the correction of stellar continuum in MIR emission
- To derive *WISE*-based SFRs conversion factors compatible for low star forming galaxies.

The structure of this thesis is organized as follows: In Chapter 2, we will describe the SDSS-*WISE* photometric data and the properties restriction applied on data selection methods. In Chapter 3, we present the results on estimated stellar contribution in the derived MIR-based SFRs and the behavior of the correlations between *WISE*-SFR indicators after the subtraction of stellar contamination. We also show comparisons between the SFRs obtained from this study and those from previous studies by referring to their intrinsic properties. Chapter 4 consists of the discussion regarding the evolution of early-type galaxies, which is based on their star forming histories and the bimodality in their intrinsic properties. Finally, in Chapter 5 we will give a brief summary, conclusion and the significance of this study. Throughout this study, the ΛCDM cosmological parameters were adopted with Ω_m= 0.3, Ω_Λ = 0.7 and H_0= 70 km s^{-1} Mpc^{-1}.

CHAPTER 2: METHODOLODY

2.1 SDSS-*WISE* Cross-matched Data

The Sloan Digital Sky Survey (SDSS) is conducted using a 2.5-meter ground-based telescope located at the Apache Point Observatory in Sunspot, New Mexico. The SDSS performed 5-optical bands of *u, g, r, i,* and *z* photometry at wavelengths 3543, 4770, 6231, 7625, 9134 Å. The survey covers ∼14,555 square degrees of the sky (35 % of the all sky). Meanwhile, Wide-field Infrared Sky Explorer (*WISE*) provides the most comprehensive view of mid-infrared sky that is currently available. *WISE* telescope was launched in December 2009 and completed the scanning for entire sky twice by early 2011. The *WISE* survey has measured the sky in four mid-infrared bandpasses centered at 3.4-, 4.6-, 12-, and 22- μm (also known as W1, W2, W3 and W4 bands) with an angular resolution of 6.1", 6.4", 6.5", and 12.0", respectively. The combination of data from SDSS and *WISE* has proven to be very powerful for a variety of studies (e.g., Yan et al., 2013; Dawson et al., 2012).

We have undertaken astrometric cross-matching between the SDSS MPA-JHU catalog and *WISE* All-sky Data Release catalog. For this study, the matching process was done via *Casjobs*, one of the SDSS database query interfaces. The unique and closest matched objects of SDSS-*WISE* identified as the brightest ones within 3" matching tolerance (∼0.5 × FWHM of the *WISE* point spread function (PSF) at 3.4 μm). The SDSS sources that show multiple matches to *WISE* object (or vice versa) are excluded from the primary sample (contains ∼679,342 SDSS-*WISE* matched galaxies), to avoid the contamination from nearby sources. In addition, the galaxy sample is conservatively constrained to have at least 3σ detection at *WISE* W3 μm and W4 μm and with signal-to-noise ratio (S/N) > 3 for Balmer emission lines (*Hα* and *Hβ*). The criterion of a high (S/N) is required for having the unconfused object in galaxy sample

and to get accurate galaxy classification into star-forming or AGN-dominated galaxies (e.g., Veilleux & Osterbrock, 1987; Kewley et al., 2001).

The sources are also restricted to lie within spectroscopic redshift range between $0.01 \leq z \leq 0.2$. The upper redshift bin is limited to 0.2, due to the redshift effects on optical emission lines. Priority for *Hα* and *Hβ* emission lines to be comfortably within the SDSS spectral coverage, which is between ~3800 Å to ~9200 Å to reduce bias. Besides, limiting the upper redshift bin could substantially reduce the uncertainties in morphology classification of the sources. On the other hand, the redshift lower limit might maximize the aperture effects on the source, as it would lower the amount of captured light. Hence, Kewley et al. (2005) suggest the lower limit for redshift bin for photometric observation should be $z > 0.04$ to ensure the captured light to be at least 20 % of the galaxy light for SDSS galaxies. However, the aperture correction method proposed by Hopkins et al. (2003) affirmed the method is working well and did not claim any aperture bias for the galaxy even at lower redshift, $z > 0.01$ (see also Brinchmann et al., 2004). This correction method is applied in the study and will be discussed further later on in Section 4.1. Consequently, there are in total of ~168,448 galaxies in secondary sample (contains ~24.8 % of the primary galaxy sample) by fulfilling all the above conditions and this sample will be utilized throughout the study.

2.2 Restriction Criterion

2.2.1 AGN Exclusion

In infrared study, identifying the active galactic nuclei (AGN) galaxies is always crucial to distinguish the origin of infrared emission, which either from the dust heated by the AGN or directly from the star forming activities within the host galaxy (e.g., Radomski et al., 2003; Sales et al., 2013; Esquej et al., 2013; Alonso-Herrero et al., 2014; Ramos Almeida et al., 2014; Hernán-Caballero et al., 2015). All the AGN

galaxies are eliminated to ensure a reliable galaxy samples for this study as AGN-related galaxies may lead to confusion and bias in SFR analysis. Generally, a more complete census of AGN can only be achieved with a multi-wavelength analysis. In this study, the AGN optical line diagnostic method of Baldwin-Phillips-Terlevich (BPT) diagram is applied to identify the AGNs. The use of this diagnostic diagram of *[NII]*6584 / *Hα* against *[OIII]*5007 / *Hβ*, necessarily require measurable *Hα*, *Hβ*, *[NII]* and *[OIII]* lines for all the sources. The host galaxies are differentiated based on the ionization mechanism of the nebular gas (e.g., Veilleux & Osterbrock, 1987; Kewley et al., 2001; Kauffmann et al., 2003a; Kewley et al., 2006; Osterbrock & Ferland, 2006; Stasińska et al., 2006; Kewley et al., 2003; Kewley & Dopita, 2003), where the galaxy with normal *HII* regions can be distinguished from normal AGNs (Seyferts and QSOs). Demarcation between star forming galaxy and AGNs proposed by Kewley et al. (2001) and Kauffmann et al. (2003a) in BPT-*[NII]* diagram (also been known as Kewley and Kauffmann curve),

$$\log \frac{[OIII]}{H\beta} \leq \frac{0.61}{(\log [NII]/\, H\alpha) - 0.47} + 1.19 \tag{2.1}$$

$$\log \frac{[OIII]}{H\beta} \leq \frac{0.61}{(\log [NII]/\, H\alpha) - 0.05} + 1.3 \tag{2.2}$$

where *[OIII] / Hβ* and *[NII] / Hα* are the flux ratio of the lines. The diagram categorized the galaxies that lie above Kewley and Kauffmann curve are likely to be dominated by AGN activities (i.e., Seyfert and LINER), while those lie below the line are categorized as star forming and composite galaxies. Figure 2.1 shows the BPT-*[NII]* line of the secondary galaxy sample. The solid line denotes the AGN-*HII* (Kewley et al., 2001) separation curve. While, the dashed line indicates the division line between the pure star forming galaxies and composite galaxies proposed by Kauffmann et al. (2003a). The blue and red dots represent the spiral and elliptical galaxies, where the morphology of

the galaxy samples determine using suitable methods explained in next subsection. Based on this scheme, all the galaxies lie above the Kewley"s curve are strictly excluded from this study. Besides that, AGN sources identified from the spectral classification provided by SDSS pipeline are also eliminated. The AGN sources from SDSS spectroscopic subclasses are appended as "QSO" and "BROADL INE" subclasses, is the candidates that show lines above 10σ level with velocity dispersion > 200 km / sec at 5σ level. In addition, AGN candidates are distinguishable from their mid-infrared colors. This method is ideally-suited to ensure a negligible contamination of AGN in galaxy samples, as the presence of obscured AGN in optical observation is detectable in MIR observation. In this study, we adopted the *WISE* color diagnostic diagram, which deduce the *WISE* (see also Wright et al., 2010) color of extragalactic populations based on several templates of SWIRE augmented by GRASIL models (Silva et al., 1998; Polletta et al., 2006, 2007) developed by Jarrett et al. (2011). The *WISE* color-color diagram can be utilized to classify the sources into stars, ellipticals, spirals, QSOs, Seyferts, ULIRGs, LIRGs and others, by interpreting the region occupied by these sources on the [W1]-[W2] versus [W2]-[W3] plane, based on the rest-frame color. The different classes of *WISE*-detected sources classified via *WISE* color-space regions, as shown in the left panel of Figure 2.2, where they are plotted in units of Vega magnitude. Distribution of mid-infrared colors, the classes illustrates that stars have MIR colors near zero magnitude and trending slightly redward in [4.6]-[12] color with the more luminous, evolved populations. For early-type field galaxies, they occupy the “green” zone and extending toward redder colors. Meanwhile, disk galaxies are located between the population of early-type galaxies and most extreme star forming galaxies, such as LIRGs (tan/brown), starbursts (yellow) and ULIRGs (orange). On the other hand, AGN classification from *WISE* color includes the QSOs, Seyferts and obscured AGN, covering from the field spirals and extending toward redder colors in [3.4]-[4.6] mag

due to their power-law mid-IR spectrum. Hence, QSOs have relatively blue colors in the short bands, while ULIRGs have the reddest overall colors. Studies by Stern et al. (2012); Assef et al. (2013) and Toba et al. (2014), showed that the *WISE* colors of AGNs have been well studied and reliable. By adopting AGN *WISE*-color definition by Stern et al. (2012) on the [W1]-[W2] and [W2]-[W3] rest-frame colors of the galaxy samples, all of the galaxies are limited to have color of [3.4]-[4.6] < 0.8 (Vega mag). This is because of the AGNs are identified to have color [3.4]-[4.6] > 0.8 mag. The right panel of Figure 2.2, shows the distribution of the remaining samples on *WISE*-color plane after the AGN cuts. Using the classifications of the *WISE* infrared host galaxies, the majority of the host galaxies are located in the *WISE* color space consisting of spiral and elliptical galaxies, which identified to have colors of [W1]-[W2] ≤ 0.5 and [W2]-[W3] ≤ 4.5. Noted that, all of the samples have reliable detections in all four *WISE* bands. These AGN-tracing method (*WISE* MIR color diagram and BPT-*[NII]* line diagnostic) have cut all the AGN candidates and yielded ∼148,118 galaxies in the sample.

2.2.2 Morphology Classification

The galaxies have been morphologically classified into spiral and elliptical galaxies by following several methods. Firstly, the morphological information of the galaxy is obtained from the Galaxy Zoo catalog (Lintott et al., 2008; Lintott et al., 2011), which is the main classification method used in this study. The Galaxy Zoo is a science program that has performed a large-scale of galaxy survey to classify the objects for the entire SDSS spectroscopic sample (around 1.5 million galaxies) via direct visual inspection by almost a million of members. This method reached accuracy comparable to those derived by expert astronomers (see Lintott et al., 2008). Categorizing the galaxy morphology is based on the obvious structural features; as such the ellipticals are

identified as „smooth‟ and bulge dominance object, while spirals are disc-dominated galaxies that have bar or spiral arm structure. The samples are constrained to have debiased vote fractions (> 0.8 votes for at least 10 voters), to avoid any uncertainties in morphology classification.

Additionally, a more restricted constraint is applied in classifying the elliptical galaxies based on their surface brightness profile by using SDSS parameter known as *fracDEV*. This parameter demonstrates the fraction of the total flux contributed by the de‟Vaucouleurs component determined from *r*-band. The *fracDEV* parameter is constrained between 0 to 1, which is functionally corresponds to the Sérsic index, *n* ranging between $1 \leq n \leq 4$ (Vincent & Ryden, 2005). In order to quantify a „clean‟ and „smooth‟ elliptical galaxy samples without morphology uncertainties, the sample is limited to have *fracDEV*> 0.9 in the *r*-band. Fulfilling the morphology constraint mentioned above, the final samples contain a total of ~2,337 elliptical galaxies and ~36,103 spiral galaxies. Figure 2.3 is the redshift distribution of the elliptical, spiral and total galaxies in the sample. The spiral galaxies declining drastically across the redshift bin 0.1 to 0.2 compared to elliptical galaxies.

2.3 *WISE* Photometric Data

Data acquisition of the selected galaxies (~38,440) from the crossed-match catalog of*WISE*-SDSS is obtain via Catalog Archive Server Jobs System, also known as *CasJobs. CasJobs* is a database and online workbench for large scientific catalogs, which the data is extracted by using SQL syntax. Due to massive datasets needed for the analysis in this study, a sample data of 15 galaxies with the relevant properties and photometric data used in this study are listed in Table 2.1 (Galaxy properties), Table 2.2

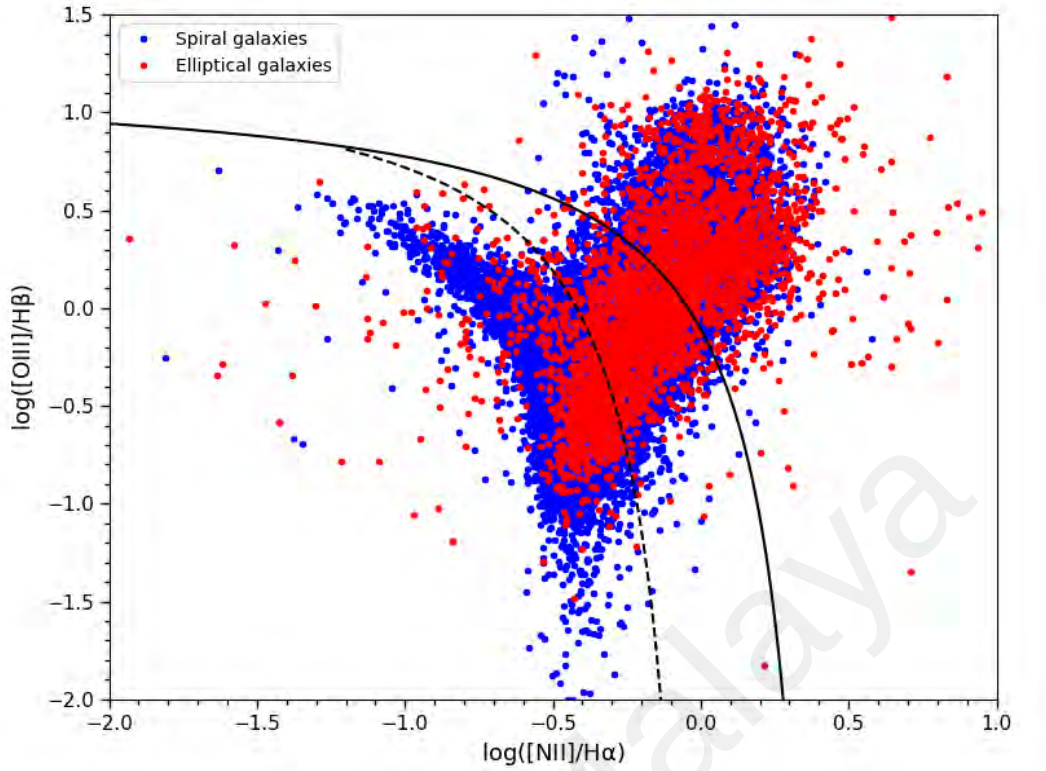

Figure 2.1: Show the BPT line diagnostic diagram of the galaxy samples at redshift $0.01 \leq z \leq 0.2$. The solid and dashed line indicates the distinguishing line for AGN sources from star forming (Kewley et al., 2001) and composite galaxies (Kauffmann et al., 2003a).

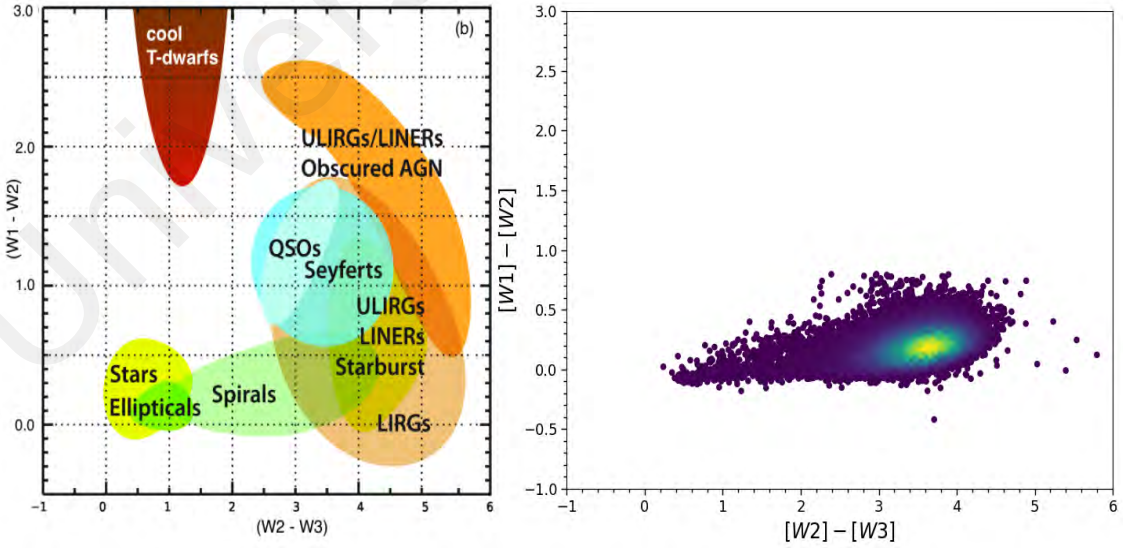

Figure 2.2: Left panel represents *WISE* color-color diagram, which is showing the classification region of various classes of galactic and extragalactic sources proposed by Jarrett et al. (2011). The right panel shows the density distribution of the data samples on the *WISE* color-color diagram, after employing the MIR color exclusion of AGN candidates defined by Stern et al. (2012).

(MIR photometry) and Table 2.3 (Optical and Emission lines photometry). *WISE* photometric calibration relies upon stars that are well characterized as K (primary) – M (secondary) giant calibrators with profile at MIR following the R-J distribution. These calibrators validate the zero magnitude system with an absolute precision of ± 1.10 %. The fluxes from these stars are measured using optimal profile (PSF) fitting. Thus, both the nature of the calibrated stars and the flux measurement method applied, both give an important implication toward photometric calibration of extended sources. The *WISE* All-Sky Data Release catalog contains detection of point-like objects (e.g., stars and unresolved galaxies) as well as resolve sources (e.g., close multiple stars and galaxies), and these objects/sources are resolved relative to *WISE* PSF in any *WISE* band. Hereby, *WISE* PSF photometry may systematically have underestimated the true brightness of extended sources as it is optimized only for point sources. Both the point-like and resolved sources can be identified through its consistency with *WISE* PSF, or the sources are previously known as extended objects that are superimposed on 2MASS Extended Source Catalog (XSC), which is indicated by the value of *WISE* extended source flag parameter (*ext_flg*). Table 2.4 explain the definition of *ext_flg* parameter, based on parameter description table of *WISE* All-Sky Data Release catalog. The magnitudes of point sources which are identified by having an *ext_flg* value = 0 are correctly measured by profile-fit photometry (*w?mpro*) and curve-of-growth corrected aperture photometry (*w?mag*). These photometry measurements also give a better estimation of the total source brightness for the unresolved sources with respect to PSF and extended/complex sources that are not associated with 2MASS Extended Source Catalog (XSC), which having the value of *ext_flg* = 1, 2, 3, and 4. Whereas, the elliptical aperture photometry measurements (*w?gmag*) is an alternative measurement for the extended, resolved and associated with 2MASS Extended Source Catalog sources (*ext_flg* = 5).

In *WISE* raw photometric measurements, the calibrated *WISE* magnitude is required to compute for the flux density of a source. The pixel value units are initially in data numbers (DN), and transformed into calibrated magnitudes by adding an instrumental zero point magnitude by, $mag_{cal} = mag_0 - 2.5l\ log_{10}\ (flux[DN])$, where mag_{cal} is the calibrated magnitude and mag_0 is the zero point magnitude. The zero point magnitude for every *WISE* band is statistically derived from the photometric measurements of the calibration stars and the predicted flux densities. For sources with constant MIR power-law spectrum ($F_v \sim v_0$), a standard zero magnitude flux density, F^0_v applied for W1, W2, W3, and W4 are 309.54, 171.79, 31.64 and 8.63 Jy, respectively in the conversion between calibrated magnitude to flux density using $F_v[\mathrm{Jy}] = F^0_v \times 10(-m_{vega}/2.5)$, where F^0_v is the standard zero magnitude flux density and m_{vega} is the *WISE* calibrated magnitude in unit of Vega magnitude. Meanwhile, the sources with a steeply rising MIR power-law spectrum or with spectrum that deviate significantly from F_v = constant, it is necessary to apply a color correction in the flux density conversion formula, $F_v[\mathrm{Jy}] = (F^{*0}_v / f_c) \times 10(-m_{vega}/2.5)$, where F^{*0}_v is the zero magnitude flux density derived for W1, W2, W3, and W4 bands are 306.68, 170.663, 29.045, and 8.284 Jy, respectively. And f_c is the color correction factor in the *WISE* bands, as described in details in *WISE* color correction table by Wright et al. (2010). However, the applied color correction applied usually appears very small ~1 % in W1, W2, and W4 bands but could be as large as ~9 % in W3 band.

Since the *WISE* photometric calibration is based on measurements of bright stars, A-K dwarfs and K/M giants, there are some discrepancies between red (typically sources with $f_v \sim v^{-2}$) and blue (stars with $f_v \sim v^2$) calibrators in W3 and W4 bands. This discrepancy is likely to be related to an error in the W4 Relative System Response (RSR), thus making the red sources appear too bright in W4 and too faint in W3. This could be resolved by requiring approximately an 8 to 10 % correction to the W4 flux.

Jarrett et al. (2011) recommend a correction to the W4 flux by a factor of 0.92 to be applied to all spiral and disk galaxies with *WISE* color of [W2 – W3] > 1.3 mag. However, for those with bulge-dominated population with WISE color of [W2 – W3] < 1.3 mag, this correction is unnecessary. The *WISE* W3 and W4 luminosities are estimated by taking the effect of redshift into consideration, where the photon energies and arrival rates are redshifted. The flux density reduced by a factor $(1 + z)^2$, thus the energy flux per unit bandwidth degraded one power of $1 + z$ and the observed photons at frequency v_0 were emitted at frequency $v_0(1 + z)$. The luminosities at 12- and 22- μm calculated by applying the following formula of flux density – luminosity relation,

$$L_v = 4D_L^2 F_v \tag{2.3}$$

where L_v is the spectral luminosity, D_L is luminosity distance and F_v is the integrated flux density of a source. The calculation of the galaxy luminosities is relative to the effective wavelength and bandwidth of the bandpass as shown in Table 2.5.

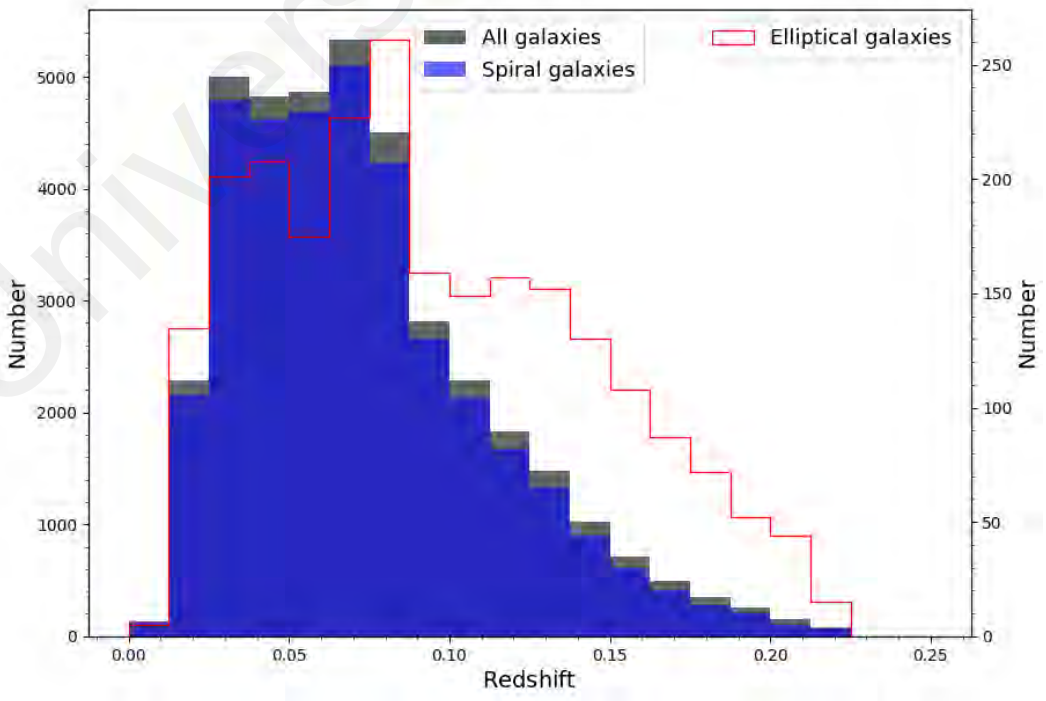

Figure 2.3: Redshift distribution of elliptical and spiral galaxy samples. The left y-axis is the scale for spiral and total galaxies, and the right y-axis is the scale for elliptical galaxies.

Table 2.1: Samples of properties of the selected galaxies.

ID	Designation	R.A.	Decl.	*z* (1)	*lumDist* (2)	*D_4000* (3)	*blend_ext_flags* (4)	*h_beta_eqw* (5)	*h_alpha_eqw* (6)
1	J095455.90-004539.9	148.73288	-0.76115921	0.08627161	329.987	1.485792	33	-1.84741	-8.237713
2	J095837.12-005546.1	149.6547	-0.92950704	0.06139873	255.57	1.946167	161	-0.3701876	-1.541347
3	J100847.83-001611.1	152.19924	-0.2698308	0.04523472	143.378	1.549541	161	-0.1802061	-3.471843
4	J101537.60+003131.1	153.90664	0.52533172	0.07067554	186.422	1.413912	33	-4.511911	-20.25242
5	J102537.42-003352.5	156.4059	-0.56463716	0.1692727	839.774	1.818063	1	-0.4866092	-1.17001
6	J102654.60-003229.3	156.72749	-0.54149707	0.03457265	141.313	1.309081	161	-2.469321	-15.57412
7	J102349.66-001513.5	155.95687	-0.25377967	0.09391025	427.081	1.640829	1	-0.3097283	-1.716329
8	J103858.45-002438.5	159.74356	-0.41071911	0.2189591	912.669	1.36794	1	-4.229593	-19.40319
9	J105654.28-002500.5	164.22617	-0.41681064	0.1085678	491.705	1.425698	33	-3.242905	-15.90502
10	J104958.87+001920.3	162.49522	0.32230856	0.03899863	76.1795	1.935942	161	-0.6635644	-0.9607223
11	J105753.64+002919.2	164.47353	0.48863994	0.06548813	315.814	1.554986	1	-2.448659	-9.786818
12	J110233.31-001727.7	165.6387	-0.29101036	0.01724125	170.957	1.665203	161	-1.890743	-4.389198
13	J111015.29-010617.9	167.56366	-1.104983	0.1090076	508.947	1.367227	1	-4.513177	-21.80468
14	J112326.98-004248.6	170.86242	-0.71357207	0.04078395	142.953	1.212951	33	-9.532088	-41.71785
15	J112146.01-002519.6	170.44164	-0.42218499	0.1308649	522.584	1.44124	1	-2.302461	-8.99471
16	J112723.46+000836.4	171.84773	0.143504	0.1347975	505.849	1.382767	1	-4.328432	-25.8096
17	J111835.82+002511.1	169.64924	0.41976742	0.02502942	100.685	1.047751	33	-12.36523	-65.11378
18	J113042.75-004902.9	172.67816	-0.81752034	0.1047876	696.346	1.351442	1	-4.165917	-17.08336
19	J112531.56+002619.1	171.38153	0.43863803	0.02592862	125.88	1.115488	33	-16.12888	-80.82957
20	J112938.57+003856.7	172.41067	0.64913156	0.1975535	963.348	1.954323	1	-0.6696309	-0.6486919

Note: Column (1) Spectroscopic redshift with *zWarning* equal to "0" from SDSS spectrograph data. Column (2) luminosity distance in Mpc. Column (3) Spectral index of 4000 Å break, follows Balogh et al. (1999) definition. Column (4) Combination of *WISE*"*ext_flg*", "*na*" and "*nb*" columns from *WISE* catalog. Column (5) and (6) are the equivalent widths of the continuum-substracted emission line computed from straight integration over the bandpasses (emission is negative) and the data obtained in Å unit.

Table 2.2: Samples of MIR photometry of the selected galaxies.

ID	*w1mpro (unc)* (1)	*w2mpro (unc)* (1)	*w3mpro (unc)* (1)	*w4mpro (unc)* (1)	*w1gmag (unc)* (2)	*w2gmag (unc)* (2)	*w3gmag (unc)* (2)	*w4gmag (unc)* (2)
1	13.057(0.025)	13.008(0.032)	9.859(0.046)	8.36(0.276)	9999(9999)	9999(9999)	9999(9999)	9999(9999)
2	11.812(0.023)	11.829(0.023)	10.591(0.084)	8.127(0.211)	11.826(0.008)	11.776(0.012)	10.908(0.093)	8.481(0.291)
3	11.608(0.023)	11.525(0.023)	8.335(0.023)	6.669(0.068)	11.506(0.006)	11.43(0.01)	8.581(0.017)	7.12(0.141)
4	11.924(0.023)	11.817(0.026)	9.008(0.04)	6.222(0.09)	12.017(0.006)	11.896(0.018)	9.603(0.046)	6.966(0.126)
5	13.86(0.029)	13.64(0.042)	11.475(0.169)	8.69(0.324)	9999(9999)	9999(9999)	9999(9999)	9999(9999)
6	11.572(0.024)	11.4(0.022)	7.508(0.017)	5.712(0.043)	11.552(0.006)	11.417(0.009)	7.972(0.016)	6.23(0.037)
7	14.112(0.03)	14.031(0.054)	12.031(0.315)	8.544(0.311)	9999(9999)	9999(9999)	9999(9999)	9999(9999)
8	14.015(0.03)	13.55(0.038)	10.522(0.073)	8.704(0.344)	9999(9999)	9999(9999)	9999(9999)	9999(9999)
9	13.228(0.026)	13.014(0.03)	9.7(0.04)	8.111(0.205)	13.332(0.01)	13.17(0.023)	10.349(0.042)	8.809(0.348)
10	11.059(0.024)	11.136(0.021)	10.246(0.058)	8.591(0.309)	10.639(0.006)	10.621(0.007)	10.017(0.084)	9.406(1.16)
11	14.611(0.034)	14.508(0.064)	11.707(0.205)	8.48(0.302)	9999(9999)	9999(9999)	9999(9999)	9999(9999)
12	12.996(0.025)	12.888(0.029)	10.867(0.108)	8.202(0.242)	12.834(0.011)	12.815(0.028)	11.086(0.12)	9.862(1.291)
13	13.11(0.024)	12.892(0.029)	9.521(0.039)	7.606(0.141)	9999(9999)	9999(9999)	9999(9999)	9999(9999)
14	12.766(0.026)	12.626(0.028)	9.137(0.031)	6.687(0.076)	9999(9999)	9999(9999)	9999(9999)	9999(9999)
15	13.471(0.025)	13.248(0.034)	10.388(0.07)	8.143(0.219)	9999(9999)	9999(9999)	9999(9999)	9999(9999)
15	13.471(0.025)	13.248(0.034)	10.388(0.07)	8.143(0.219)	9999(9999)	9999(9999)	9999(9999)	9999(9999)
16	13.6(0.026)	13.047(0.03)	9.376(0.035)	6.873(0.072)	9999(9999)	9999(9999)	9999(9999)	9999(9999)
17	12.402(0.022)	12.203(0.025)	7.964(0.018)	4.75(0.025)	12.566(0.008)	12.406(0.016)	8.729(0.012)	5.485(0.02)
18	13.669(0.026)	13.318(0.036)	10.228(0.064)	7.93(0.186)	9999(9999)	9999(9999)	9999(9999)	9999(9999)
19	13.2(0.026)	13.031(0.03)	8.985(0.03)	6.583(0.062)	9999(9999)	9999(9999)	9999(9999)	9999(9999)
20	13.94(0.028)	13.726(0.045)	11.911(0.281)	8.415(0.29)	9999(9999)	9999(9999)	9999(9999)	9999(9999)

Note: (1) Show the W1, W2, W3, and W4 magnitude measured with profile-fitting photometry, or the magnitude of the 95 % confidence brightness upper limit if the W1/W2/W3/W4 flux measurement has (SNR) < 2, in unit of Vega mag. (2) Show the W1, W2, W3, and W4 magnitude of source measured in the elliptical aperture. The value of 9999 indicate missing or no recorded values.

Table 2.3: Samples of Optical and Emission lines photometry of the galaxies.

ID	*h_beta_flux (err)* (1)	*h_alpha_flux (err)* (1)	*modelMag_u* (2)	*modelMag_g* (2)	*modelMag_r* (2)	*modelMag_i* (2)	*modelMag_z* (2)
1	64.29(4.02)	266.53(5.18)	18.424	16.840	16.024	15.586	15.275
2	22.76(8.68)	142.95(13.11)	17.682	15.620	14.680	14.218	13.873
3	52.92(7.08)	347.37(11.83)	16.751	15.118	14.388	14.002	13.715
4	398.29(7.86)	1720.13(16.23)	17.292	15.880	15.092	14.695	14.380
5	6.44(3.91)	17.92(3.4)	20.866	18.617	17.338	16.843	16.445
6	244.57(6.21)	1454.47(15.12)	16.877	15.349	14.574	14.166	13.829
7	6.94(2.31)	24.66(2.34)	20.129	18.188	17.206	16.768	16.412
8	39.26(2.18)	195.48(4.63)	19.792	18.468	17.465	16.968	16.626
9	83.75(3.41)	427.22(5.71)	18.819	17.316	16.467	16.029	15.711
10	90.55(13)	161.93(18.25)	16.400	14.429	13.538	13.099	12.765
11	24.27(1.67)	107.44(2.06)	19.848	18.117	17.310	16.892	16.605
12	79.81(5.89)	234.17(8.3)	17.746	16.148	15.403	15.032	14.727
13	120.32(4.01)	599.98(8.09)	18.746	17.333	16.500	16.037	15.704
14	497.87(6.39)	1786.37(15.36)	17.113	15.969	15.411	15.103	14.871
15	59.07(3.29)	226.2(4.49)	19.132	17.547	16.658	16.236	15.899
16	84.08(2.75)	450.08(4.69)	19.356	17.910	17.134	16.675	16.435
17	1254.6(12.96)	4352.19(30.37)	16.570	15.722	15.215	14.988	14.772
18	63.98(2.69)	296.29(4.41)	18.663	17.615	16.883	16.481	16.192
19	541.45(5.92)	2280.82(16.58)	17.407	16.484	15.999	15.746	15.544
20	9.65(4.45)	15.65(5.72)	20.838	18.626	17.292	16.749	16.379

Note: (1) 1e-17 erg/s/cm^2 are the line flux from Gaussian fit to continuum subtracted data. (2) Show the magnitude (in mag) calculated uses the better of the two fits (de Vaucouleurs and exponential model fits) in the *r*-band as a matched aperture to calculate the flux in all bands. Provides the best available SDSS colors for extended objets.

Table 2.4: *WISE* extended source flag (*ext_flg*).

ext _flg	**Definition**
0	The source shape is consistent with a point-source and the source is not associated with or superimposed on a 2MASS XSC source
1	The profile-fit photometry goodness-of-fit, *w?rchi2* , is > 3.0 in one or more bands
2	The source falls within the extrapolated isophotal footprint of a 2MASS XSC source
3	The profile-fit photometry goodness-of-fit, *w?rchi2* , is > 3.0 in one or more bands, and the source falls within the extrapolated isophotal footprint of a 2MASS XSC source
4	The source position falls within 5" of a 2MASS XSC source
5	The profile-fit photometry goodness-of-fit, *w?rchi2* , is > 3.0 in one or more bands and the source position falls within 5" of a 2MASS XSC source

Table 2.5: Effective Wavelength and Bandwidth of *WISE* Filters

Filter	**Effective wavelength (μm)**	**Bandwidth (Hz)**	**Reference**
W1	3.356 (0.0132)	1.75E+13 (3.04E+10)	Jarrett et al. (2011)
W2	4.6028 (0.0168)	1.46E+13 (1.18E+10)	Jarrett et al. (2011)
W3	11.5608 (0.0446)	1.13E+13 (8.58E+9)	Jarrett et al. (2011)
W4	22.00883 (0.1184)	2.49E+12 (4.02E+9)	Jarrett et al. (2011)

2.4 Research Process Flow Diagram

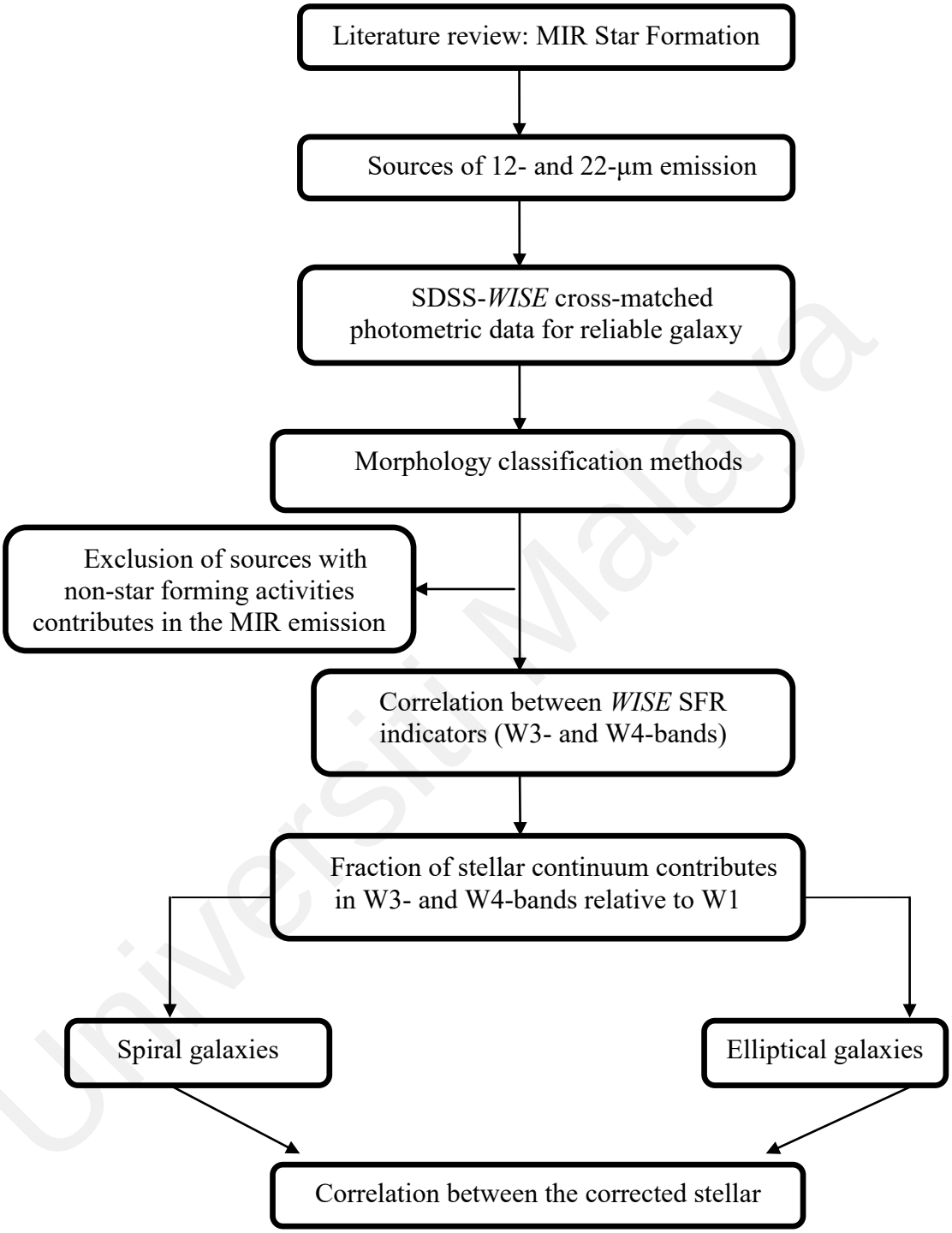

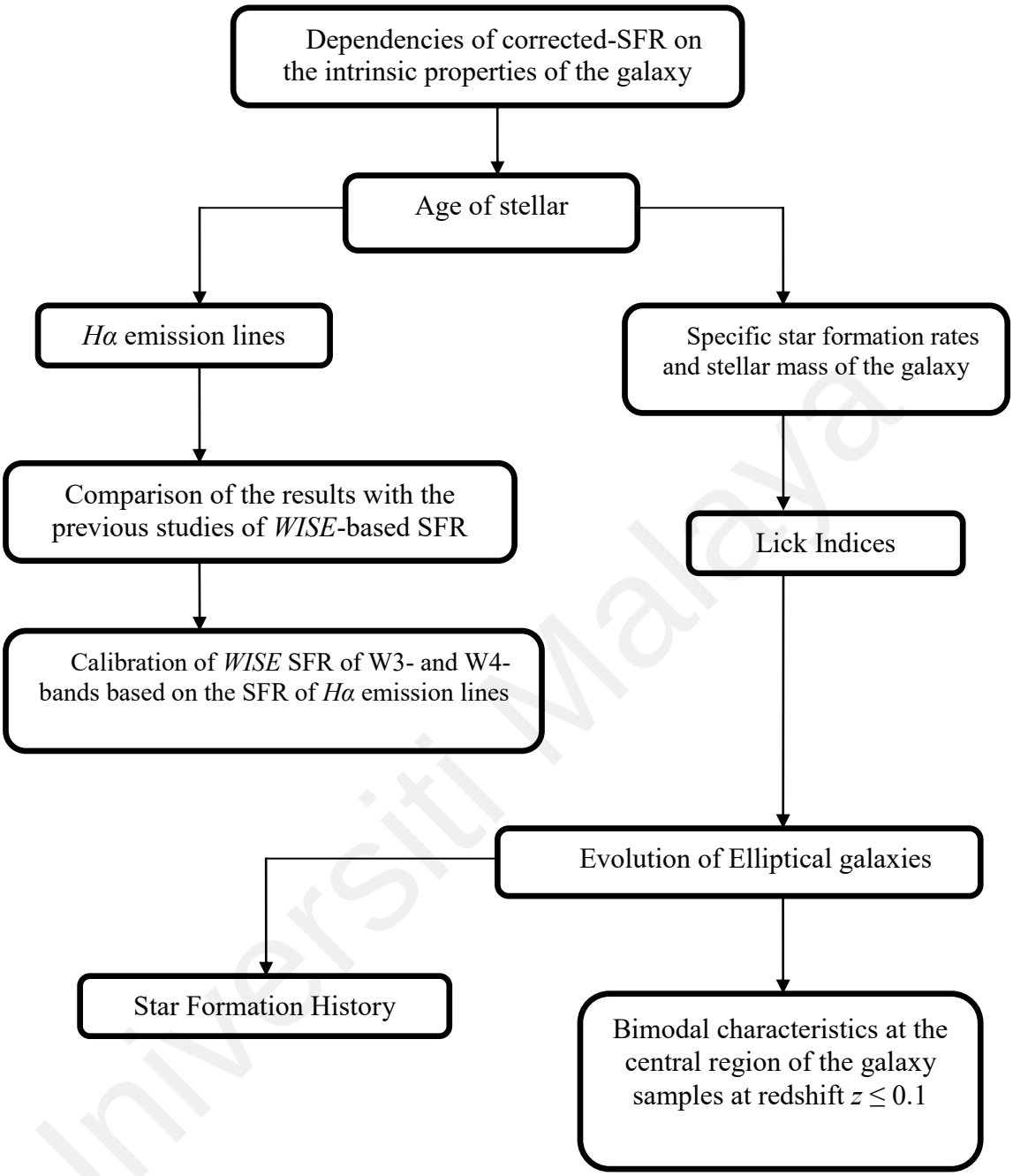

CHAPTER 3: RESULTS AND DISCUSSION

3.1 *WISE*-based Star Formation Rates

The advent of Wide-field Infrared Survey Explorer (*WISE*) have provide the whole sky mapping and also complemented with higher sensitivity with better angular resolution compare to previous IR space telescope such as Spitzer and Herschel. The sources of MIR emission described that the emissions at *WISE* W3 (12 μm) and W4 (22 μm) bands has a nontrivial relationship with the star forming activities in the galaxy. *WISE* W3 band is hypothesized to be a reliable indicator of SFR as the emission mainly coming from the Polycyclic Aromatic Hydrocarbon (PAH) features at 6.2, 7.7, 8.6, 11.2, and 12.7 μm, the deep silicate absorption feature at about 9.7 μm. For the *WISE* W4 band, the star formation activity is directly traced from the warm dust emission associated with massive star formation. The emission from these bands are also showed purely dominated by very small grains (VSGs), which always peak inside the HII regions and hence closely correlated to active star formation (e.g., Leger & Puget, 1984; Allamandola et al., 1985; Draine & Anderson, 1985; Boulanger & Perault, 1988). The MIR emission from these *WISE* W3 and W4 bands are considered to be good tracers to estimate the global star formation of the galaxy. A consistent correlation between these two SFR indicators showed that the emission is attributed exclusively from the star forming regions in the galaxy. The relationship between the *WISE* SFR indicators of W3 and W4 are examined in the study by adopting the empirical relations proposed from Lee et al. (2013),

$$SFR_{W3}(M_{\odot}yr^{-1}) = 9.54 \times 10^{-10} L_{W3}^{1.03}(L_{\odot}) \quad (3.1)$$

$$SFR_{W4}(M_{\odot}yr^{-1}) = 4.25 \times 10^{-9} L_{W4}^{0.96}(L_{\odot}) \quad (3.2)$$

where SFR_{W3} and SFR_{W4} are the SFR of a galaxy derived from the luminosity at W3 and W4 bands, respectively. All fluxes used in this study are the rest-frame fluxes, which have been corrected for the redshift effect by adopting the rest-frame SED model and by performed the k-correction methods by Hogg (1999).

3.2 Another Contributor for MIR Emission

In MIR spectrum, the thermal emission from dust claimed to be originated from the pure star formation in the galaxy. However, the emission could also be the results of dust-heated from active galactic nuclei (AGNs; Netzer et al., 2007; Mullaney et al., 2011), Asymptotic Giant Branch (AGB) circumstellar dust (e.g., Bressan et al., 1997; Piovanet al., 2003) and old stellar populations (e.g., Walterbos & Schwering, 1987; Bendo et al., 2010; Boquien et al., 2016; Davies et al., 2016; Leja et al., 2017). The activities of the active galactic nuclei (AGN) in the galaxy could also potentially give an impact on MIR SFRs. The near- and mid-IR emission of AGNs, arise from hot and warm dust heated by nuclear emission (e.g., Polletta et al., 2000; Shi et al., 2005; Hines et al., 2006; Jiang et al., 2006). Several authors have claimed that the obscured AGNs could contribute a substantial fraction that can reach up to 50 % of the infrared background (Almaini et al., 1999; Fabian & Iwasawa, 1999). About 80 MIR spectra of luminous and ultraluminous infrared galaxies have been analyzed by Tran et al. (2001), have found that the average contributions of star formation to the infrared luminosity are 82 - 94% for low-luminosity sources (LIR < $10^{12.4}$ $L_{\odot}$) and 44 – 55 % for high luminosity sources (LIR ≥ $10^{12.4}$ $L_{\odot}$). For proper measurements of the star forming activities in the galaxy, all the galaxy samples with AGN signs that visible in optical lines ratio and MIR are strictly need to be removed from the galaxy samples.

LINERS and AGNs are eliminated from the SFR indicator calibration as their *Hα* emission is not the result of the star formation. Thus, optical BPT diagnostic diagram is very useful to differentiate between star forming galaxies, composite and AGNs. This BPT diagnostic identified the classes of the galaxies based on the basis of their spectral emission lines *[OIII]λ*5007/*Hβ* and *[NII]λ*6583/*Hα* flux ratios. The sources were categorized according to the boundaries defined by Kewley et al. (2001) and Kauffmann et al. (2003a), where those located above the Kewley et al. (2001) delineation are classified as pure Seyfert 2. While, those lie in between these curves of demarcations are classified as composites and for those lies below Kauffmann et al. (2003a) curve are classified as pure star forming galaxies. There are ∼15,000 AGNs from the primary samples based on the applied BPT-diagram designation. To validate a negligible AGN contamination, the AGNs are also considered to be identified by using the *WISE* MIR color criterion of Stern et al. (2005). This method restricted to include the sample only and with *WISE* color [3.4]-[4.6] < 0.8 mag. Consequently, this restriction has removed the obscured AGNs for a more reliable galaxy sample coincides with the objective of this research. Both of these AGN-tracer methods have been utilized in this study, as mentioned in Section 2.2.1.

Besides that, the excess flux associated to circumstellar dust has showed that it can be observed in the MIR spectrum (beyond ∼10 μm) of Asymptotic Giant Branch (AGB) stars. As this subject has been identified in a number of studies (e.g., Bressan et al., 1997; Athey et al., 2002; Martini et al., 2013). This emission is more significant in early-type galaxies, which have much less interstellar dust compared to the active star forming galaxies. In the diffuse interstellar medium (ISM), the circumstellar dust emission have been often dwarfed by the emission from dust. Thus, the inference made only from the integrated *WISE* photometry is not reliable for those with low specific star formation rates (SSFR) as the contribution of circumstellar dust at 12- and 22- μm will

mimic an SSFR of 2×10^{-12} yr^{-1} (Simonian & Martini, 2016). However, the effect of circumstellar dust for larger sSFR values is still necessary to be subtracted out. The relations derived by Simonian & Martini (2016) are used in this work to quantify the circumstellar dust effect and subtracted out for better estimation on galaxy SFR. The adopted equations by Simonian & Martini (2016) shown as follows,

$$\log \nu L_{W3} = 1.03 \log L_{W1} + 30.58 \quad (3.3)$$

$$\log \nu L_{W4} = 0.97 \log L_{W1} + 30.72 \quad (3.4)$$

where L_{W1} is the "in-band" luminosity in solar luminosities, and νL_ν is the spectral luminosity of the band in erg s^{-1} . The fraction of AGB circumstellar dust in MIR spectrum of the galaxy samples could contributes with an average fraction of ~8.47 × 10^{-2} and ~1.103 × 10^{-1} at 12- and 22- μm, respectively in spiral galaxies. Meanwhile, the contribution of circumstellar dust is quite higher in elliptical galaxies, with average of AGB dust contribution ~0.45 and ~0.32 at 12- and 22- μm. The correction applied on local star forming galaxies with sSFR ~10−10 yr^{-1} are seems negligible. This shows a consistent agreement with previous work, where the MIR emission of AGB-dust is significant from galaxies that contain relatively little diffuse dust, including low-metallicity and/or non-star forming galaxies (Villaume et al., 2015; Davis et al., 2014; Cluver et al., 2014). Besides, this effect is at maximum for the intermediate age of galaxy (~0.1 to 3 Gyr) and also when at minimum presence of diffuses dust.

3.3 Stellar Contribution at 12- and 22- μm

3.3.1 Derivation Formula of Stellar Contribution

Villaume et al. (2015) claimed that flux at the short wavelength in IR spectrum (W1 and W2 bands) is largely dominated by the stellar continuum and not sensitive to dust. Compare to the optical bands, near-IR is significantly less suffered from the obscuring

dust and gas; the *V*-band suffering from the extinction about 15 times larger than that in the 3.4 μm band assuming a Milky Way-like extinction law (Schlafly & Finkbeiner, 2011; Yuan et al., 2013). Additionally, the metallicity dependence in the near-IR decreases dramatically relative to that seen in the optical (e.g., Norris et al., 2014, 2016). This insensitivity towards the age and metallicity has particularly useful implication for the study on the stellar emission of massive galaxies. Herein, *WISE* W1 band in the integrated galaxy spectrum is considered fully contributed from the spectrum of stellar population in the galaxy. Thus, W1 band is a good indicator that can be utilized to properly scale the fraction of stellar continuum that still remains in MIR wavelengths at W3 and W4 bands (Helou et al., 2004; Wu et al., 2005). A template of elliptical galaxy spectrum is selected to determine the contribution of stellar continuum in the galaxy samples. This selection is correlated to the fact that most of elliptical galaxy is a dust-poor galaxy (negligible in W1 band) and dominated by old stellar population, which is not associated to the current star formation. This study makes use the spectral energy distribution (SED) of NGC 5018, which is an elliptical galaxy located in Virgo constellation at redshift $z\sim0.009413$ as a SED template. The stellar population in NGC 5018 is consisting of old population (Bertola et al., 1993). This galaxy is also having trivial existence of optical emission lines, where it experienced a negligible ongoing star formation and nuclear activities (not an AGN-host galaxy) in the galaxy.

From the *WISE* signal formula by Wright et al. (2010), the stellar contribution at W3 and W4 bands is computed by using the rest-frame SED of NGC 5018 with the assumption that flux density at W1 band is dust-free. The stellar contribution at *WISE* W3 and W4 bands relative to W1 band (hereafter denoted as η_{w3} and η_{w4}) estimated as follows,

$$\eta_i = \frac{\int R(i)\lambda F_\lambda(i)d\lambda}{\int R(W1)\lambda F_\lambda(W1)d\lambda}, where\ i = \mathrm{W3}\ and\ \mathrm{W4} \quad (3.5)$$

R(i) is the *WISE* QE-based Relative Spectral Response and λF_λ represents the integrated flux density at W3 or W4 bands. From the calculation, the average fraction of stellar contributes in W3 and W4 bands are η_{w3} = 0.125 and η_{w4} = 0.0107 with a very small scatter less than 0.01 for $z \leq 0.2$. The average value obtained for η_{w3} prominently higher than η_{w4}, which is well-correspond to the fact that the W3 band is the widest *WISE* bandpass and also closer to the NIR wavelength (is where the stellar continuum decreases along the spectrum). This value obtained is comparable to the one obtained in previous studies of Jarrett et al. (2012, hereafter called as J12) and Lee et al. (2013, hereafter called as L13). They have showed that the estimation values of stellar continuum contributed at W3 bands are ~0.15 and ~0.1 for J12 and L13, respectively. In the literature for a well-studied IR data from Spitzer, they scaled the stellar continuum at 3.6 μm to that at 8 μm, and obtained a factor of 0.26 and 0.232 claimed by Helou et al. (2004) and Wu et al. (2005). This thus convinced the contribution of stellar continuum is increasing at shorter wavelength.

3.3.2 Stellar Contribution Corrected-SFR

Generally, contribution of stellar continuum is very important in NIR and MIR studies as it may give significant impact on the SFR of the galaxies. To prevail over the contribution of stellar continuum in *WISE* W3 and W4 SFR indicators, the stellar contribution factors at W3 and W4 are then used to calculate for the stellar-continuum corrected SFR. The stellar correction factors estimated in this study is used to directly subtract the stellar continuum from the estimated flux densities of the galaxy samples. The corrected flux densities from the stellar emission calculated as below,

$$f_v(i_{corr}) = f_v(i) - \eta_i f_v(W1),\ where\ i = W3\ and\ W4 \quad (3.6)$$

where η_i is the stellar contribution parameters and f_v is the flux density. This correction has been performed on both spiral and elliptical galaxy samples. The spiral galaxies give an average contribution of stellar continuum is ~3.69 % at W3 and ~0.19 % at W4 band. Meanwhile, elliptical galaxies have showed an average contribution of ~13.94 % at W3 and ~0.7 % at W4 band. The contribution of stellar continuum is clearly higher in ellipticals compare to spirals due to the high fraction of dust emission and lacking of old stars in most of the spiral galaxies. However, the most extreme case for the non-star forming elliptical galaxy in this study has show that the contribution can reached as high as 89.5 % at W3 and 10 % at W4 band. In this situation, the W3 emission is not suitable to estimate the star formation in this galaxy. The SFR of both spiral and elliptical galaxies have been quantified at W3 and W4 bands by adopting the SFR formula from Lee et al. (2013), and indicated as SFR_{W3} and SFR_{W4} hereafter. Meanwhile, for the corrected stellar contribution SFR, are indicated as $SFR_{W3(corr)}$ and $SFR_{W4(corr)}$. To study the impact on the correlation between these SFR indicators, before and after the reduction of stellar emission on the galaxy samples, has been illustrated in Figure 3.1. This Figure 3.1 shows the comparison between the uncorrected (top) and corrected (bottom) stellar contribution SFR of *WISE* W4- versus W3-band. The left panel represent the correlation of *WISE* SFRs in spiral galaxies and on the right panel represent for the elliptical galaxies. The color-coded indicates the redshift bins covering $0.01 \leq z \leq 0.2$ and the black solid line is the one-to-one relation. The residual plot showed at the bottom of every panel. First and foremost, all the plots in Figure 3.1 give a good correlation between *WISE* SFR indicators with a slight offset towards W3. This pattern can be observed clearly where most of the data lie just below the one-to-one relation. The SFR derived from W3 consistently give a bigger value compared to the SFR derived from W4 band. This overestimation can possibly caused by the higher contribution of stellar continuum in W3 band compare to that in W4. However, the

offset apparently still remain even after the reduction of stellar continuum (showed in bottom panels). This matter probably suggesting that the offset is originated from the 11.3 μm PAH emission, which is a prominent feature in W3 band that reflects the recent star forming activities (e.g., Jarrett et al., 2012; Shipley et al., 2016; Kokusho et al., 2017). Thus, this have caused the calibration done by Lee et al. (2013) might suffer from the metallicity bias, where the metal-poor galaxies show much lower SFR compared to SFR of *Hα*.

Statistically, the average residual scattering for both spirals and ellipticals at the top panels give the same amount of ~0.45 dex. Nevertheless, a slightly tight correlation is showed between the corrected stellar contributions SFRs for both spiral and elliptical galaxies with the average scattering of ~0.43 and ~0.41 dex, respectively. There are very slight changes in the offset and the slope of the SFRs relation for spiral galaxies after the stellar correction has been applied. This clarify that the stellar contribution is less important in spiral galaxies at least for those at redshift smaller than 0.2. On the contrary, elliptical galaxies experienced significant changes, which give a better correlation between the *WISE* SFRs after the subtraction of stellar continuum. The slope of $SFR_{W4(corr)}$ - $SFR_{W3(corr)}$ has changed from $m = 0.92$ to $m = 0.8$. This is substantially caused by the elliptical population that is located at redshift $z \leq 0.1$, which is the population that mostly affected by the stellar correction (~63.5 % of the total elliptical galaxies in the sample in this redshift bin). Besides that, the scattering for the corrected SFR relation drops to 0.41 dex, and makes the SFR relations diverged towards one-to-one relation. Distinguished by the redshift bins, the elliptical galaxy samples at lower redshift bin $z \leq 0.1$ exhibit bigger statistical changes of RMSE from 0.44 to 0.38 dex. Whilst, for those lie within redshift bin $0.1 \leq z \leq 0.2$, experienced minor decreasing in RMSE from 0.47 to 0.46 dex. The physical parameters of the affected elliptical galaxies have been examined and discussed in the following section.

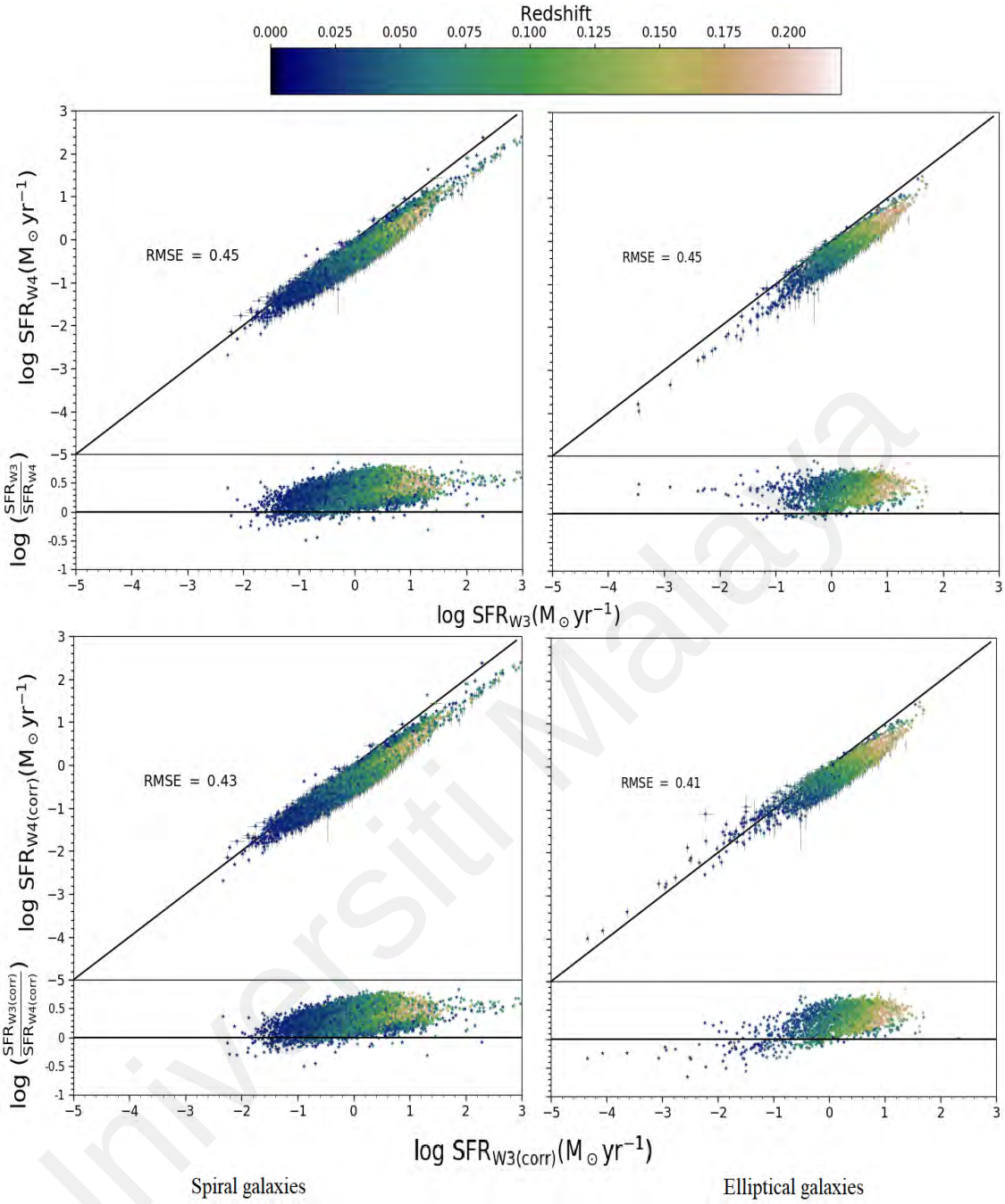

Figure 3.1: Top: Comparison between W3-based SFR and W4-based SFR for spiral (left) and elliptical (right) galaxies. Bottom: Comparison between the corrected stellar contribution of SFR_{W3} and SFR_{W4} for spiral (left) and elliptical (right) galaxies. The solid lines indicate the one-to-one relation. The color-coded shows the spectroscopic redshift of the galaxies. The error bars represent the 1σ uncertainties of the sample.

3.4 Comparisons with Literature

3.4.1 Stellar Population Age

The intrinsic properties of these elliptical galaxies are further probed, to observe their dependency towards the stellar continuum correction. The age of stellar population in the galaxies is one of the important properties that can be investigated from the spectral feature, which able to reveal the presence of stars with different ages in the galaxy. Zaritsky et al. (1995) and Kauffmann et al. (2003) have showed that the mean age of the stellar population can be determined from the strength of 4000 Å break, or hereafter called as D_n4000 spectral index. The D_n4000 spectral index is defined as the ratio of the average flux density between 4050 - 4250 Å and 3750 - 3950 Å (Bruzual et al., 1983). There are the presence of the absorption metallic lines within these wavelength ranges and a large number of overlapping lines in a narrow wavelength region. These features resulting an observable discontinuity in the optical spectrum of a galaxy. The main contribution to the opacity comes from the ionized metals in the atmosphere of old cool stars, which produce the absorption lines. In the galaxy that consists of cool stars and lack of hot blue star, the opacity increases and the D_n4000 index will be large. Thus, for the galaxy dominated by the hot blue stars will have a smaller D_n4000 index. Balogh et al. (1999) have introduced the 4000 Å break ratio by using narrower continuum bands that are between 3850 - 3950 Å and 4000 - 4100 Å. The benefit of this idea can give the index with considerably less sensitive towards reddening effects. This study has adopted the index derived from SDSS MPA-JHU spectroscopic catalog using the narrow definition measured following Balogh et al. (1999) method. The distribution of D_n4000 index in the galaxy samples of this study covered a wide range between $0 < D_n4000 \leq 2.38$ for both galaxy morphologies within redshift $0.01 \leq z \leq 2.0$, as shown in Figure 3.2. The plot shows a typical property between the observed spiral and elliptical galaxies (e.g., Kauffmann et al., 2003a; Padmanabhan et al., 2004), where the average

D_n4000 index for the selected spirals (~1.35; blue histogram) is smaller than the average of selected ellipticals (~1.57; red-lined histogram).

The relationship between the stellar age and the *WISE* SFRs is illustrated in the Figure 3.3. The color-scale represents the D_n4000 spectral index of the galaxy. While, the dashed line is the separator between the high (SFR > 1 $M_\odot$ yr^{-1}) and low (SFR ≤ 1 $M_\odot yr^{-1}$) star forming galaxy. For the purpose of this study, the elliptical galaxies is categorized into two subclasses; where the first one is the elliptical galaxies with young stellar age (D_n4000 < 1.5; left panel) and the other one is the elliptical galaxies with old stellar age (D_n4000 ≥ 1.5; right panel). Noted that the relation of SFRs for the galaxy with young stellar age gives small changes of RMSE value from ~0.45 to ~0.43 dex after the stellar contribution correction has been applied. The inconspicuous impact of stellar contribution within these galaxies quiet similar to the spiral galaxy population showed earlier. Meanwhile, the galaxy with older stellar population demonstrates a better correlation between the corrected *WISE* SFR of W3 and W4. The offset of $SFR_{W4(corr)}$ -$SFR_{W3(corr)}$ relations significantly decreasing from ~0.42 to ~0.33 dex and thus, deviates toward the one-to-one relation. Additionally, the galaxies that particularly lie below the dashed line experienced an obvious change in their corrected SFRs. This indicates that stellar continuum have a higher significance that contributes in the elliptical galaxy population, which dominated by old stellar population with low star forming activities.

In order to verify this argument, the comparisons have been done with the previous studies of *WISE*-based SFRs done by Jarrett et al. (2012) and Chang et al. (2015, hereafter known as C15). From Figure 3.4, the relationships between *WISE*-based SFR of W3 and W4 (top panels) of the samples are determined by using the conversion factors proposed by C15 (left) and J12 (right). The bottom panels show the relationship

of the *WISE*-based SFRs that have been subtracted for the stellar continuum with respect to their above panels. Here on, we focus more on investigating the old age elliptical galaxies. Both of the relations derived from J12 and C15 give a better correlation after applying the stellar correction factors at W3 and W4 bands. In C15 case, the RMS relative to one-to-one relation changed from ~0.42 to ~0.35 dex, meanwhile for J12, the RMS reduces from ~0.34 to ~0.29 dex. Both results from these studies have showed an excellent consistency to the previous result obtained in Figure 3.3, which adopted the SFR formulas from L13.

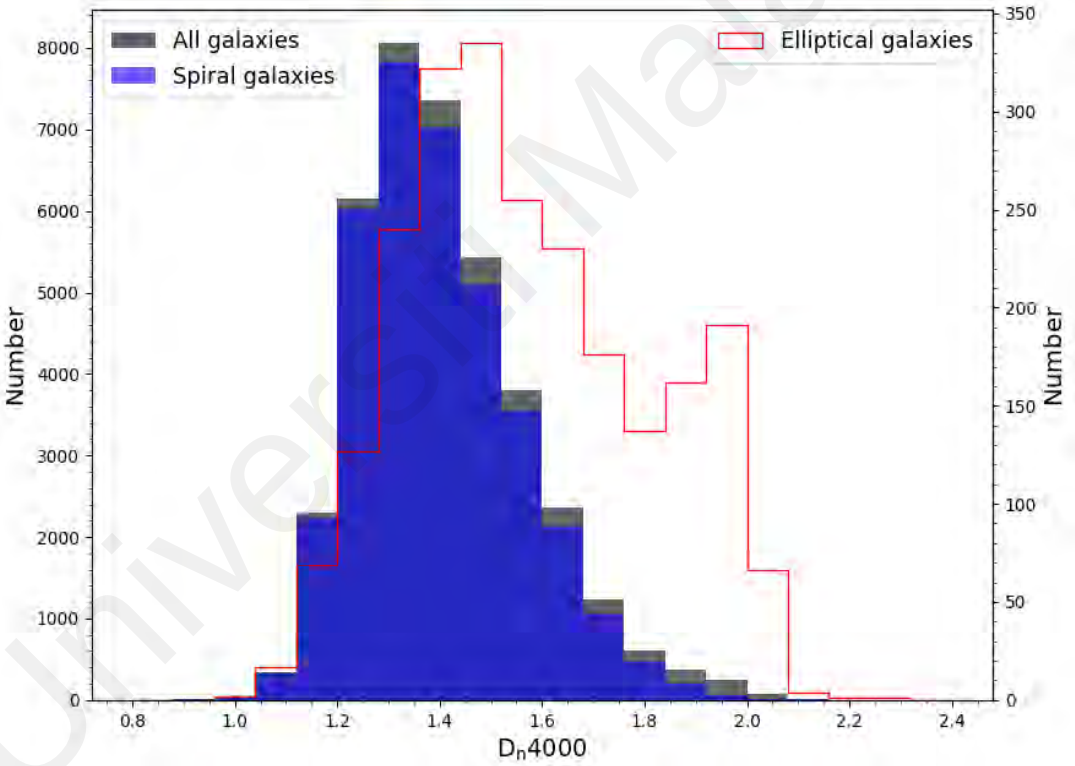

Figure 3.2: Distribution of D_n4000 index (follow the definition by Balogh et al., 1999) of the galaxy samples within redshift $0.01 \leq z \leq 2.0$.

The calibrations of SFR done by J12, L13, and C15 were performed using different methods and based on various sample properties; as such, the galaxy sample sizes, morphologies, redshifts, and also the range of SFRs. The L13 done the SFR derivation is basically facilitated by ~105,753 of star forming galaxies that located at redshift range of $0.01 < z < 0.3$. This big survey of galaxies gives the samples a wide range of SFRs, which is between 0.1 $M_{\odot}\mathrm{yr}^{-1}$ to 100 $M_{\odot}\mathrm{yr}^{-1}$. Meanwhile, the work of J12 was based on 17 well-resolved, nearby galaxies (< 60 Mpc) with small SFRs range between 0.03 $M_{\odot}\mathrm{yr}^{-1}$ and 4 $M_{\odot}\mathrm{yr}^{-1}$. Besides of using a small number of the galaxies, the author considered the samples that consist of diverse morphologies (3 bulge-dominated ellipticals, 13 disk and barred spirals, and 1 barred irregulars). The empirical calibrations have also been investigated by C15 by using ~858,365 of star forming galaxies with wider SFRs range between 0.01 $M_{\odot}\mathrm{yr}^{-1}$ to 100 $M_{\odot}\mathrm{yr}^{-1}$ in *WISE* W3 and W4 bands. The technique applied in the calibration also attributes to systematic differences, where the calibration carried out by J12, have used the SFRs of GALEX UV fluxes and the standard Spitzer/MIPS 24 μm adopted from Rieke et al. (2009). On the other hand, the conversions done by L13 are based on the SFRs estimated from Brinchmann et al. (2004). All these studies of *WISE*-based SFRs done by J12, L13, and C15 are strongly require the stellar continuum correction to be utilized in their derived SFR formulas in order to determine the SFR of old stellar population galaxy. Although these SFR empirical formulas calibrated from previous studies performed using different approaches, the result still highlight the importance of stellar continuum in MIR emission. This also emphasized that, an extra caution is needed in the calibration of SFRs when using *WISE* 12- and 22- μm emission. We further observed into the galaxy Balmer emission lines properties in the next section.

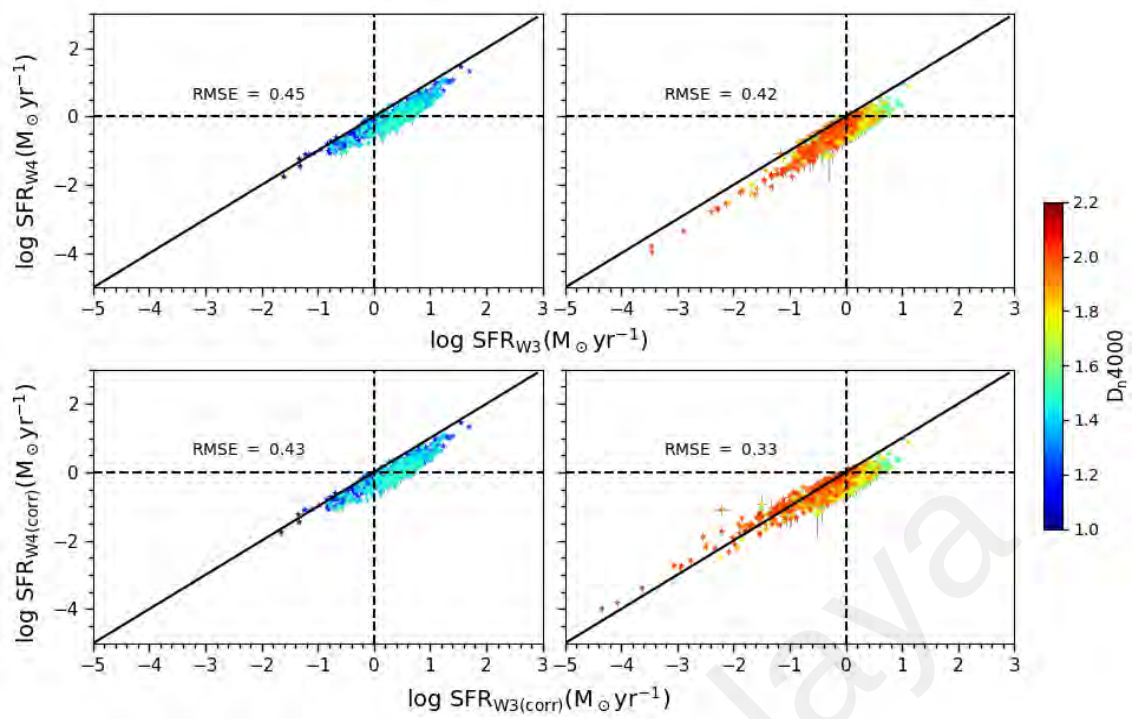

Figure 3.3: Comparison between the uncorrected (top) and corrected (bottom) stellar contribution of SFR_{W4}-SFR_{W3} relation for elliptical galaxies with young stellar population (left panel; $D_n4000 < 1.5$) and old stellar population (right panel; $D_n4000 \geq 1.5$). The color-coded show the D_n4000 indices, the solid line indicates one-to-one relation and the dashed line is the separator between high and low star forming galaxies. The error bars represent the 1σ uncertainties.

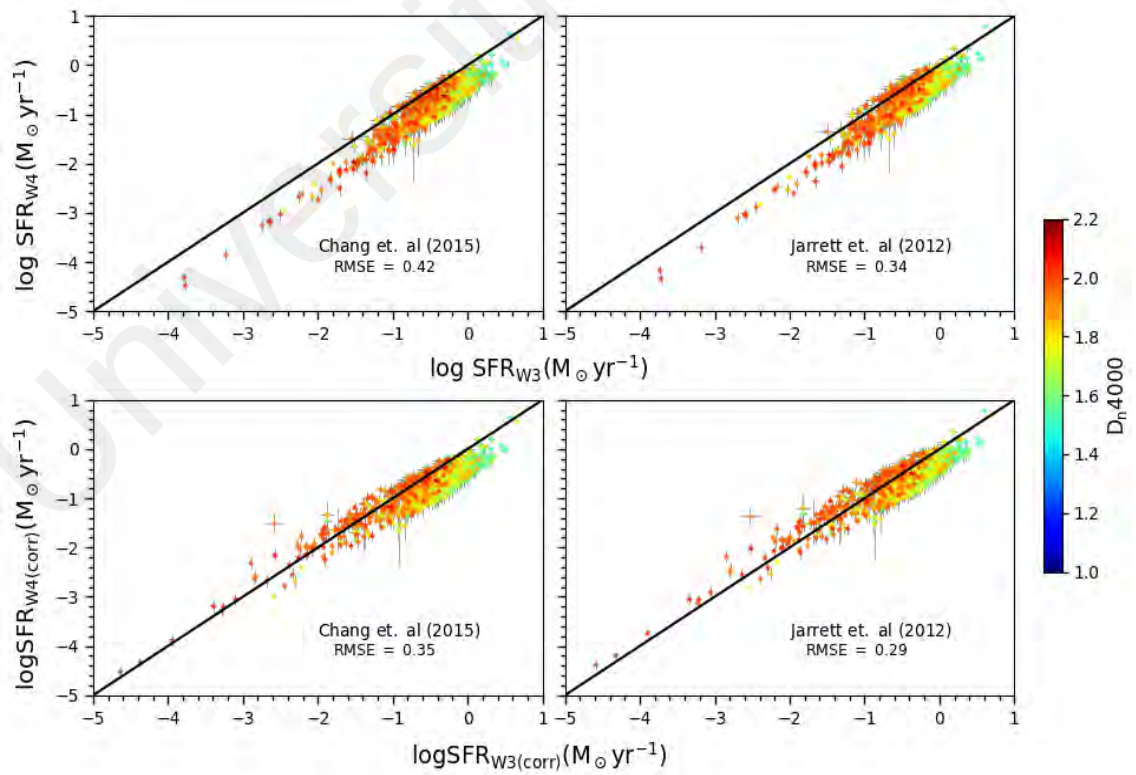

Figure 3.4: Comparison between the uncorrected (top) and corrected (bottom) stellar contribution of SFR_{W4}-SFR_{W3} relations derived by Chang et al. (2015, left panels) and Jarrett et al. (2012, right panels). The solid and dashed lines represent the one-to-one relation and the separator between the high (SFR ≥ 1 $M_\odot yr^{-1}$) and the low (SFR ≤ 1 $M_\odot yr^{-1}$) star forming galaxies, respectively. The error bars represent the 1σ uncertainties for the sample.

3.4.2 SFR of *Hα* emission as SFR Reference Indicators

In star forming galaxies, *Hα* photons were arises from the recombination of gas ionized by young hot stars. Recently, SFR inferred from the *Hα* emission is widely used, due to the good capability to measure directly the current SFR in the galaxies regardless of the reddening effect. Thus, in this study, the *Hα* luminosity of the galaxy was adopted to be the reference SFR indicator in the calibration of *WISE*-based SFR. The consistency between the SFRs derived from *Hα* emission lines and the corrected *WISE* SFR of W3 and W4, were also evaluated in this section. The estimation of *Hα*-based SFR (hereafter $SFR_{H\alpha}$) is probed by using the calibration given by Kennicutt Jr (1998),

$$SFR_{H\alpha}(M_{\odot}yr^{-1}) = \frac{L_{H\alpha}}{1.27 \times 10^{34}\ W} \tag{3.7}$$

where $L_{H\alpha}$ is the luminosity of *Hα* lines. In order to obtain the global SFR of the SDSS galaxies, the measured *Hα* flux from the fiber spectrum was converted into the one that covered the entire galaxy. It is an important correction to be done to reduce the aperture bias in every galaxy due to the limited emission detected through the SDSS 3" aperture fiber. The aperture correction was applied follows the method proposed by Hopkins et al. (2003, hereafter H03). This approach applied the aperture correction factor defined as,

$$A = 10^{-0.4}(m_{total} - m_{fiber}) \tag{3.8}$$

where m_{total} is the total galaxy magnitude derived from *r*-band Petrosian magnitude and m_{fiber} is the *r*-band fiber magnitude. Both of the magnitudes were derived from the *r*-band because of a less scatter distribution compare to other optical bands. The H03 method assume that the measured emission through the fiber is representing the flux from entire galaxy, which might be a caveat as the aperture correction may be biased

due to the divergences in galaxy properties. Ensuring a reliable $SFR_{H\alpha}$ with deficiently affected to dust reddening, the luminosity of $H\alpha$ emission of the samples is corrected for the foreground galactic extinction using the extinction law of $R_v = 3.1$ as discussed by O'Donnell (1994) and Schlegel et al. (1998). The obscuration correction is another crucial correction that necessary to be applied on $H\alpha$ flux functioning as the internal dust obscuration corrector. It was derived by using the corrected stellar absorption of Balmer decrement and the Milky Way obscuration curve with $R_v = 4.05$ (Cardelli et al., 1989; Calzetti, 2001). The corrected Balmer decrement of stellar absorption defined as $S_{H\alpha} / S_{H\beta}$, and S is calculated from,

$$S = \frac{EW + EW_c}{EW} F \tag{3.9}$$

where S is the corrected stellar absorption line flux, EW is the equivalent width of the line, EW_c is the correction for stellar absorption and F is the observed line flux. In the calculation, Case B was adopted with the normalized intrinsic Balmer decrement, $H\alpha/H\beta$ of 2.86 at T = 104 K for the low electron densities of $n_e = 10^2$ cm^{-3} (Brocklehurst, 1971; Dopita & Sutherland, 2003; Osterbrock & Ferland, 2006). The recommended correction factor referencing to H03 for stellar absorption EW is EW_c = 1.3 Å. This value is claimed to be a reasonable approximation for SDSS pipeline spectral line measurements. This correction value is then applied on the samples and the correlation between the *WISE*-based SFR and SFR of $H\alpha$ luminosity is examined. Figure 3.5 show the SFR of $H\alpha$ as the function of SFR W3-based (left) and SFR W4-based (right). The color-coded in the figure represents the mean stellar age, while the dashed line indicate the one-to-one relation. The SFR relations derived using the EW_c adopted from H03 is least-squares fitted (represent as the dash-dotted line) in the plot, and this relation exhibit offset relative from the one-to-one relations of ~0.2 and ~0.36 dex for $SFR_{H\alpha}$-SFR_{W3} and $SFR_{H\alpha}$-SFR_{W4}, respectively. To evaluate the significance of

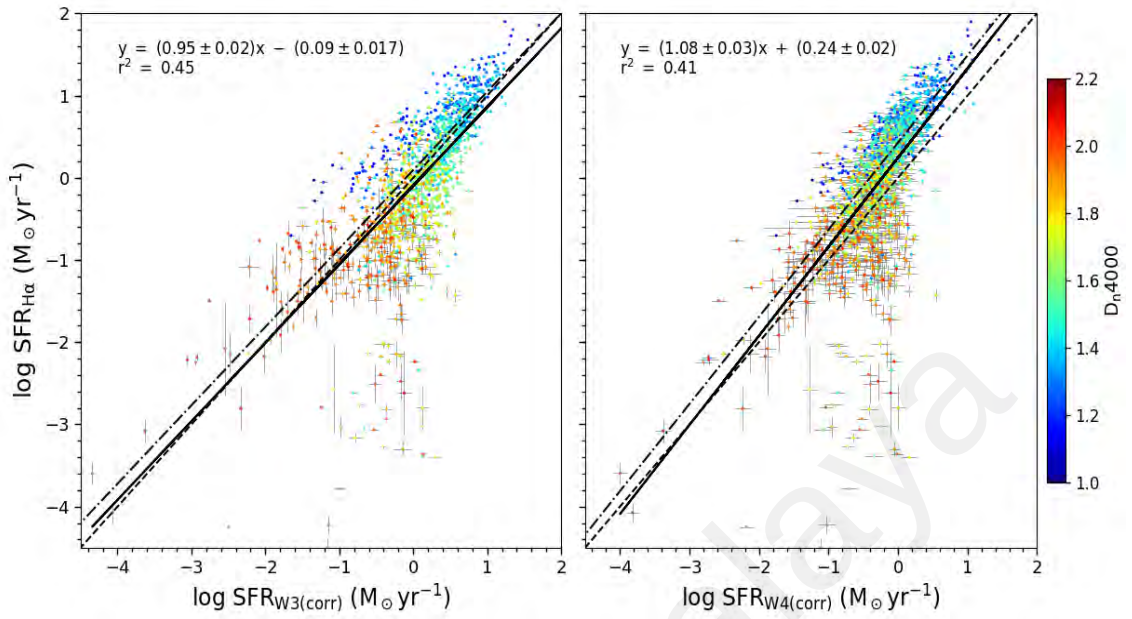

Figure 3.5: Comparison of *Hα* SFR with SFRs of W3 (left) and W4 (right). The lines in both plots indicate the least-squares fit of the data (solid line), the one-to-one relation (dashed line) and the fitted line for the SFR relations derived using the EW_c=1.3 Å (dash-dotted line). The color-coded of the diagram shows the D_n4000 spectral index. The error bars represent the 1σ uncertainties.

H03 stellar correction factor, a range of values of stellar correction *EW* also have been considered in the calculation. The range of stellar correction *EW* used is between 0.7 Å to 2 Å, proposed by several literature (e.g., Poggianti & Barbaro, 1997; Georgakakis et al., 1999; Miller & Owen, 2001; Kewley et al., 2002; Hopkins et al., 2003). However, statistically inconspicuous results were obtained compared to result calculated using stellar correction from H03. The correction *EW* applied to correct the stellar absorption of optical lines is further explored, by employed the specific values of stellar absorption of each galaxies. This stellar absorption is derived from the SDSS MPA-JHU catalog. The absorptions are derived from the spectra fitted into the templates with appropriate redshift and velocity dispersion (more detail for the stellar absorption *EW* described in Tremonti et al., 2004). The obtained correction factors are then subtracted from every galaxy individually and their relations of $SFR_{H\alpha}$-SFR_{W3} and $SFR_{H\alpha}$-SFR_{W4} are plotted in

Figure 3.5 (represented by the dots) and the least-squares fitted (represented by solid line). Noted that these relationships (correction *EW* adopted from SDSS spectra-fitted) are deviated from the one-to-one relations with a smaller scattering ~0.1 and ~0.19 dex for $SFR_{H\alpha}$-SFR_{W3} and $SFR_{H\alpha}$-SFR_{W4}. Consequently, a stronger correlation for these relationships is obtained compared to the relations derived by using the H03 correction constant, which give considerably larger offset.

Referring to Poggianti & Barbaro (1997) and Miller & Owen (2001), the strength of the 4000 Å break is showed to be corresponding to the correction of stellar absorption. Thus, the discrepancy occurred are might associated from the *Hα* and *Hβ* Balmer lines that assumed can be corrected using the same amount of stellar absorption, for all types of galaxy. This issue results in a higher value of the derived Balmer decrements. The relationship between the D_n4000 index and stellar absorption is illustrated in Figure 3.6. Since the galaxy samples span a broad range of 4000 Å break, they classified into two group based on their D_n4000 index. From Figure 3.6, the galaxies dominated with old stellar population (red) is distributed to have smaller stellar absorption *EW* of *Hα* compare to those with young population (blue), with mean values of 1.5 Å and 2.2 Å, respectively. Whereas, the mean values of *Hβ* stellar absorption for both old and young stellar population are higher compare to *Hα*, which are 2.1 Å and 2.8 Å. However, the old galaxies consistently show lower stellar absorption for both *Hα* and *Hβ* compare to population of young galaxies. Corollary of the results demonstrated in Figure 3.6, the obscuration correction for old galaxies is quantified to be much lower than the young galaxies, with an average of obscuration correction of 0.3 for the old galaxies and 1.5 for the young galaxies (shows in Figure 3.7). The huge difference in properties between these two galaxy populations, suggesting that a better obscuration correction can be derived by using the specific values of *EW* correction for stellar absorption for each

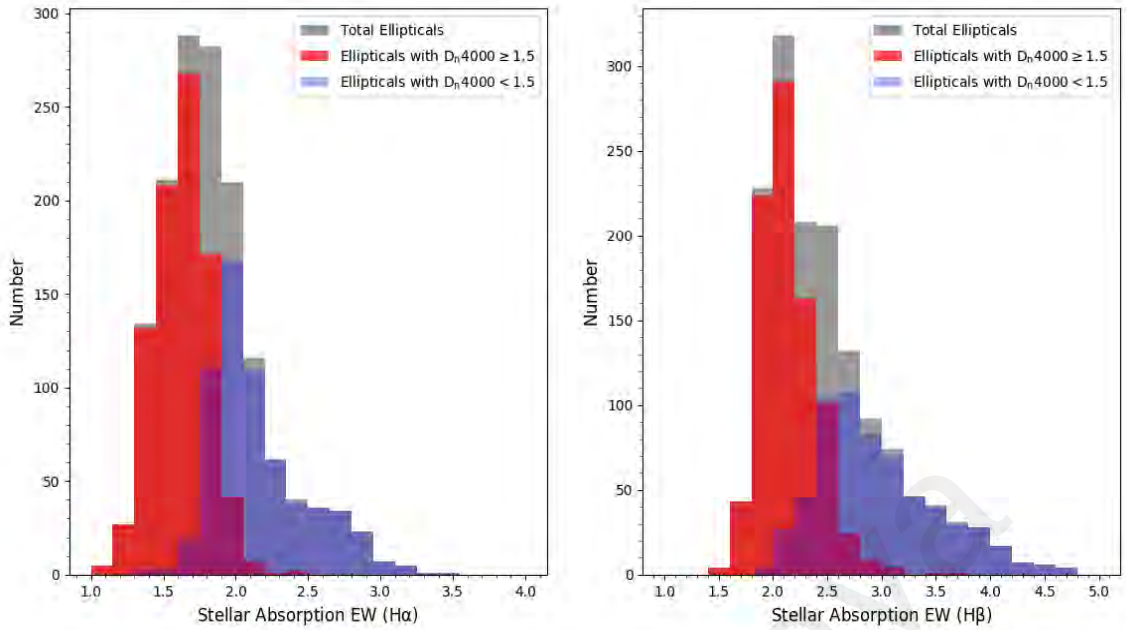

Figure 3.6: Histogram shows the distribution of stellar absorption *EW* at *Hα* (left) and *Hβ* (right) emission lines of the galaxy samples adopted from SDSS MPA-JHU catalog.

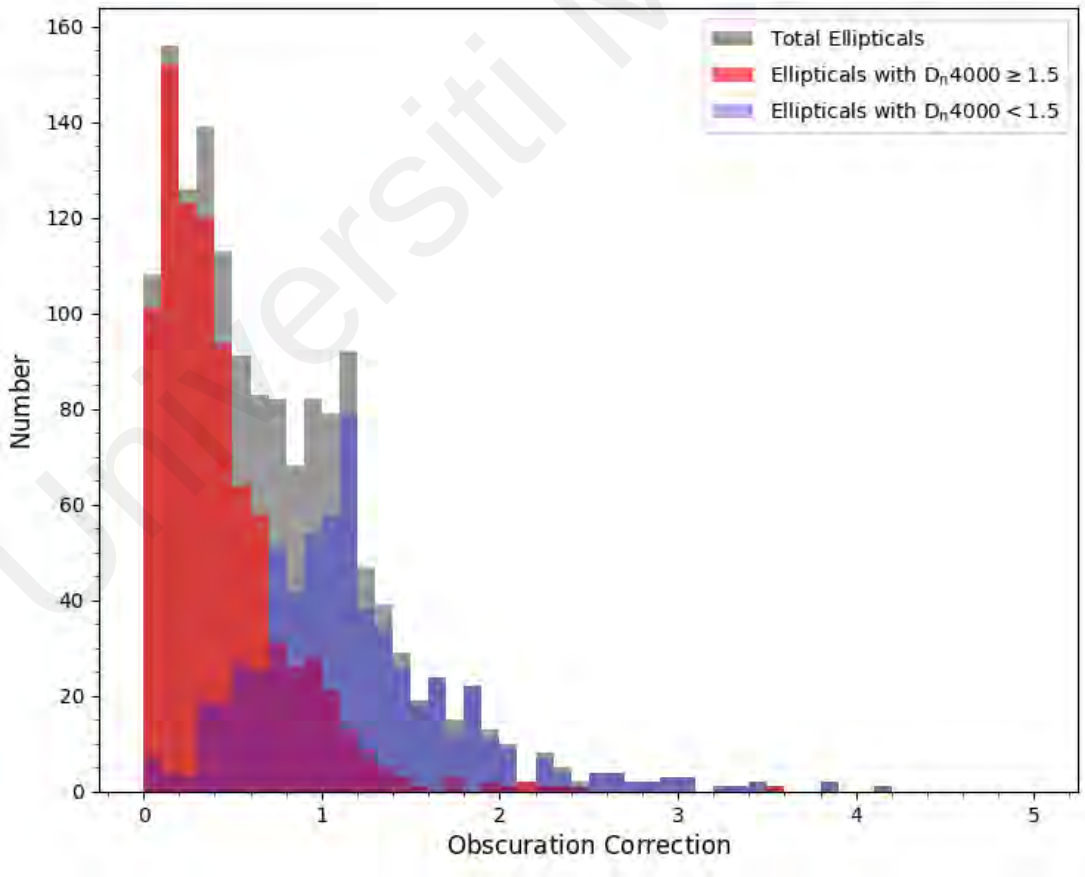

Figure 3.7: Distribution of obscuration correction to *Hα* emission line luminosities of the galaxy samples, which derived from the stellar absorption-corrected Balmer decrement and obscuration curve assumption from Cardelli et al. (1989).

galaxies, instead of using the median values for the whole groups. This is the most plausible explanation for the discrepancy when applying a standard correction factor of stellar absorption for both *Hα* and *Hβ* lines. In this study, the correction *EW* for stellar absorption is adopted individually for each galaxy from SDSS MPA-JHU catalog, instead of using 1.3 Å, which is not applicable to account for the underlying stellar absorption in galaxy samples. The result concludes that there is a strong agreement between *WISE* SFR indicators and SFR of *Hα* luminosities, which is reliable to be the reference indicator of SFR. The calibration of *WISE* W3 and W4 SFR based on the SFR of *Hα* is carried out next.

3.4.3 SFR Calibration

Proven that the stellar continuum in MIR windows might contributes to the overestimation of "real" SFR of the galaxies. Therefore, the measured *Hα*-based SFR of the samples from previous section is then used to derive reliable *WISE* SFRs conversion factors based on the elliptical galaxies by using W3- and W4-band indicators. Figure 3.8 shows the empirical calibration of SFRs at 12 μm (W3; left panel) and 22 μm (W4; right panel) luminosities. The calibration is based on the reference SFR indicator of *Hα* luminosities. The distributions of the elliptical galaxy samples have a tighter correlation between SFR and W4 luminosities, compared to the W3 luminosities. The relation is least-squares fitted and represent as the black solid lines. The empirical formulas for the SFR of *WISE* W3 and W4 are obtained as follows,

$$\log SFR_{W3}(M_{\odot}yr^{-1}) = (0.98 \pm 0.02)\log L_{W3}(L_{\odot}) - (8.72 \pm 0.24) \qquad (3.10)$$

$$\log SFR_{W4}(M_{\odot}yr^{-1}) = (1.04 \pm 0.03)\log L_{W4}(L_{\odot}) - (8.83 \pm 0.27) \qquad (3.11)$$

This Figure 3.8 is also complemented with another *WISE* SFR conversion factors proposed by Chang et al. (2015, dotted line), Lee et al. (2013, triangles) and Jarrett et al.

(2012, dashed line). Referring to this plot, the conversions of SFR_{W3} derived from this study appears to have an average offset of ~0.16, ~0.48 and ~0.53 dex relative to conversions derived from L13, J12, and C15, respectively. Whilst, the conversion of W4-band derived from this study give higher values of W4 SFR compare to other studies in the literature. The offset between the conversion factor for SFR_{W4} from this study and L13, J12, and C15 are ~0.4, ~0.63 and ~0.76 dex, respectively. The offset showed could be caused by the differences in SFR estimation technique and sample selection as we have discussed above. We summarized the SFR calibration based on W3- and W4- bands from the literature in Table 3.1.

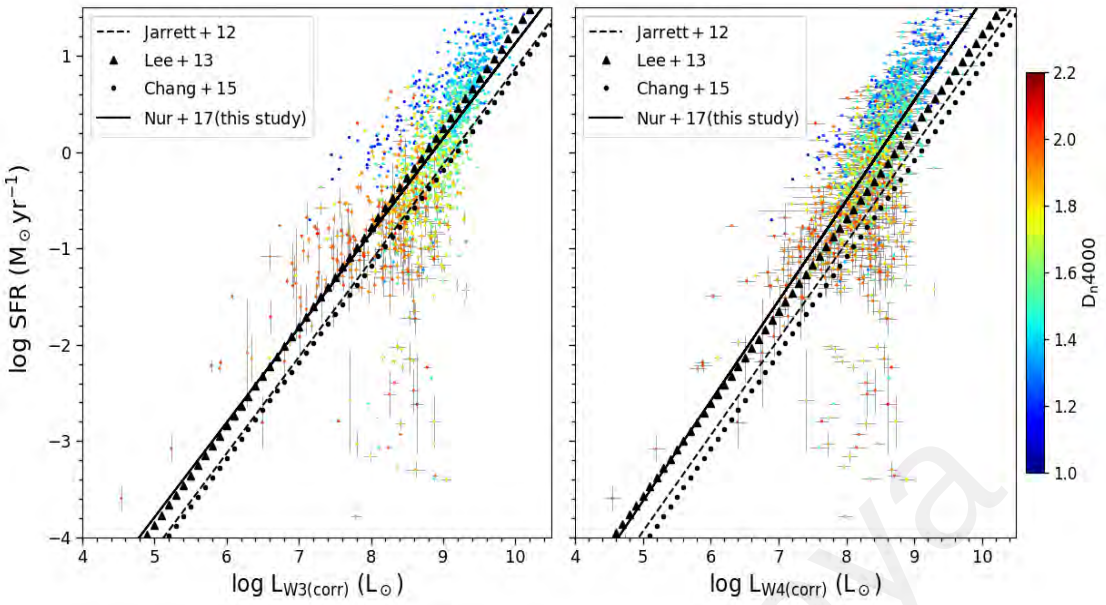

Figure 3.8: SFR calibrations based on 12 µm (left) and 22 µm (right) luminosities. The lines indicate the conversions of SFR derived by Chang et al. (2015, dotted line), Lee et al. (2013, triangles), Jarrett et al. (2012, dashed line), and this study (black solid line). The error bars represent the 1σ uncertainties for the sample.

Table 3.1: SFR Calibration for *WISE* W3- and W4-based luminosities.

Reference	SFR of *WISE* W3 and W4			
	Jarret et al. (2012)	Lee et al. (2013)	Chang et al. (2015)	This study
Calibrator	24 µm	*Hα*	UV-MIR SED modelling	*Hα*
SFR conversion	Rieke et al. (2009)	SDSS MPA-JHU; Brinchmann et al.	Chang et al. (2015)	Kennicutt (1998)
SFR range ($M_\odot yr^{-1}$)	0.03 - 4	3 - 100	10^{-3} - 100	10^{-4} - $10^{1.4}$
W3-band coeffecient (1)	c = -9.13 ± 0.03	m = 1.03 ± 0.01 n = -9.02 ± 0.02 c = -8.78 ± 0.03	c = -9.18	m = 0.98 ± 0.02 n = -8.72 ± 0.02
W4-band coefficient (1)	c = -8.94 ± 0.01	m = 0.96 ± 0.01 n = -8.37 ± 0.02 c = -8.80 ± 0.03	c = -9.08	m = 1.04 ± 0.03 n = -8.83 ± 0.27

Note: (1) W3- and W4-bands coefficients of m, n, and c are the coefficients for SFR equations of log SFR_{MIR} = $m$log L_{MIR}+ n and log SFR_{MIR} = log L_{MIR}+ c. The SFR and L are expressed in units of M⊙yr^{-1} and L⊙, respectively.

CHAPTER 4: EVOLUTION IN ELLIPTICAL GALAXIES

4.1 Bimodality in Early-type Galaxies

The evolution of the galaxies is a mysterious phenomenon but yet there are many evidences of star formation evolution that is investigable and can be traced. One of them is by probing the contribution of SFR to the growth of the galaxy using the parameter of specific SFRs (SSFRs). The SSFR parameter indicates the fraction of the new star formed in the galaxy, which defined as the SFR normalized by its stellar mass,

$$SSFR\,[yr^{-1}] = \frac{SFR\,[M_{\odot}yr^{-1}]}{M\,[M_{\odot}]} \tag{4.1}$$

where M is the stellar mass of the galaxies in solar mass unit. Several literatures have showed that the rest-frame luminosities around NIR wavelength are well-qualified to probe the old stellar components that dominating the stellar mass of the galaxies (e.g., Hancock et al., 2007; Lin et al., 2011; Ko et al., 2012). Therefore, a number of studies have been done and claimed that the *WISE* W1 band luminosity exhibit a well-established relation with the stellar mass of the galaxy (Jarrett et al., 2012). Especially for the early-type galaxies, which have little PAH emission (Wen et al., 2013). In this study, the galaxy stellar mass is estimated from the *WISE* W1 band (3.4 μm) luminosity by utilized the derived conversion factor from Hwang et al. (2012),

$$\log(M_{star}\,/\,M_{\odot}) = \log(\nu L_{\nu}\,(3.4\,\mu m)/L_{\odot})(1.14\,\pm\,0.02) - (0.11\,\pm\,0.17) \tag{4.2}$$

This conversion factor is applicable to our galaxy samples, since almost all the contaminated SED from AGN activities have been excluded. The relationship between the SSFRs of the corrected W3 and W4 luminosities as a function of stellar mass is studied with the dependence upon the age of stellar population in the galaxy. Figure 4.1 shows the SSFR of W3 and W4, $SSFR_{W3}$ and $SSFR_{W4}$, as the function of galaxy stellar

mass, M_{star} in the left and right panels, respectively. The color-code of the plots defined by the D_n4000 spectral index. Noted from this Figure 4.1, relationship between $SSFR_{W4}$ and stellar mass give a tighter correlation and a smaller scattering compare to $SSFR_{W3}$. However, both of these relations show almost the same distribution, where the galaxy with stellar age of $D_n4000 \geq 1.5$ are distributed at high density within the range of stellar mass between $10 \leq \log M_{star} \leq 11.4$ and have lower value of SSFR between $-12.5 \leq \log SSFR \leq -11$. Meanwhile, galaxies with $D_n4000 < 1.5$, have a wider range of stellar mass, which is between $8.4 \leq \log M_{star} \leq 11$ and have higher value of SSFRs within range of $-11 \leq \log SSFR \leq -10$. Both plots in Figure 4.1, illustrated the bimodal nature in the distribution of intrinsic properties of elliptical galaxies in our sample. As might be seen from the data distribution, galaxies with old stellar populations are concentrated only at high stellar mass compared to galaxies with young stellar populations, which have a wider range of stellar mass. In addition to that, noted that the old galaxies have a smaller value of SSFRs compare to the young galaxies, which is highly distributed at a higher value of SSFRs. In brief, the sample of elliptical galaxies is split into two distinct populations:

i) Galaxies with high SSFRs have low values of D_n4000 index and stellar mass

ii) Galaxies with low SSFRs have high values of D_n4000 index and stellar mass

These population behavior have been quantified in a number of papers (e.g., Kauffmann et al., 2003b; Brinchmann et al., 2004; Bauer et al., 2005; Salim et al., 2007), stating that the massive galaxies, which normally dominated with old stars, have a lower fraction of current star formation and vice versa. Based on these bimodal characteristics, a clearer separation between two regimes is showed at some point around SSFRs $\sim$10 - 11 yr^{-1} for both $SSFR_{W3}$ and $SSFR_{W4}$. This separations seen to have the similarities to the division of the SSFRs between the bulge-dominated red

sequences galaxies and disk blue cloud ones (e.g., Brinchmann et al., 2004; Schiminovich et al., 2007; Bothwell et al., 2009). However, some bulge-dominated galaxy appear to have high SSFRs with a very low stellar mass, which makes this population is comparable to the typical disk galaxies (SSFRs > 10^{-11} yr^{-1}; Schiminovich et al., 2007; Cheung et al., 2013). From the analysis, an elliptical galaxy population with SSFR > 10^{-11} yr^{-1} is found, which mimics the behavior of typical star forming spiral galaxy in terms of their stellar mass and the age of stellar populations. The recent literatures have discovered the blue galaxies literature (e.g., Schawinski et al., 2006, 2007; Tempel, 2011), which have demonstrate the importance of photometric color in the analysis of the morphology-related properties of the galaxies. For better understanding of the photometric properties of our samples, the elliptical galaxies are categorized into star forming elliptical (SFEGs), which have SSFR ≥ 10^{-11} yr^{-1} and those with SSFR < 10^{-11} yr^{-1}, categorized as non-star forming or quiescent elliptical galaxies (non-SFEGs). Table 4.1 illustrated the percentage obtained from this classification, where there are ∼69.7 % of SFEGs and ∼30.3 % of non-SFEGs that classified according to their SSFR of W3. Meanwhile, classification based on SSFR of W4, shows that there are ∼40.8 % and ∼59.2 % of SFEGs and non-SFEGs, respectively in the samples.

The color-magnitude relation (CMR) of the galaxy samples are illustrated as in Figure 4.2, where the left panel show the plot of $u - r$ Petrosian color versus stellar mass, and the right panel show the relation of $u - r$ Petrosian color versus r-band absolute Petrosian magnitude, M_r. The SFEGs and non-SFEGs are represented by the blue and red dots in both plots. According to optical photometric surveys, there are bimodality showed in the optical color distribution of the galaxies (Strateva et al., 2001; Hogg et al., 2003; Blanton et al., 2003). The analysis of the color-magnitude distribution of the galaxy samples will reveals the star formation characteristics of the galaxies that

distributed in the red-sequence, blue cloud and "green valley" regions. We adopted the CMR properties of the star forming elliptical galaxies from Huang & Gu (2009) as the CMR references for the galaxy samples in this study. The average values of CMR properties from Huang & Gu (2009), $u - r$ = 2.1 mag and M_r = -21.06 mag are represented in the Figure 4.2 by the solid lines in the left and right panels. Figure 4.2 indicates the density distribution of the galaxy samples within similar range of M_r , for non-SFEGs are significantly dominated in the red-sequence region, while the SFEGs are dominated in the bluer color region compare to the non-SFEGs. Nevertheless, there are also a population of SFEGs that existed with indistinguishable $u - r$ color from the typical $u - r$ color of the non-SFEGs.

Our galaxy samples give an average value for $u - r$ = 2.2 mag and M_r= -21.2 mag (represented as the dashed line in Figure 4.2), which is comparable to the average values of elliptical star forming galaxy from Huang & Gu (2009). These CMR distribution of the samples, have strengthen the existence of the elliptical galaxies (∼35.4 %) that posses the star forming properties, which mimics the CMR of spiral population. This is because, this population is tending to have lower stellar mass and brighter M_r that much alike to the typical blue cloud galaxies. The analysis also shows that more than half of the sample of elliptical galaxies carries the physical properties of the typical quiescent galaxies, which normally distributed in the red-sequence region of color-color relation.

Referring to the aperture correction applied on the SFR of $H\alpha$ luminosities (as mentioned in Section 3.4.2), this correction is estimated to account for the limited amount of emission that detected through the 3" diameter fiber. This correction implicitly assumes that the emission measured through the 3" fiber represents the characteristic of the whole galaxy and hence the star forming region estimated from this aperture is assume to be uniformly distributed over the galaxy. Thus, we look into

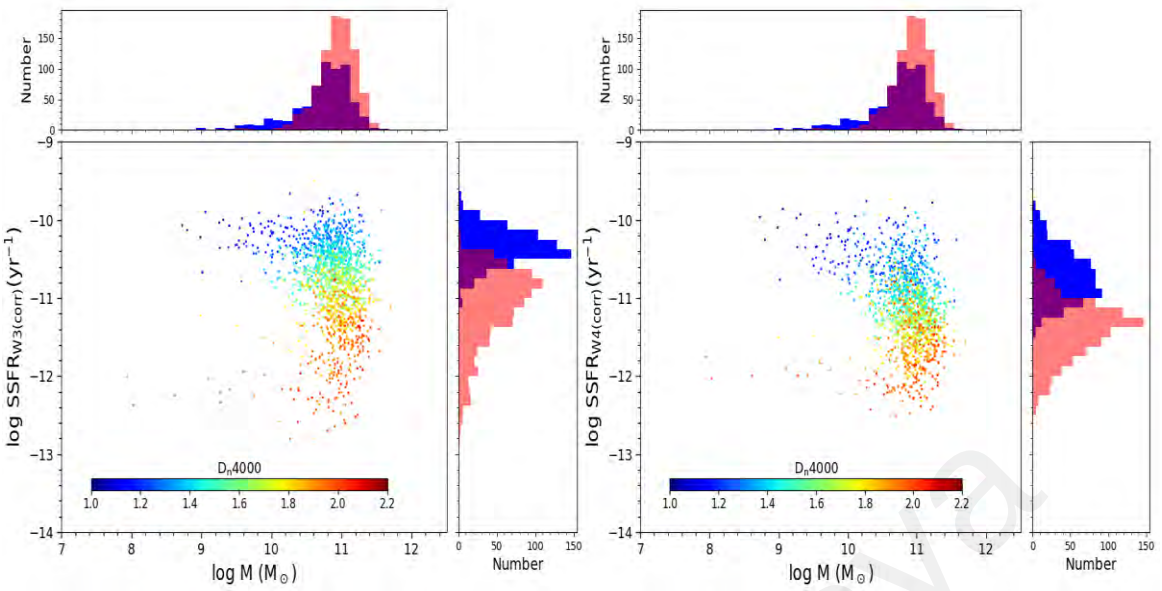

Figure 4.1: Specific Star Formation Rates of W3 (left) and W4 (right) as a function of stellar mass of elliptical galaxies. The color-coded of the diagram shows the D_n4000 spectral index. Histogram: Distributions of y- and x-parameters. Blue indicates the young stellar population galaxy (D_n4000 < 1.5) and red indicates the galaxy with old stellar population ($D_n4000 \geq 1.5$).

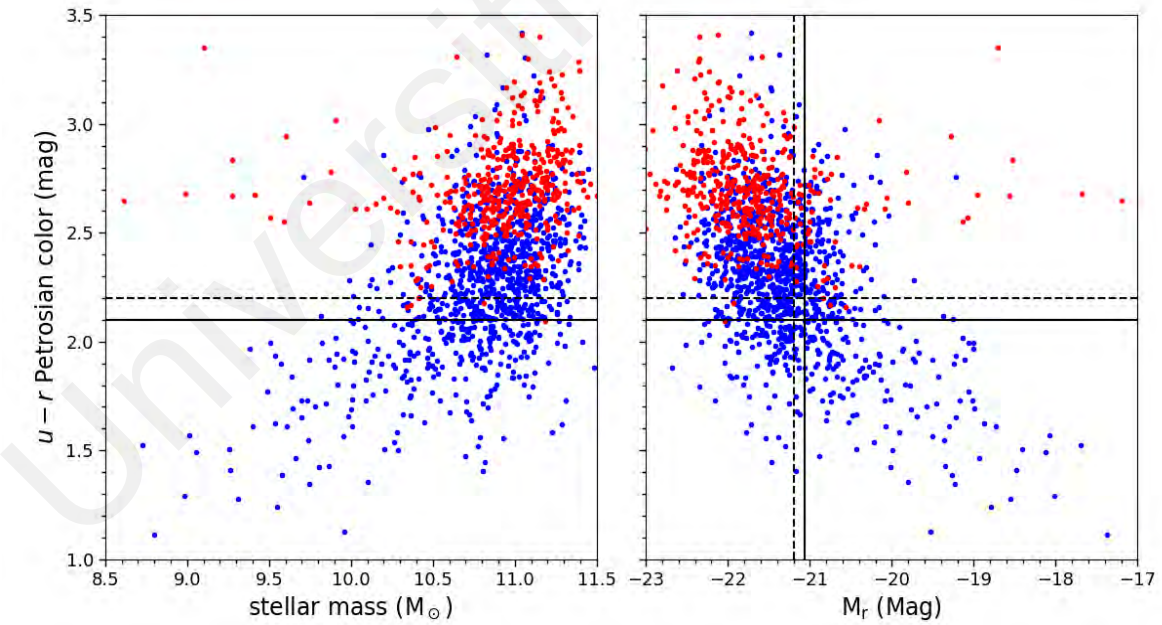

Figure 4.2: Shows the Color-magnitude relations (CMR) of $u - r$ Petrosian color as a function of stellar mass (left) and r-band absolute magnitude, M_r (right). The blue and red dots represent the SFEGs and non-SFEGs, respectively as defined according to this study. The solid lines show the average value for the elliptical star forming galaxy adopted from Huang & Gu (2009, $u - r$ = 2.1 mag and M_r = -21.06 mag). The dashed lines indicate the average parameter values obtained from this study.

aperture correction further to see how they vary with other galaxy parameters. In Figure 4.3, shows the distribution of the aperture correction of elliptical galaxies over the redshift between $0.01 \leq z \leq 0.2$ (left panel), complemented with color-coded of the age of stellar population in the galaxies. The aperture correction across the lower redshift bin, $0.01 \leq z \leq 0.12$ and the old stellar population galaxies perceived a consistently higher aperture correction at specific redshift compare to the young stellar population galaxies. However, at higher redshift bin, $0.12 \leq z \leq 0.2$, the aperture correction between these two galaxy populations reached unity. Meanwhile, on the right panel of Figure 4.3 is the relation of aperture correction as a function of galaxy size, where the galaxy size is estimated from the *r*-band Petrosian radius of the galaxies. Clearly, the relation shows that the larger galaxies required a bigger aperture correction (Hopkins et al., 2008). Additionally, Figure 4.4 shows the variation in ratio of SFRs of *Hα* and 12 μm emission along the aperture correction of the samples. Regardless to small amount of galaxies, the relation is recognized to be flat, as would be desired for an aperture correction. The flatness in the relation may reflects the derived SFRs have no bias for most of the D_n4000 spectral index ($1 \leq z \leq 2.2$) and redshift smaller than 2.2. However, there is small number of galaxies, which demonstrated having a higher SFR of W3 than SFR of *Hα*. Most of them are the elliptical galaxies that consist of old stellar population at higher redshift. Contrast to the discrepancy appears in Hopkins et al. (2008), where the galaxies with largest aperture corrections have slightly overestimated the $SFR_{H\alpha}$.

Furthermore, related to the fact that D_n4000 spectral index is obtained from the SDSS spectra observed through a small 3" aperture fiber. Thereby, the size of the aperture fiber corresponds to a physical scale of ~5.535 kpc for an object observed at $z = 0.1$. Inferred that the light collected from this diameter mainly comes from the central region of galaxies for most of the samples, which lie at redshift $z \leq 0.1$. For further details, the SDSS *u*, *g*, *r*, *i* and *z*-band images of 210 elliptical galaxies from the sample are

presented in Appendix. They are representing the sample of elliptical galaxies at redshift $0.01 \leq z \leq 0.1$ in this study, which widely covered all the D_n4000 spectral indices from this study. Therefore, the galaxies at lower redshift, $z \leq 0.1$, the age of stellar population is representing the age of the stellar that concentrated at the central region of the galaxies. Implying that the samples with young stellar population galaxies have a centrally concentrated star forming regions, whereas the old galaxies have passive central regions. This hence suggest that, those SFEGs and non-SFEGs have divergent stellar properties or activities at their central regions. This also emphasized that the elliptical galaxies can possibly have two different origins, which allowed the existence of two different properties in their central regions. Next section, we further discuss on the history of the star formation in these galaxy populations.

Table 4.1: Percentage of SFEG and non-SFEG classified based on $SSFR_{W3}$ and $SSFR_{W4}$.

Classified from	$SSFR_{W3}$	$SSFR_{W4}$
SFEG	69.7 %	40.8 %
non-SFEG	30.3 %	59.2 %

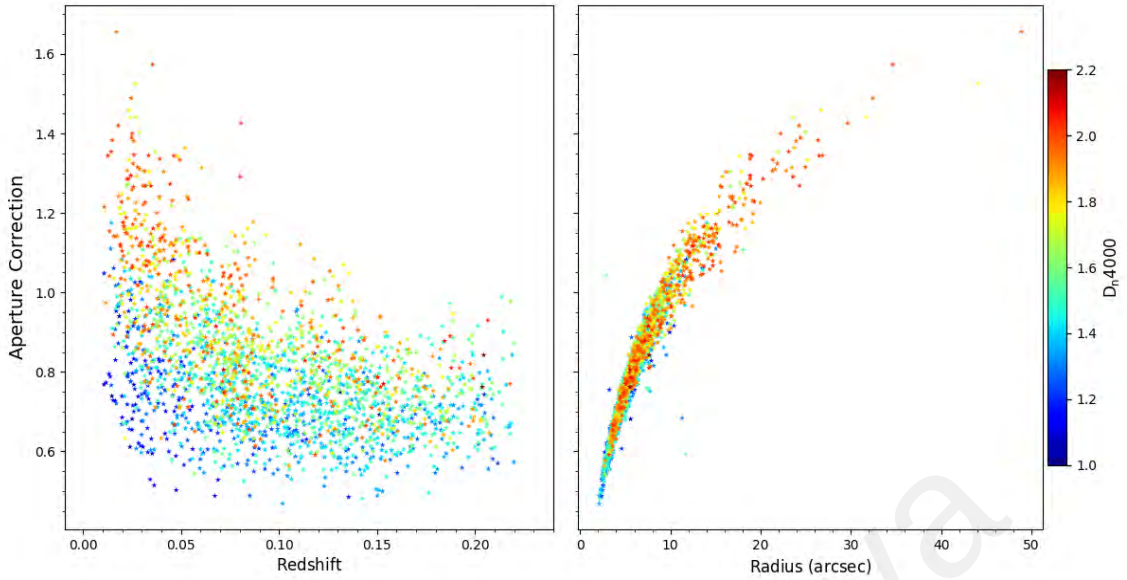

Figure 4.3: Relation of aperture correction as a function of redshift (left) and galaxy size (right).

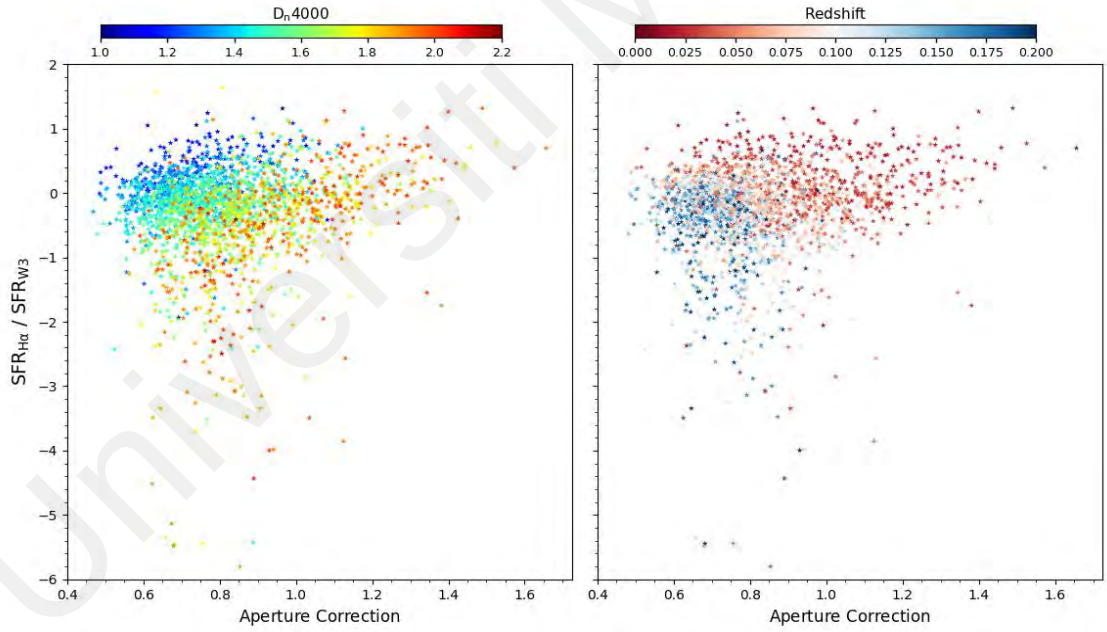

Figure 4.4: SFRs ratio between *Hα* and *WISE* W3 luminosities as a function of the aperture correction, with color-coded of D_n4000 spectral index (left) and redshift (right).

4.2 Star Formation History

The observable segregation in the properties of elliptical galaxy populations from previous section, may associated to the star formation history (SFH) of the galaxies. In galaxy evolution studies, modern merger hypothesis (Hopkins et al., 2008) is still remains controversial in making of a conclusion for elliptical galaxy formation in the Universe. However, this hypothesis is the most acceptable to explain the phenomenon that is so-called "blue-to-red" migration (Faber et al., 2007; Eliche-Moral et al., 2010; Gonçalves et al., 2012), where the increasing of red sequence galaxies over cosmic time were believed to be strongly related to the transformation of nearly equal mass of blue disk galaxies into one quiescent, red early-type galaxies (ETGs) via gas-rich major merger. Haines et al. (2015) have tested the modern merger hypothesis by built a model of SFH. The prediction of the model is based on the presence of strong and centrally concentrated burst of the star formation in the merger remnant. This SFH model has characterized the SFR as a function of time for an arbitrary stellar population that allowed distinguishing the two possible evolution paths after the initial large burst. The first path is the model for galaxy that has continuity in star formation throughout lifetime and the second path is the galaxy with additional burst atop a continuously-declining SFH. This SFH model qualitatively distinguished these galaxies by comparing their measured Balmer Lick indices ($H\gamma$ and $H\delta$) with the D_n4000 index, on the Balmer-D_n4000 parameter space, which divided into four regions.

The Region 1 contains the model of continuous star formation with $D_n4000 \lesssim 1.35$ index, where normally dominated by the typical late-type star forming galaxies or galaxies with recent small bursts. For Region 2, it consists of model with radial indices of $1.35 \lesssim D_n4000 \lesssim 1.6$, which has a typical characteristic decay time of star formation around 2 Gyr and simulate the galaxies with old populations with a few additional new

stars. The third region (Region 3) has the radial indices of $D_n4000 \gtrsim 1.6$, and it is the overlapping region of continuous and burst models. In this region, the galaxy could be quiescent, early-type galaxies, which might contain at most 5 % bursts that have ages $\gtrsim$ 1 Gyr. In Region 4, the models span with the indices $D_n4000 \gtrsim 1.6$ and are located above the continuous SFH models. This region contains the galaxies that have undergone a recent burst of star formation in the last ~2 Gyrs. Herein, from the Balmer-D_n4000 plane of SFH model, the first and fourth regions show a slightly decreasing Balmer index gradients and generally increasing D_n4000 indices at large radii. The galaxies lie in these regions is likely to be the candidates of recent gas-rich major mergers, as they exhibit the burst-like SFH and consist of very young stellar ages in their cores. The Region 2 was predicted to have only the smooth elliptical morphologies and SFHs consistent with weak, but ongoing star formation. Meanwhile, the galaxies lie within Region 3 usually has a steep positive Balmer index gradients and a steep negative gradient of D_n4000. Thus, this characteristics act as an indicative of domination of very old stellar ages in the central regions. Those lie within this region are least likely to be remnants of recent gas-rich major mergers. The SFH of the galaxy samples are examined by utilizing the SFH model by Haines et al. (2015), which determined the galaxy evolution by using the measured Lick indices of $H\delta_A$ and $H\gamma_A$ from MPA-JHU spectroscopic catalog (as described in Brinchmann et al., 2004). This method can be achieved by taking the average values of these Lick indices, $< H\delta_A, H\gamma_A > \equiv (H\delta_A + H\gamma_A)/2$ (Kauffmann et al., 2003). This Lick indices represent the equivalent widths of $H\delta_A$ and $H\gamma_A$ absorption in the galaxies with wide central bandpass (~40 Å as using the Balmer indices with A-definition) to trace the young stellar populations (e.g., Haines et al., 2015). Referring to previous section, the galaxy samples have been into two groups that defined to be SFEGs (SSFR $\geq 10^{-11}\mathrm{yr}^{-1}$) and non-SFEGs (SSFR $< 10^{-11}\mathrm{yr}^{-1}$), which identified from both W3 and W4 bands emission.

Figure 4.5 shows the implemented SFH model on Balmer-D_n4000 plane for the elliptical galaxies classified based on their $SSFR_{W3}$ (top panel) and $SSFR_{W4}$ (bottom panel). First and foremost, our galaxy samples have the measured indices that span nearly the entire model, and hence this indicates that our samples possess a wide range of SFHs. The distribution of the galaxies on Balmer-D_n4000 plane is simplified in Table 4.2. Most of the non-SFEGs (represented as red dots) are found dominating the Region 3 for both plots in Figure 4.5, where ~99.9 % and ~75.4 % of the total non-SFEGs (based in W3 and W4 classification), distributed in the top and bottom panels, respectively. On the other hand, the majorities of SFEGs (represented as blue dots) are dispersed across Region 1 and 2 in both plots of Figure 4.5. The top and bottom panels show that ~85.7 % and ~88.5 % of SFEGs, distributed within both Region 1 and Region 2. The results obtained, reveal an observable consistency to the model prediction, where majority of SFEGs can be found in Region 1 and Region 2, on the other hand, the non-SFEGs are highly distributed in the Region 3 of Balmer-D_n4000 plane. Only a very small amount of remaining SFEGs and non-SFEGs are allocated in other regions and thus carries non-statistical significance. Meanwhile, noticed that the percentages of the SFEGs and the non-SFEGs located in Region 4 are almost negligible. This implied that the SFEGs might have undergone continuous star forming activities and the star formation of the SFEGs might not be triggered by recent burst activities. Additionally, all of our samples are smooth elliptical galaxies, which were identified with no peculiarity in their morphology. Hence, they are unlikely to be the remnants of recent mergers. For a direct comparison, the spiral galaxy samples have been applied on this Balmer-D_n4000 plane, and they indeed dominated within Region 1 and Region 2. The spiral galaxies are represented as gray dots in Figure 4.5. Therefore, this clearly indicates that most of the spiral galaxies have undergone continuous star formation throughout their lifetime. Comparatively, most of the SFEGs lie in similar regions to the

spiral galaxies, hence suggesting that the SFEGs have a tendency to maintain a continuous star formation activity as the spiral galaxies do. It is strongly agreed that the star forming activities, which performed by the spiral galaxies have take place in the spiral arm. However, there are no observable spiral patterns in the SFEGs. Consequently, these results have suggested that the SFEGs might have some unknown mechanisms that able to stimulate the continuity of star formation activities in the elliptical galaxies. Nevertheless, the origins of the star formation activities in the SFEGs are still remained unclear.

Table 4.2: Percentage of Elliptical Galaxies distributed on Balmer- D_n4000 plane.

Classification	W3 band		W4 band	
	SFEG (%)	non-SFEG (%)	SFEG (%)	non-SFEG (%)
Region 1	14.57	0.00	15.70	0.40
Region 2	39.90	0.74	16.96	16.01
Region 3	14.90	29.49	7.80	42.60
Region 4	0.33	0.07	0.34	0.19

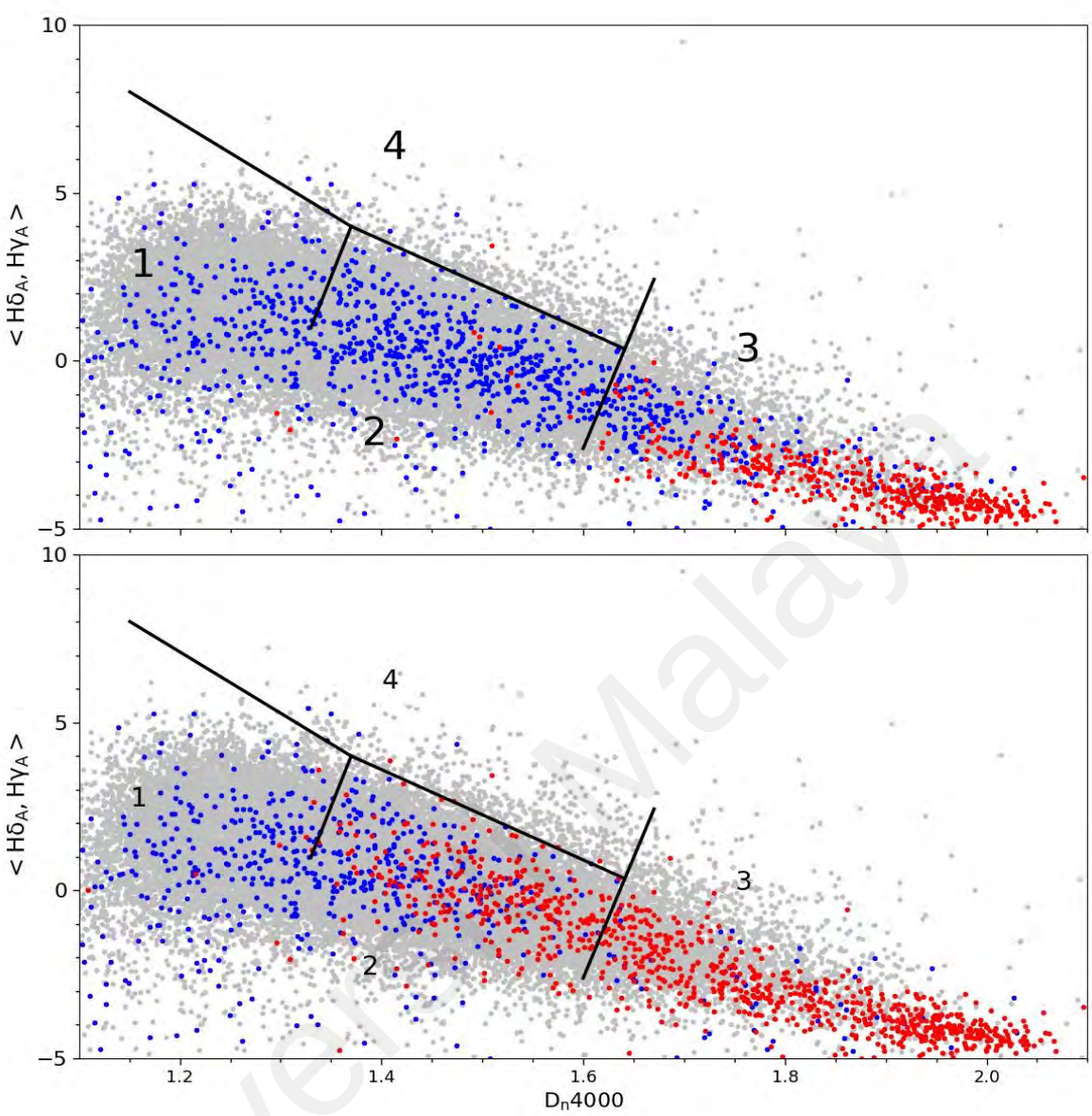

Figure 4.5: Distribution of galaxies on the Balmer absorption versus 4000 Å break strength plane. The black solid line represents the SFH of Haines et al. (2015) model with the numbered regions (1, 2, 3, and 4) have same definitions as in Haines et al. (2015). The blue, red and gray dots represent the SFEGs, non-SFEGs and spiral galaxies, respectively.

CHAPTER 5: SUMMARY AND CONCLUSION

Mid-infrared (MIR) emission of star-forming galaxies is dominated by the blackbody radiation from warm dust, young stellar population and emission features attributed to PAHs. Thus, the MIR emission from the star-forming galaxies have shown a great dependency between the rate of star formation and dust content (and thus metallicity), geometry, and temperature. However, the MIR emission are complex to be directly compared to the rate of star formation for certain galaxies, as it may include the contributions from dust heated by old stellar populations ("galactic cirrus"), AGNs, and the Rayleigh-Jeans tail of stellar spectra. This issue might cause bias in MIR SFR calibration, and need to be correct for future application.

This study of the star formation activities is performed based on a large sample of star forming galaxies collected from SDSS MPA-JHU catalog, and photometrically crossed-matched to *WISE* All-Sky Data Release catalog. The selected samples are located within redshift $0.01 \leq z \leq 0.2$, and these samples are complemented with reliable detections of signal-to-noise ratio, (SNR) ≥ 3 at all *WISE* bands. These samples are morphology-identified into spiral or elliptical galaxy populations using Galaxy Zoo and SDSS parameter. The finalized galaxy samples consist of ~36,103 spiral galaxies and ~2,337 elliptical galaxies. The galaxy samples are considered to have negligible AGN contamination and also AGB circumstellar dust emission have been subtracted out. This study probes the mid-infrared (MIR) star formation rate indicators at 12- and 22-μm, by using *WISE* W3 and W4 bands. The conclusion obtained from this study is as follows:

- The correlation of star formation rates of *WISE* W3 and W4 bands have been examined and the result shows a strong correlation between these MIR-SFR indicators, regardless to a consistent pattern that seems to be an overestimation

of SFR at 12 μm (W3) emission across the redshift range ($0.01 \leq z \leq 0.2$) for both spiral and elliptical galaxies.

- The contribution of stellar continuum at 12- and 22- μm, which contributed by the R-J tails of stellar continuum, has been estimated for all the galaxy samples, relative to the near-infrared emission at 3.4 μm. The corollary of stellar continuum emission at 12- and 22- μm of the galaxy samples has showed a significant contribution in the elliptical galaxies. The estimated fraction of stellar continuum at W3 or W4 bands relative to W1 band are $\eta_{w3} = 0.125 \pm 0.001$ and $\eta_{w4} = 0.0107 \pm 0.0003$, respectively. Hence, the study has shown that the stellar continuum emission could contribute to MIR fluxes with an average overestimation of ~13.95 % and ~0.77 % from *WISE* W3 and W4 observed fluxes. However, for the extreme case, the stellar continuum could contribute nearly as high as ~89.5 % at W3 and ~10 % at W4 band.
- The SFR of W3- and W4-band have been estimated exclusively from the star forming region of the galaxy, by employing the calculated η_{w3} and η_{w4}. These parameters are used as the correction factors of stellar contribution at 12- and 22- μm, in order to derive the stellar contribution corrected SFRs. Both of the corrected SFR of W3 and W4 give a better correlation, especially between the old stellar population elliptical galaxies. The results obtained by using calibrated *WISE* SFR, derived from previous studies also strongly agreed on SFRs correlation pattern and the affected properties of elliptical galaxy populations. Thus, inferred that the SFR of the galaxy is considerably good without the contamination of stellar contribution.
- The affected galaxy populations from the corrected stellar continuum emission have been identified based on their intrinsic properties, with the most affected population being the low star forming elliptical galaxies with old stellar

population (SFR $\leq 1\ M_{\odot}\mathrm{yr}^{-1}$ and $D_n4000 \geq 1.5$). These elliptical galaxies give a better correlation of corrected $\mathrm{SFR_{W3}}$-$\mathrm{SFR_{W4}}$. Meanwhile, for the case of the elliptical galaxies with high star forming and/or young stellar population, stellar contribution seems unremarkable.

- Conversion factor of *WISE* SFR of W3 and W4 luminosities have been derived in this study based on the reference SFR of *Hα* luminosities. The derived SFR conversions are shown as Equation 3.10 and 3.11. The calibration carried out using elliptical galaxies with low star forming activities (SFR range between 10^{-4} to $10^{1.5}\ M_{\odot}\mathrm{yr}^{-1}$) and lie in local Universe within redshift $0.01 \leq z \leq 0.2$. These SFR conversion equations are compatible for the low star forming galaxies. Consequently, the results deduce that extra caution is needed in SFR calibration of *WISE* indicators, especially for the unsuitable galaxy populations that could lead into SFR biases.

We also have studied the evolutions of elliptical galaxies and noticed remarkable bimodalities in elliptical galaxies, where the SFEGs exhibit a similar distribution of spiral galaxies on the Balmer Lick-D_n4000 plane of star formation history model adopted from Haines et al. (2015). The non-SFEGs, on the other hand distributed in the region that predicted by the model for typical early-type, quiescent galaxy. The results show the continuous decay of SFR in SFEGs, and this emphasizing that the SFEGs have tendency in maintaining the continuous star formation activities in lifetime. Furthermore, there is no observable peculiarity in the morphology of the samples; we proposed that the formation of SFEGs is less likely caused by major merger. Briefly, a caution should be taken in the estimation of SFR using MIR emission especially for elliptical or low star forming galaxies. This is regarding to the MIR emission that could overestimate the SFR due to emission contributed by stellar continuum with an average overestimation of ~13.95 % and ~0.77 % at 12- and 22- μm. This study has shown that

the most affected population is the low star forming elliptical galaxies with the old stellar population and we also proposed a SFR conversion factor with *WISE*-based indicators for the targeted population.

These findings are very useful for future application, as the SFR is a very important parameter in the study of the galaxy evolution. The fractions of stellar contribution at mid-infrared wavelength (to be exact at 12- and 22- μm) in this study have shown a significant connection to the intrinsic properties of the galaxy samples, as well as the SFH of the elliptical galaxies. Hence, it is important to well-understand the mechanism contributes from multiwavelength observation to understand more on the evolution of our universe. The application of the method proposed in this study for future research of "new population" of elliptical galaxies that currently discovered is highly recommended. Main contribution of this study is the beneficial knowledge of star forming elliptical galaxy evolutions detected at mid-infrared wavelength, which is not widely studied in literature. The lack of studies on elliptical galaxy at infrared wavelength observation is probably due to the non-star forming properties and very low detection at mid-infrared emission. The literature on the other hand is more focus on the research of star forming galaxies. By carried out one of a large mid-infrared survey of elliptical galaxies at local Universe, this study contributes for a better understanding of elliptical galaxy population at 12- and 22- μm emission based on their intrinsic properties and also contributes to the galaxy evolution research in multiwavelength observation, which is very important in this the study of astrophysics and astronomy.

REFERENCES

Allamandola, L., Tielens, A., & Barker, J. (1985). Polycyclic aromatic hydrocarbons and the unidentified infrared emission bands-auto exhaust along the Milky Way. *The Astrophysical Journal*, *290*, L25–L28.

Almaini, O., Lawrence, A., & Boyle, B. (1999). The AGN contribution to deep submillimetre surveys and the far-infrared background. *Monthly Notices of the Royal Astronomical Society, 305*(3), L59–L63.

Alonso-Herrero, A., Ramos Almeida, C., Esquej, P., Roche, P., Hernán-Caballero, A., Hönig, S. F., … Telesco, C. M. (2014). Nuclear 11.3 μm PAH emission in local active galactic nuclei. *Monthly Notices of the Royal Astronomical Society*, *443*(3), 2766–2782.

Alonso-Herrero, A., Rieke, G. H., Rieke, M. J., Colina, L., Pérez-González, P. G., & Ryder, S. D. (2006). Near-infrared and star-forming properties of local luminous infrared galaxies. *The Astrophysical Journal, 650*(2), 835-849.

Antonucci, R. (1993). Unified models for active galactic nuclei and quasars. *Annual Review of Astronomy and Astrophysics, 31*, 473–521.

Antonucci, R., & Miller, J. S. (1985). Spectropolarimetry and the nature of NGC 1068. *The Astrophysical Journal, 297*, 621–632.

Assef, R. J., Stern, D., Kochanek, C. S., Blain, A. W., Brodwin, M., Brown, M. J., … Yan, L. (2013). Mid-infrared selection of active galactic nuclei with the wide-field infrared survey explorer: II. Properties of WISE-selected active galactic nuclei in the NDWFS boötes field. *The Astrophysical Journal, 772*(1), 26-44.

Athey, A., Bregman, J., Bregman, J., Temi, P., & Sauvage, M. (2002). Mid-infrared observation of mass loss in elliptical galaxies. *The Astrophysical Journal, 571*(1), 272-281.

Balogh, M. L., Morris, S. L., Yee, H., Carlberg, R., & Ellingson, E. (1999). Differential galaxy evolution in cluster and field galaxies at z ≈ 0.3. *The Astrophysical Journal, 527*(1), 54-79.

Bauer, A., Drory, N., Hill, G., & Feulner, G. (2005). Specific star formation rates to redshift 1.5. *The Astrophysical Journal Letters, 621*(2), L89-L92.

Bendo, G., Wilson, C., Pohlen, M., Sauvage, M., Auld, R., Baes, M., … Zeilinger, W. W. (2010). The Herschel space observatory view of dust in M81. *Astronomy & Astrophysics, 518*, L65-L68.

Bertola, F., Burstein, D., & Buson, L. M. (1993). NGC5018 a metal-poor giant elliptical. *The Astrophysical Journal, 403*(2), 573–576.

Blain, A. W., Smail, I., Ivison, R. J., & Kneib, J. -P. (1999). The history of star formation in dusty galaxies. *Monthly Notices of the Royal Astronomical Society, 302*(4), 632–648.

Blanton, M. R., Hogg, D. W., Bahcall, N. A., Baldry, I. K., Brinkmann, J., Csabai, I., … Weinberg, D. H. (2003). The broadband optical properties of galaxies with redshifts 0.02< z< 0.22. *The Astrophysical Journal, 594*(1), 186-207.

Boquien, M., Kennicutt, R., Calzetti, D., Dale, D., Galametz, M., Sauvage, M., … Tabatabaej, F. (2016). Towards universal hybrid star formation rate estimators. *Astronomy & Astrophysics, 591*, A6.

Boselli, A., Sauvage, M., Lequeux, J., Donati, A., & Gavazzi, G. (2003). Mid-IR emission of galaxies in the Virgo cluster: III. The data. *Astronomy & Astrophysics, 406*(3), 867–877.

Bothwell, M. S., Kennicutt, R. C., & Lee, J. C. (2009). On the interstellar medium and star formation demographics of galaxies in the local universe. *Monthly Notices of the Royal Astronomical Society, 400*(1), 154–167.

Boulanger, F., & Perault, M. (1988). Diffuse infrared emission from the galaxy: I. Solar neighborhood. *The Astrophysical Journal, 330*, 964–985.

Bressan, A., Granato, G. L., & Silva, L. (1998). Modelling intermediate age and old stellar populations in the infrared. *Astronomy & Astrophysics, 332*, 135-148.

Brinchmann, J., Charlot, S., White, S., Tremonti, C., Kauffmann, G., Heckman, T., & Brinkmann, J. (2004). The physical properties of star-forming galaxies in the low-redshift universe. *Monthly Notices of the Royal Astronomical Society, 351*(4), 1151–1179.

Brocklehurst, M. (1971). Calculations of level populations for the low levels of hydrogenic ions in gaseous nebulae. *Monthly Notices of the Royal Astronomical Society, 153*(4), 471–490.

Bruzual, A. (1983). Spectral evolution of galaxies: I. Early-type system. *The Astrophysical Journal, 273*, 105–127.

Calzetti, D. (2001). The dust opacity of star-forming galaxies. *Publications of the Astronomical Society of the Pacific, 113*(790), 1449-1485.

Calzetti, D., Kennicutt, R., Engelbracht, C., Leitherer, C., Draine, B., Kewley, L., … Walter, F. (2007). The calibration of mid-infrared star formation rate indicators. *The Astrophysical Journal, 666*(2), 870-895.

Calzetti, D., Kennicutt Jr, R., Bianchi, L., Thilker, D., Dale, D., Engelbracht, C., … Lindler, D. (2005). Star formation in NGC 5194 (M51a): The panchromatic view from GALEX to Spitzer. *The Astrophysical Journal, 633*(2), 871-893.

Cardelli, J. A., Clayton, G. C., & Mathis, J. S. (1989). The relationship between IR, optical, and UV extinction. *Astrophysical Journal, 345*, 245–256.

Chang, Y.-Y., van der Wel, A., da Cunha, E., & Rix, H.-W. (2015). Stellar masses and star formation rates for 1M galaxies from SDSS + WISE. *The Astrophysical Journal Supplement Series, 219*(1), 8-24.

Cheung, E., Athanassoula, E., Masters, K. L., Nichol, R. C., Bosma, A., Bell, E. F., … Willett, K. W. (2013). Galaxy Zoo: Observing secular evolution through bars. *The Astrophysical Journal, 779*(2), 162-179.

Cimatti, A., Daddi, E., Renzini, A., Cassata, P., Vanzella, E., Pozzetti, L., … Zamorani, G. (2004). Old galaxies in the young universe. *Nature, 430*(6996), 184-187.

Cluver, M., Jarrett, T. H., Hopkins, A. M., Driver, S., Liske, J., Gunawardhana, M., … Wilkins, S. M. (2014). Galaxy and Mass Assembly (GAMA): Mid-infrared properties and empirical relations from WISE. *The Astrophysical Journal, 782*(2), 90-106.

Condon, J. (1992). Radio emission from normal galaxies. *Annual Review of Astronomy and Astrophysics, 30*(1), 575–611.

Cowie, L. L., Songaila, A., & Barger, A. J. (1999). Evidence for a gradual decline in the universal rest-frame ultraviolet luminosity density for z< 1. *The Astronomical Journal, 118*(2), 603-612.

Cram, L., Hopkins, A., Mobasher, B., & Rowan-Robinson, M. (1998). Star formation rates in faint radio galaxies. *The Astrophysical Journal, 507*(1), 155-160.

Daddi, E., Renzini, A., Pirzkal, N., Cimatti, A., Malhotra, S., Stiavelli, M., … Windhorst, R. A. (2005). Passively evolving early-type galaxies at $1.4 < z < 2.5$ in the Hubble ultra deep field. *The Astrophysical Journal, 626*(2), 680-697.

Dale, D. A., Silbermann, N. A., Helou, G., Valjavec, E., Malhotra, S., Beichman, C. A., … Corwin, G. (2000). ISO mid-infrared observations of normal star-forming galaxies: The key project sample. *The Astronomical Journal, 120*(2), 583-603.

Davies, L., Driver, S., Robotham, A., Grootes, M., Popescu, C., Tuffs, R., … Bourne, N. (2016). Gama/H-atlas: A meta-analysis of SFR indicators–comprehensive measures of the SFR–M* relation and cosmic star formation history at $z < 0.4$. *Monthly Notices of the Royal Astronomical Society, 461*(1), 458–485.

Davis, T. A., Young, L. M., Crocker, A. F., Bureau, M., Blitz, L., Alatalo, K., … Weijmans, A-. M. (2014). The ATLAS^{3D} project: XXVIII. Dynamically driven star formation suppression in early-type galaxies. *Monthly Notices of the Royal Astronomical Society, 444*(4), 3427–3445.

Dawson, K. S., Schlegel, D. J., Ahn, C. P., Anderson, S. F., Aubourg, É., Bailey, S., … Zheng, Z. (2012). The baryon oscillation spectroscopic survey of SDSS: III. *The Astronomical Journal, 145*(1), 10-50.

Donoso, E., Yan, L., Tsai, C., Eisenhardt, P., Stern, D., Assef, R., ... Stanford, S. (2012). Origin of 12 μm emission across galaxy populations from WISE and SDSS surveys. *The Astrophysical Journal, 748*(2), 80-90.

Dopita, M. A., & Sutherland, R. S. (2003). What is the diffuse universe? In Astrophysics of the diffuse universe. *The Astrophysical Journal, 292*, 1-9.

Draine, B., & Anderson, N. (1985). Temperature fluctuations and infrared emission from interstellar grains. *The Astrophysical Journal, 292*, 494–499.

Efstathiou, A., & Rowan-Robinson, M. (1995). Dusty discs in active galactic nuclei. *Monthly Notices of the Royal Astronomical Society, 273*(3), 649–661.

Eggen, O., Lynden-Bell, D., & Sandage, A. (1962). Evidence from the motions of old stars that the galaxy collapsed. *The Astrophysical Journal, 136*, 748-766.

Elbaz, D., Dickinson, M., Hwang, H., Díaz-Santos, T., Magdis, G., Magnelli, B., … Wilson, G. (2011). GOODS–Herschel: An infrared main sequence for star-forming galaxies. *Astronomy & Astrophysics, 533*, A119.

Eliche-Moral, M. C., Prieto, M., Gallego, J., Barro, G., Zamorano, J., López-Sanjuan, C., … Munoz-Mateos, J. C. (2010). On the buildup of massive early-type galaxies at z < 1: I. Reconciling their hierarchical assembly with mass downsizing. *Astronomy & Astrophysics, 519*, A55.

Esquej, P., Alonso-Herrero, A., González-Martín, O., Hönig, S. F., Hernán-Caballero, A., Roche, P., … Packham, C. (2013). Nuclear star formation activity and black hole accretion in nearby Seyfert Galaxies. *The Astrophysical Journal, 780*(1), 86-100.

Faber, S., Willmer, C., Wolf, C., Koo, D., Weiner, B., Newman, J. A., ... Yan, R. (2007). Galaxy luminosity functions to z~1 from DEEP2 and COMBO-17: Implications for red galaxy formation. *The Astrophysical Journal, 665*(1), 265-294.

Fabian, A., & Iwasawa, K. (1999). The mass density in black holes inferred from the X-ray background. *Monthly Notices of the Royal Astronomical Society, 303*(2), L34–L36.

Fukugita, M., Nakamura, O., Turner, E. L., Helmboldt, J., & Nichol, R. (2004). Actively star-forming elliptical galaxies at low redshifts in the Sloan Digital Sky Survey. *The Astrophysical Journal Letters, 601*(2), L127-L130.

Gallego, J., Zamorano, J., Aragon-Salamanca, A., & Rego, M. (1995). The current star formation rate of the local universe. *The Astrophysical Journal Letters, 455*(1), L1-L4.

Georgakakis, A., Mobasher, B., Cram, L., Hopkins, A., Lidman, C., & Rowan-Robinson, M. (1999). The phoenix survey: Optical and near-infrared observations of faint radio sources. *Monthly Notices of the Royal Astronomical Society, 306*(3), 708–726.

Glazebrook, K., Blake, C., Economou, F., Lilly, S., & Colless, M. (1999). Measurement of the star formation rate from Hα in field galaxies at z = 1. *Monthly Notices of the Royal Astronomical Society, 306*(4), 843–856.

Gonçalves, T. S., Martin, D. C., Menéndez-Delmestre, K., Wyder, T. K., & Koekemoer, A. (2012). Quenching star formation at intermediate redshifts: Downsizing of the mass flux density in the green valley. *The Astrophysical Journal, 759*(1), 67-78.

Goto, T., Arnouts, S., Inami, H., Matsuhara, H., Pearson, C., Takeuchi, T. T., … Treister, E. (2010). Luminosity functions of local infrared galaxies with AKARI: Implications for the cosmic star formation history and AGN evolution. *Monthly Notices of the Royal Astronomical Society, 410*(1), 573–584.

Goto, T., Nichol, R. C., Okamura, S., Sekiguchi, M., Miller, C. J., Bernardi, M., … Subbarao, M. (2003). Hδ-strong galaxies in the Sloan Digital Sky Survey: I. The catalog. *Publications of the Astronomical Society of Japan, 55*(4), 771–787.

Haines, T., McIntosh, D., Sánchez, S., Tremonti, C., & Rudnick, G. (2015). Testing the modern merger hypothesis via the assembly of massive blue elliptical galaxies in the local universe. *Monthly Notices of the Royal Astronomical Society, 451*(1), 433–454.

Hancock, M., Smith, B. J., Struck, C., Giroux, M. L., Appleton, P. N., Charmandaris, V., … Reach, W. T. (2007). Large-scale star formation triggering in the low-mass ARP 82 system: A nearby example of galaxy downsizing based on UV/optical/mid-IR imaging. *The Astronomical Journal, 133*(2), 676-693

Heckman, T. M., & Best, P. N. (2014). The coevolution of galaxies and supermassive black holes: Insights from surveys of the contemporary universe. *Annual Review of Astronomy and Astrophysics, 52*, 589–660.

Helou, G. (1986). The IRAS colors of normal galaxies. *The Astrophysical Journal, 311*, L33–L36.

Helou, G., Roussel, H., Appleton, P., Frayer, D., Stolovy, S., Storrie-Lombardi, L., … Smith, H. A. (2004). The anatomy of star formation in NGC 300. *The Astrophysical Journal Supplement Series, 154*(1), 253-258.

Hernán-Caballero, A., Alonso-Herrero, A., Hatziminaoglou, E., Spoon, H. W., Almeida, C. R., Santos, T. D., ... Esquej, P. (2015). Resolving the active galactic nucleus and host emission in the mid-infrared using a model-independent spectral decomposition. *The Astrophysical Journal, 803*(2), 109-124.

Hines, D. C., Backman, D. E., Bouwman, J., Hillenbrand, L. A., Carpenter, J. M., Meyer, M. R., … Su, K. Y. L. (2006). The formation and evolution of planetary systems (FEPS): Discovery of an unusual debris system associated with HD 12039. *The Astrophysical Journal, 638*(2), 1070-1079.

Hogg, D. W. (1999). *Distance measures in cosmology* (pp. 15). Princeton, NJ: arXiv.

Hogg, D. W., Blanton, M. R., Eisenstein, D. J., Gunn, J. E., Schlegel, D. J., Zehavi, I., ... York, D. G. (2003). The overdensities of galaxy environments as a function of luminosity and color. *The Astrophysical Journal Letters, 585*(1), L5-L9.

Holmberg, E. (1958). *A photographic photometry of extragalactic nebulae* (V. 136, pp. 1). Lund, Sweden: Meddelanden fran Lunds Astronomiska Observatorium Serie II.

Hopkins, A. M., Miller, C., Nichol, R., Connolly, A., Bernardi, M., Gómez, P., … Ivezić, Ž. (2003). Star formation rate indicators in the Sloan Digital Sky Survey. *The Astrophysical Journal, 599*(2), 971-991.

Hopkins, P. F., Cox, T. J., Kereš, D., & Hernquist, L. (2008). A cosmological framework for the co-evolution of quasars, supermassive black holes, and elliptical galaxies: II. Formation of red ellipticals. *The Astrophysical Journal Supplement Series, 175*(2), 390-422.

Huang, S., & Gu, Q.-S. (2009). Recent star-forming activity in local elliptical galaxies. *Monthly Notices of the Royal Astronomical Society, 398*(4), 1651–1667.

Hubble, E. (1926). *No. 324. Extra-galactic nebulae* (V. 324, pp. 1-49). Washington, US: Contribution from the Mount Wilson Observatory/Carnegie Institution of Washington.

Hubble, E. P. (1936). *The The realm of the nebulae* (Vol. 25). New Haven, US: Yale University Press.

Hughes, T., & Cortese, L. (2009). The migration of nearby spirals from the blue to red sequence: AGN feedback or environmental effects? *Monthly Notices of the Royal Astronomical Society: Letters, 396*(1), L41–L45.

Hwang, H. S., Geller, M. J., Kurtz, M. J., Dell‟Antonio, I. P., & Fabricant, D. G. (2012). Shels: Optical spectral properties of WISE 22 μm selected galaxies. *The Astrophysical Journal, 758*(1), 25-41.

Im, M., Faber, S., Gebhardt, K., Koo, D. C., Phillips, A. C., Schiavon, R. P., … Willmer, C. N. (2001). Are there blue, massive E/S0 galaxies at z < 1? kinematics of blue spheroidal galaxy candidates. *The Astronomical Journal, 122*(2), 750-763.

Jarrett, T., Cohen, M., Masci, F., Wright, E., Stern, D., Benford, D., … Yan, D. L. (2011). The Spitzer-WISE survey of the ecliptic poles. *The Astrophysical Journal, 735*(2), 112-144.

Jarrett, T., Masci, F., Tsai, C., Petty, S., Cluver, M., Assef, R. J., … Wright, E. (2012). Extending the nearby galaxy heritage with WISE: First results from the WISE enhanced resolution galaxy atlas. *The Astronomical Journal, 145*(1), 6-39.

Jiang, L., Fan, X., Hines, D. C., Shi, Y., Vestergaard, M., Bertoldi, F., … Brinkmann, J. (2006). Probing the evolution of infrared properties of z~6 quasars: Spitzer observations. *The Astronomical Journal, 132*(5), 2127-2134.

Kannappan, S. J., Guie, J. M., & Baker, A. J. (2009). E/S0 galaxies on the blue color-stellar mass sequence at z= 0: Fading mergers or future spirals? *The Astronomical Journal, 138*(2), 579-597.

Kauffmann, G., Heckman, T. M., White, S. D., Charlot, S., Tremonti, C., Brinchmann, J., … York, D. (2003a). Stellar masses and star formation histories for 10^5 galaxies from the Sloan Digital Sky Survey. *Monthly Notices of the Royal Astronomical Society, 341*(1), 33–53.

Kauffmann, G., Heckman, T. M., White, S. D., Charlot, S., Tremonti, C., Peng, E. W., … York, D. (2003). The dependence of star formation history and internal structure on stellar mass for 10^5 low-redshift galaxies. *Monthly Notices of the Royal Astronomical Society, 341*(1), 54–69.

Kennicutt Jr, R. C. (1998). Star formation in galaxies along the Hubble sequence. *Annual Review of Astronomy and Astrophysics, 36*(1), 189–231.

Kennicutt Jr, R. C., & Kent, S. M. (1983). A survey of H-alpha emission in normal galaxies. *The Astronomical Journal, 88*, 1094–1107.

Kewley, L., & Dopita, M. (2003). The AGN-starburst connection in infrared merging galaxies. *Galaxy Evolution: Theory & Observations, 17*, 83–84.

Kewley, L., Geller, M., & Jansen, R. (2003). [OII] as a SFR indicator and the cosmic star formation history. *Bulletin of the American Astronomical Society*, *35*, 1404-1437.

Kewley, L. J., Dopita, M., Sutherland, R., Heisler, C., & Trevena, J. (2001). Theoretical modeling of starburst galaxies. *The Astrophysical Journal, 556*(1), 121-140.

Kewley, L. J., Dopita, M. A., Leitherer, C., Davé, R., Yuan, T., Allen, M., … Sutherland, R. (2013). Theoretical evolution of optical strong lines across cosmic time. *The Astrophysical Journal, 774*(2), 100-116.

Kewley, L. J., Geller, M. J., Jansen, R. A., & Dopita, M. A. (2002). The Hα and infrared star formation rates for the nearby field galaxy survey. *The Astronomical Journal, 124*(6), 3135-3143.

Kewley, L. J., Groves, B., Kauffmann, G., & Heckman, T. (2006). The host galaxies and classification of active galactic nuclei. *Monthly Notices of the Royal Astronomical Society, 372*(3), 961–976.

Kewley, L. J., Jansen, R. A., & Geller, M. J. (2005). Aperture effects on star formation rate, metallicity and reddening. *Publications of the Astronomical Society of the Pacific, 117*(829), 227-244.

Kewley, L. J., Maier, C., Yabe, K., Ohta, K., Akiyama, M., Dopita, M. A., … Yuan, T. (2013). The cosmic BPT diagram: Confronting theory with observations. *The Astrophysical Journal Letters, 774*(1), L10-L15.

Ko, J., Im, M., Lee, H. M., Lee, M. G., Kim, S. J., Shim, H., … Takagi, T. (2012). AKARI observation of the North Ecliptic Pole (NEP) supercluster at z= 0.087: Mid-infrared view of transition galaxies. *The Astrophysical Journal, 745*(2), 181-202.

Kokusho, T., Kaneda, H., Bureau, M., Suzuki, T., Murata, K., Kondo, A., ... Yamagishi, M. (2017). A star formation study of the ATLAS3D early-type galaxies with the AKARI All-sky Survey. *Astronomy & Astrophysics, 605*, A74-A77.

Lee, J. C., Hwang, H. S., & Ko, J. (2013). The calibration of star formation rate indicators for WISE 22 μm-selected galaxies in the Sloan Digital Sky Survey. *The Astrophysical Journal, 774*(1), 62-71.

Leger, A., & Puget, J. (1984). Identification of the „unidentified" IR emission features of interstellar dust? *Astronomy and Astrophysics, 137*, L5–L8.

Leja, J., Johnson, B. D., Conroy, C., van Dokkum, P. G., & Byler, N. (2017). Deriving physical properties from broadband photometry with prospector: Description of the model and a demonstration of its accuracy using 129 galaxies in the local universe. *The Astrophysical Journal, 837*(2), 170-204.

Lilly, S. J., Le Fevre, O., Hammer, F., & Crampton, D. (1996). The Canada-France redshift survey: The luminosity density and star formation history of the universe to z~1. *The Astrophysical Journal Letters, 460*(1), L1-L4.

Lin, Y.-T., Stanford, S. A., Eisenhardt, P. R., Vikhlinin, A., Maughan, B. J., & Kravtsov, A. (2011). Baryon content of massive galaxy clusters at z= 0-0.6. *The Astrophysical Journal Letters, 745*(1), L3-L7.

Lintott, C., Schawinski, K., Bamford, S., Slosar, A., Land, K., Thomas, D., … Vandenberg, C. (2011). Galaxy Zoo 1: Data release of morphological classifications for nearly 900 000 galaxies. *Monthly Notices of the Royal Astronomical Society, 410*(1), 166–178.

Lintott, C. J., Schawinski, K., Slosar, A., Land, K., Bamford, S., Thomas, D., … Berg, J. V. (2008). Galaxy zoo: Morphologies derived from visual inspection of galaxies from the Sloan Digital Sky Survey. *Monthly Notices of the Royal Astronomical Society, 389*(3), 1179–1189.

Lonsdale Persson, C. J., & Helou, G. (1987). On the origin of the 40-120 micron emission of galaxy disks a comparison with H-alpha fluxes. *The Astrophysical Journal, 314*, 513–524.

Martini, P., Dicken, D., & Storchi-Bergmann, T. (2013). The origin of dust in earlytype galaxies and implications for accretion onto supermassive black holes. *The Astrophysical Journal, 766*(2), 121-143.

Mazzei, P., & De Zotti, G. (1994). Far-IR properties of early type galaxies. *The Astrophysical Journal, 426*(1), 97-104.

McIntosh, D. H., Wagner, C., Cooper, A., Bell, E. F., Kereš, D., van den Bosch, F. C., … Christian, A. M. (2014). A new population of recently quenched elliptical galaxies in the SDSS. *Monthly Notices of the Royal Astronomical Society, 442*(1), 533–557.

Miller, N. A., & Owen, F. N. (2001). Current star formation in post-starburst galaxies? *The Astrophysical Journal Letters, 554*(1), L25-L31.

Moorwood, A. F., van der Werf, P. P., Cuby, J. G., & Oliva, T. (2000). H-alpha emitting galaxies and the cosmic star formation rate at z= 2.2. *Astronomy & Astrophysics, 509*, L5-L9.

Mullaney, J., Alexander, D., Goulding, A., & Hickox, R. C. (2011). Defining the intrinsic AGN infrared spectral energy distribution and measuring its contribution to the infrared output of composite galaxies. *Monthly Notices of the Royal Astronomical Society, 414*(2), 1082–1110.

Murphy, E., Chary, R.-R., Dickinson, M., Pope, A., Frayer, D., & Lin, L. (2011). An accounting of the dust-obscured star formation and accretion histories over the last 11 billion years. *The Astrophysical Journal, 732*(2), 126-142.

Netzer, H. (2015). Revisiting the unified model of active galactic nuclei. *Annual Review of Astronomy and Astrophysics, 53*, 365–408.

Netzer, H., Lutz, D., Schweitzer, M., Contursi, A., Sturm, E., Tacconi, L. J., … Lord, S. (2007). Spitzer Quasar and ULIRG Evolution Study (QUEST): II. The spectral energy distributions of palomar-green quasars. *The Astrophysical Journal, 666*(2), 806-816.

Norris, M. A., Meidt, S., Van de Ven, G., Schinnerer, E., Groves, B., & Querejeta, M. (2014). Being WISE: I. Validating stellar population models and M/L ratios at 3.4 and 4.6 μm. *The Astrophysical Journal, 797*(1), 55-63.

Norris, M. A., Van de Ven, G., Schinnerer, E., Crain, R. A., Meidt, S., Groves, B., … Theuns, T. (2016). Being WISE II: Reducing the influence of star formation history on the mass-to-light ratio of quiescent galaxies. *The Astrophysical Journal, 832*(2), 198-211.

O'Donnell, J.E. (1994). Rv - dependant optical and near-ultraviolet extinction. *The Astrophysical Journal, 422,* 158–163.

Osterbrock, D. E., & Ferland, G. J. (2006). *Astrophysics of gas nebulae and active galactic nuclei*. Sausalito, US: University Science Books.

Padmanabhan, N., Seljak, U., Strauss, M. A., Blanton, M. R., Kauffmann, G., Schlegel, D. J., … Ivezic, Z. (2004). Stellar and dynamical masses of ellipticals in the Sloan Digital Sky Survey. *New Astronomy, 9*(5), 329–342.

Phillips, M., Jenkins, C., Dopita, M., Sadler, E., & Binette, L. (1986). Ionized gas in elliptical and S0 galaxies: I. A survey for H-alpha and forbidden [N II] emission. *The Astronomical Journal, 91*, 1062–1085.

Pier, E. A., & Krolik, J. H. (1992). Infrared spectra of obscuring dust tori around active galactic nuclei: I. Calculational method and basic trends. *The Astrophysical Journal, 401*, 99–109.

Piovan, L., Tantalo, R., & Chiosi, C. (2003). Shells of dust around AGB stars: Effects on the integrated spectrum of single stellar populations. *Astronomy & Astrophysics, 408*(2), 559–579.

Poggianti, B., & Barbaro, G. (1997). Indicators of star formation: 4000 break and balmer lines. *Astronomy & Astrophysics, 325*, 1025-1030.

Polletta, M., Courvoisier, T.-L., Hooper, E., & Wilkes, B. J. (2000). The far-infrared emission of radio loud and radio quiet quasars. *Astronomy & Astrophysics, 362,* 75-96.

Polletta, M., Tajer, M., Maraschi, L., Trinchieri, G., Lonsdale, C., Chiappetti, L., … Tresse, L. (2007). Spectral energy distributions of hard x-ray selected active galactic nuclei in the XMM-newton medium deep survey. *The Astrophysical Journal, 663*(1), 81-102.

Polletta, M., Wilkes, B. J., Siana, B., Lonsdale, C. J., Kilgard, R., Smith, H. E., … Shupe, D. L. (2006). Chandra and Spitzer unveil heavily obscured quasars in the SWIRE/Chandra survey. *The Astrophysical Journal, 642*, 673-693.

Quintero, A. D., Hogg, D. W., Blanton, M. R., Schlegel, D. J., Eisenstein, D. J., Gunn, J. E., ... Goto, T. (2004). Selection and photometric properties of K + A galaxies. *The Astrophysical Journal, 602*(1), 190-199.

Radomski, J. T., Pina, R. K., Packham, C., Telesco, C. M., De Buizer, J. M., Fisher, R. S., … Robinson, A. (2003). Resolved mid-infrared emission in the narrow-line region 80 of NGC 4151. *The Astrophysical Journal, 587*(1), 117-122.

Ramos Almeida, C., Alonso-Herrero, A., Esquej, P., González-Martín, O., Riffel, R., García-Bernete, I., … Álvarez, C. (2014). A mid-infrared view of the inner parsecs of the Seyfert Galaxy MRK 1066 using Canari Cam/GTC. *Monthly Notices of the Royal Astronomical Society, 445*(2), 1130–1143.

Rieke, G., Alonso-Herrero, A., Weiner, B., Pérez-González, P., Blaylock, M., Donley, J., … Marcillac, D. (2009). Determining star formation rates for infrared galaxies. *The Astrophysical Journal, 692*(1), 556-573.

Roussel, H., Sauvage, M., Vigroux, L., & Bosma, A. (2001). The relationship between star formation rates and mid-infrared emission in galactic disks. *Astronomy & Astrophysics, 372*(2), 427–437.

Rowan-Robinson, M., & Crawford, J. (1989). Models for infrared emission from IRAS galaxies. *Monthly Notices of the Royal Astronomical Society, 238*(2), 523–558.

Rowan-Robinson, M., Mann, R., Oliver, S., Efstathiou, A., Eaton, N., Goldschmidt, P., … Gonzalez-Serrano, J. I. (1997). Observations of the Hubble deep field with the infrared space observatory: V. Spectral energy distributions, starburst models and star formation history. *Monthly Notices of the Royal Astronomical Society, 289*(2), 490–496.

Sales, D. A., Pastoriza, M. G., Riffel, R., & Winge, C. (2013). Polycyclic aromatic hydrocarbon in the central region of the Seyfert 2 Galaxy NGC 1808. *Monthly Notices of the Royal Astronomical Society, 429*(3), 2634–2642.

Salim, S., & Rich, R. M. (2010). Star formation signatures in optically quiescent early-type galaxies. *The Astrophysical Journal Letters, 714*(2), L290-L294.

Salim, S., Rich, R. M., Charlot, S., Brinchmann, J., Johnson, B. D., Schiminovich, D., … Sukyoung, K. Y. (2007). UV star formation rates in the local universe. *The Astrophysical Journal Supplement Series, 173*(2), 267-292.

Sauvage, M., Blommaert, J., Boulanger, F., Cesarsky, C., Cesarsky, D., Desert, F., … Vigroux, L. (1996). ISOCAM mapping of the whirlpool galaxy M51. *Astronomy and Astrophysics, 315*, L89–L92.

Sauvage, M., & Thuan, T. X. (1994). The far-infrared properties of the CfA galaxy sample. 2: Gas, dust, and star formation along the Hubble sequence19. *The Astrophysical Journal, 429*, 153–171.

Schade, D., Lilly, S., Crampton, D., Ellis, R., Le Fevre, O., Hammer, F., … Broadhurst, T. (1999). Hubble space telescope imaging of the CFRS and LDSS redshift surveys: III. Field elliptical galaxies at 0.2< z< 1.0. *The Astrophysical Journal, 525*(1), 31-46.

Schawinski, K., Khochfar, S., Kaviraj, S., Yi, S. K., Boselli, A., Barlow, T., … Szalay, A. (2006). Suppression of star formation in early-type galaxies by feedback from supermassive black holes. *Nature, 442*(7105), 888–891.

Schawinski, K., Lintott, C., Thomas, D., Sarzi, M., Andreescu, D., Bamford, S. P., … Sukyoung, K. Y. (2009). Galaxy zoo: A sample of blue early-type galaxies at low redshift. *Monthly Notices of the Royal Astronomical Society, 396*(2), 818-829.

Schawinski, K., Thomas, D., Sarzi, M., Maraston, C., Kaviraj, S., Joo, S.-J., ... Silk, J. (2007). Observational evidence for AGN feedback in early-type galaxies. *Monthly Notices of the Royal Astronomical Society, 382*(4), 1415-1431.

Schiminovich, D., Wyder, T. K., Martin, D. C., Johnson, B. D., Salim, S., Seibert, M., … Sukyoung, Y. (2007). The UV-optical color magnitude diagram: II. Physical properties and morphological evolution on and off of a star-forming sequence. *The Astrophysical Journal Supplement Series, 173*(2), 315-341.

Schlafly, E. F., & Finkbeiner, D. P. (2011). Measuring reddening with Sloan Digital Sky Survey stellar spectra and recalibrating SFD. *The Astrophysical Journal, 737*(2), 103-115.

Schlegel, D. J., Finkbeiner, D. P., & Davis, M. (1998). Maps of dust infrared emission for use in estimation of reddening and cosmic microwave background radiation foregrounds. *The Astrophysical Journal, 500*(2), 525-553.

Schmitt, D., HR ti, Armus, L., Giavalisco, M., Heckman, T., Kennicutt Jr, R., Leitherer, C., … Meurer, G. (2006). Ultraviolet-to-far-infrared properties of local star-forming galaxies. *The Astrophysical Journal, 643*(1), 173-185.

Shi, F., Kong, X., Wicker, J., Chen, Y., Gong, Z.-Q., & Fan, D.-X. (2012). Star formation rate indicators in Wide-field infrared survey preliminary release. *Journal of Astrophysics and Astronomy, 33*(2), 213–220.

Shi, Y., Rieke, G., Hines, D., Neugebauer, G., Blaylock, M., Rigby, J., … Alonso-Herrero, A. (2005). Far-infrared observations of radio quasars and FR II radio galaxies. *The Astrophysical Journal, 629*(1), 88-99.

Shipley, H. V., Papovich, C., Rieke, G. H., Brown, M. J., & Moustakas, J. (2016). A new star formation rate calibration from polycyclic aromatic hydrocarbon emission features and application to high-redshift galaxies. *The Astrophysical Journal, 818*(1), 60-79.

Siebenmorgen, R., Heymann, F., & Efstathiou, A. (2015). Self-consistent two-phase AGN torus models-SED library for observers. *Astronomy & Astrophysics, 583*, A120-A137.

Silva, L., Granato, G. L., Bressan, A., & Danese, L. (1998). Modeling the effects of dust on galactic spectral energy distributions from the ultraviolet to the millimeter band. *The Astrophysical Journal, 509*(1), 103-117.

Simonian, G. V., & Martini, P. (2016). Circumstellar dust, PAHs, and stellar populations in early-type galaxies: Insights from GALEX and WISE. *Monthly Notices of the Royal Astronomical Society, 464*, 3920-3936.

Stalevski, M., Fritz, J., Baes, M., Nakos, T., & Popović, L. Č. (2012). 3D radiative transfer modelling of the dusty tori around active galactic nuclei as a clumpy two-phase medium. *Monthly Notices of the Royal Astronomical Society, 420*(4), 2756–2772.

Stasińska, G., Fernandes, R. C., Mateus, A., Sodré, L., & Asari, N. V. (2006). Semiempirical analysis of Sloan Digital Sky Survey galaxies: III. How to distinguish AGN hosts. *Monthly Notices of the Royal Astronomical Society, 371*(2), 972-982.

Steidel, C. C., Adelberger, K. L., Giavalisco, M., Dickinson, M., & Pettini, M. (1999). Lyman-break galaxies at z>~4 and the evolution of the ultraviolet luminosity density at high redshift. *The Astrophysical Journal, 519*(1), 1-17.

Stern, D., Assef, R. J., Benford, D. J., Blain, A., Cutri, R., Dey, A., … Madsen, Kristin (2012). Mid-infrared selection of active galactic nuclei with the Wide-field Infrred Survey Explorer: I. Characterizing WISE-selected active galactic nuclei in COSMOS. *The Astrophysical Journal, 753*(1), 30-47.

Stern, D., Eisenhardt, P., Gorjian, V., Kochanek, C. S., Caldwell, N., Eisenstein, D., … Willner, S. P. (2005). Mid-infrared selection of active galaxies. *The Astrophysical Journal, 631*(1), 163-168.

Strateva, I., Ivezić, Ž., Knapp, G. R., Narayanan, V. K., Strauss, M. A., Gunn, J. E., … York, D. (2001). Color separation of galaxy types in the Sloan Digital Sky Survey imaging data. *The Astronomical Journal, 122*(4), 1861-1874.

Sullivan, M., Treyer, M. A., Ellis, R. S., Bridges, T. J., Milliard, B., & Donas, J. (2000). An ultraviolet-selected galaxy redshift survey: II. The physical nature of star formation in an enlarged sample. *Monthly Notices of the Royal Astronomical Society, 312*(2), 442–464.

Tadhunter, C. (2008). An introduction to active galactic nuclei: Classification and unification. *New Astronomy Reviews, 52*(6), 227–239.

Temi, P., Brighenti, F., & Mathews, W. G. (2005). Mid-infrared emission from elliptical galaxies: Sensitivity to stellar age. *The Astrophysical Journal Letters, 635*(1), L25-L28.

Temi, P., Brighenti, F., & Mathews, W. G. (2009). Spitzer observations of passive and starforming early-type galaxies: An infrared color–color sequence. *The Astrophysical Journal, 707*(2), 890-902.

Tempel, E. (2011). Tracing galaxy evolution by their present-day luminosity function. *Open Astronomy, 20*(2), 241–250.

Tinsley, B. M., & Gunn, J. E. (1976). Evolutionary synthesis of the stellar population in elliptical galaxies: I. Ingredients, broad-band colors and infrared features. *The Astrophysical Journal, 203*, 52–62.

Toba, Y., Oyabu, S., Matsuhara, H., Malkan, M. A., Gandhi, P., Nakagawa, T., … Yano, K. (2014). Luminosity and redshift dependence of the covering factor of active galactic nuclei viewed with WISE and Sloan Digital Sky Survey. *The Astrophysical Journal, 788*(1), 45-80.

Tojeiro, R., Masters, K. L., Richards, J., Percival, W. J., Bamford, S. P., Maraston, C., ... Thomas, D. (2013). The different star formation histories of blue and red spiral and elliptical galaxies. *Monthly Notices of the Royal Astronomical Society, 432*(1), 359-373.

Trager, S., Faber, S., Worthey, G., & González, J. J. (2000). The stellar population histories of early-type galaxies: II. Controlling parameters of the stellar populations. The *Astronomical Journal, 120*(1), 165-188.

Tran, Q., Lutz, D., Genzel, R., Rigopoulou, D., Spoon, H., Sturm, E., ... Wart, N. (2001). ISOCAM-CVF 5-12μm spectroscopy of ultraluminous infrared galaxies. *The Astrophysical Journal, 522*(2), 527-543.

Tremonti, C. A., Heckman, T. M., Kauffmann, G., Brinchmann, J., Charlot, S., White, S. D., … Brinkmann, J. (2004). The origin of the mass-metallicity relation: Insights from 53,000 star-forming galaxies in the Sloan Digital Sky Survey. *The Astrophysical Journal, 613*(2), 898-913.

Tresse, L., & Maddox, S. J. (1998). The Hα luminosity function and star formation rate at z~0.2. *The Astrophysical Journal, 495*(2), 691-697.

Treyer, M. A., Ellis, R. S., Milliard, B., Donas, J., & Bridges, T. J. (1998). An ultravioletselected galaxy redshift survey: New estimates of the local star formation rate. *Monthly Notices of the Royal Astronomical Society, 300*(1), 303–314.

Urry, C. M., & Padovani, P. (1995). Unified schemes for radio-loud active galactic nuclei. *Publications of the Astronomical Society of the Pacific, 107*(715), 803-845.

Urry, M. (2003). The AGN paradigm for radio-loud objects. *Astronomical Society of the Pacific, 290*, 3-10.

Veilleux, S., & Osterbrock, D. E. (1987). Spectral classification of emission-line galaxies. *The Astrophysical Journal Supplement Series, 63*, 295–310.

Villaume, A., Conroy, C., & Johnson, B. D. (2015). Circumstellar dust around AGB stars and implications for infrared emission from galaxies. *The Astrophysical Journal, 806*(1), 82-99.

Vincent, R. A., & Ryden, B. S. (2005). The dependence of galaxy shape on luminosity and surface brightness profile. *The Astrophysical Journal, 623*(1), 137-147.

Walterbos, R., & Schwering, P. (1987). Infrared emission from interstellar dust in the Andromeda galaxy. *Astronomy and Astrophysics, 180*, 27–49.

Wen, X.-Q., Wu, H., Zhu, Y.-N., Lam, M. I., Wu, C.-J., Wicker, J., … Zhao, Y.-H. (2013). The stellar masses of galaxies from the 3.4 μm band of the WISE all-sky survey. *Monthly Notices of the Royal Astronomical Society, 433*(4), 2946-2957.

Wright, E. L., Eisenhardt, P. R., Mainzer, A. K., Ressler, M. E., Cutri, R. M., Jarrett, T., … Tsai, -C. W. (2010). The Wide-field Infrared Survey Explorer (WISE): Mission description and initial on-orbit performance. *The Astronomical Journal, 140*(6), 1868-1881.

Wu, H., Cao, C., Hao, C.-N., Liu, F.-S., Wang, J.-L., Xia, X.-Y., … Young, C. K.-S. (2005). PAH and mid-infrared luminosities as measures of star formation rate in Spitzer first look survey galaxies. *The Astrophysical Journal Letters, 632*(2), L79-L82.

Xilouris, E. M., Madden, S., Galliano, F., Vigroux, L., & Sauvage, M. (2004). Dust emission in early-type galaxies: The mid-infrared view. *Astronomy & Astrophysics, 416*(1), 41–55.

Yan, L., Donoso, E., Tsai, C.-W., Stern, D., Assef, R., Eisenhardt, P., … Riechers, D. A. (2013). Characterizing the mid-infrared extragalactic sky with WISE and SDSS. *The Astronomical Journal, 145*(3), 55-70.

Yuan, F.-T., Takeuchi, T. T., Buat, V., Heinis, S., Giovannoli, E., Murata, K. L., … Burgarella, D. (2011). Akari/IRC broadband mid-infrared data as an indicator of the star-formation rate. *Publications of the Astronomical Society of Japan, 63*(6), 1207–1217.

Yuan, H.-B., Liu, X.-W., & Xiang, M.-S. (2013). Empirical extinction coefficients for the GALEX, SDSS, 2MASS and WISE passbands. *Monthly Notices of the Royal Astronomical Society, 430*(3), 2188–2199.

Zabludoff, A. I., Zaritsky, D., Lin, H., Tucker, D., Hashimoto, Y., Shectman, S. A., … Kirshner, R. P. (1995). The environment of "E + A" galaxies. *The Astrophysical Journal, 466*, 104-113.

Zaritsky, D., Zabludoff, A. I., & Willick, J. A. (1995). Spectral classification of galaxies along the Hubble sequence. *The Astronomical Journal, 110*(4), 1602-1613.

Zhu, Y.-N., Wu, H., Cao, C., & Li, H. -N. (2008). Correlations between mid-infrared, far-infrared, Hα, and FUV luminosities for Spitzer SWIRE field galaxies. *The Astrophysical Journal, 686*(1), 155-171.